ABSTRACT

Title of Dissertation: DEVELOPMENT OF NOVEL AG-BASED ANTIMICROBIAL MATERIALS: ANTIMICROBIAL EFFICACY AND POTENTIAL APPLICATIONS IN FOOD

Lei Mei, Doctor of Philosophy, 2020

Dissertation directed by: Associate Professor, Qin Wang, Department of Nutrition and Food Science

Silver (Ag) and Ag-based compounds have been used as broad-spectrum antimicrobial agents for centuries for their great antimicrobial activities against many different strains of bacteria, fungi, and viruses. Though the development of Ag-based antimicrobial agents have made a great advancement in the past decades, many challenges remain to be addressed: 1) constructing sustained-release delivery system of antimicrobials to ensure prolonged antimicrobial efficacy; 2) reducing antimicrobial agents' toxicity to human; 3) minimizing the risk of causing potential environmental pollution by incompletely degraded antimicrobial agents residues. To meet these challenges, two novel Ag-based antimicrobial agents have been developed: Ag nanoclusters (AgNCs) and alkynyl Ag modified CS (Ag-CS). Further studies were conducted to investigate their synthesis routes, chemical and physical properties, antimicrobial efficiencies, cytotoxicity, and potential applications.

AgNCs with particle size of 2-4 nm were successfully synthesized and embedded into zein films to form a novel antimicrobial coating material. AgNCs endowed bright fluorescence with emissions between 620-650 nm and the synthesis conditions were optimized by adjusting the irradiation time, light sources, and concentrations of synthesis materials. The antimicrobial efficacy and cytotoxicity of AgNCs were then systematically evaluated and compared with those of $AgNO_3$ as well as larger Ag nanoparticles (AgNPs) with diameters of 10 nm (AgNP10) and 60 nm (AgNP60). AgNCs presented a comparable dose-dependent antimicrobial efficacy to $AgNO_3$, but had a significantly lower toxicity towards human cells than that of $AgNO_3$. Further, AgNCs presented a much greater antimicrobial capacity than AgNP10 and AgNP60, which indicated that the administration dose of AgNCs for antimicrobial applications could be dramatically reduced compared to that of AgNPs.

Ag-CS were prepared by modifying the alkynyl Ag group on the backbone of chitosan (CS) through chemical reactions. Experiment results indicated that Ag-CS exhibited a sustained release of Ag for over 5 days whereas Ag acetate (AgOAc) infused CS released 91.18±2.07 % of its Ag in 4 h. Ag-CS was proved to have potent bacteria inhibition and inactivation efficiencies that were stronger than AgOAc at the same equivalent Ag concentration. By coating on shrimps and strawberries, Ag-CS greatly extent their shelf lives under cold storage conditions.

# DEVELOPMENT OF NOVEL AG-BASED ANTIMICROBIAL MATERIALS: ANTIMICROBIAL EFFICACY AND POTENTIAL APPLICATIONS IN FOOD AREA

by

Lei Mei

Dissertation submitted to the Faculty of the Graduate School of the
University of Maryland, College Park, in partial fulfillment
of the requirements for the degree of
Doctor of Philosophy
2020

Advisory Committee:
Dr. Qin Wang, Chair
Dr. Rohan V. Tikekar
Dr. Liangli Yu
Dr. Yang Tao
Dr. Yaguang Luo

# Dedication

To my parents for their financial, moral, continual and unrelenting support.

To my husband for his understanding, support and encouragement.

To my daughter for bringing me tremendous joy.

# Acknowledgements

My PhD journey at University of Maryland is filled with encourage, support, friendship, preservation, determination, joys, and, of course, difficulties. There have been tremendous memories that I will remember for my whole life.

First of all, I would like to express my deep gratitude to my advisor, Dr. Qin Wang, who has guided me throughout my graduate study with dedicated support, encouragement, and patience. Her insight, enthusiasm, knowledge was invaluable in formulating my research questions and methodology. I also thank her for encouraging me to freely pursue my research interest and providing me with the best research environment possible.

I also would like to thank all my other committee members: Dr. Rohan Tikekar, Dr. Yaguang Luo, Dr. Yang Tao, and Dr. Liangli Yu. I sincerely appreciate their support and guidance in finishing this dissertation. Their insightful suggestions broadened my professional experience and prepared me for future challenges. Also, I appreciate Dr. Lee's lab, Nanocenter, Surface Analysis Center for their technical supports.

Special thank goes to my labmates, Jinglin Zhang, Zi Teng, Yongguang Guan, Yuan Li, and Peihua Ma for providing me valuable research comments and suggestions as well as shaping our lab an encouraging, comfortable, and joyful research environment.

Finally, I would like to give my deepest gratitude to my families. I thank my parents for their consistent support and encouragement, their optimism and tenacity silently encouraging me pursuing so far in my research. I also would especially thank my husband for always being supportive, encouraging, and caring. Thank him for spending a lot of time taking care of our kid at this moment, and this allowed me to be more focused on finishing my dissertation. I also thank my kid for bringing me a lot of joy and making my life more tasty.

Without you, nothing is possible. I am more than glad to thank you all at this special moment.

# Table of Contents

# List of Tables

# List of Figures

# List of Abbreviations

| **Abbreviations** | **Definitions** |
|---|---|
| AgNPs | Silver nanoparticles |
| PEG | Polyethylene glycols |
| PAA | Polyacrylamides |
| SDS | Sodium dodecyl sulfate |
| CTAC | Cetyltrimethylammonium chloride |
| CTAB | Cetyltrimethylammonium bromide |
| TEM | Transmission electron microscopy |
| EPS | Extracellular polymeric substance |
| AgNCs | Ag Nanoclusters |
| HAADF | High angel annular dark field |
| STEM | Scanning transmission electron microscopy |
| OPML-XRD | Oriented particulate monolayer X-ray diffraction |
| PE | Polyethylene |
| MRSA | Methicillin-resistant *S. aureus* |
| LB | Lysogeny broth |
| ZnO NPs | Zinc oxide nanoparticles |
| $TiO_2$ NPs | Titanium dioxide nanoparticles |
| GMs | Graphene materials |
| NA | not applicable |
| PLA | Polylactic acid |
| PP | Polypropylene |
| WVP | Water vapor permeability |
| WS | Water solubility |
| UV | Ultraviolet |

| | |
|---|---|
| LDPE | Low density polyethylene |
| EtOH | Ethanol |
| PPH | Homopolymer of polypropylene |
| PPB | Block copolymer of polypropylene |
| PPR | Random copolymer of polypropylene |
| CuNPs | Copper nanoparticles |
| TiNPs | Titanium nanoparticles |
| GRAS | Generally recognized as safe |
| PMAA | Poly methacrylic acid |
| $AgNO_3$ | Silver nitrate |
| AgNP10 | Ag nanoparticles with diameter of 10 nm |
| AgNP60 | Ag nanoparticles with diameter of 60 nm |
| AgNP550 | Ag nanoparticles with diameter of 550 nm |
| SPR | Surface plasmon resonance |
| FTIR | Fourier transform Infrared |
| NMR | Nuclear magnetic resonance |
| ROS | Reactive oxygen species |
| AMP | Antimicrobial peptides |

# Chapter 1: Literature Review

*Adapted from Mei, L.; Wang, Q. Advances in Using Nanotechnology Structuring Approaches for Improving Food Packaging. Annual Review of Food Science and Technology 2020, 11, 339-364.*

Microbial contamination usually increases the risk of foodborne illness, shortens the shelf life of food products, and causes huge economic losses to the food industry. One approach to combat microbial contamination in the food supply chain is to develop novel antimicrobial materials with high efficiencies, which can be incorporated into food packaging materials and interact with food or headspace in the package to extend the shelf life of food products, thus enhance food safety with little influence on food quality.[1]

In this chapter, generally used antimicrobial agents in food area are briefly introduced. Then, an elaborate overview of current state of the art of Ag-based antimicrobial agents was given. Meanwhile, the commercial availability, antimicrobial mechanism, antimicrobial efficacy, and applications of Ag-based antimicrobial agents in the food area are summarized and discussed. Lastly, the background and advances of two major research subjects of this dissertation: AgNCs and Ag-CS are illustrated.

## *1.1 Overview of antimicrobial agents used in food area*

Different antimicrobial agents are incorporated into packaging materials to improve food safety and extend shelf lives of food products. The antimicrobial agents used in packaging materials include naturally derived antimicrobial agents (e.g., essential oils and enzymes), synthetic inorganic materials (e.g., ZnO, $TiO_2$, and Ag), and organic compounds (e.g., nisin, lysozyme, curcumin).[2] Their antimicrobial activities are derived from several mechanisms, such as damaging cell membrane integrity,[3] impairing biomolecules (e.g., DNA and protein) inside cells,[4] regulating metabolic systems,[5] and exerting oxidative stresses.

### 1.1.1 Naturally-derived antimicrobial agents

Naturally-derived antimicrobial agents have gained much attention by consumers and the food industry, for they are generally safer than other antimicrobial agents and consumers prefer natural over synthetic products. These natural antimicrobial compounds can be obtained from different sources including plants, animal, bacteria, algae and fungi.[6] Natural antimicrobials used in antimicrobial food packages can be classified based on different origins and components.

#### 1.1.1.1 Plant volatile oils and secondary metabolites

The antimicrobial activity of plant volatile oils and extracts has been recognized for years. Studies showed that some oils extracted from different plants such as

lemongrass, oregano and bay can inhibit the growth of organisms of Gram-positive bacteria, Gram-negative bacteria, and yeast with a minimum inhibitory concentration (MIC) less than 2.0% (v/v).[7] Applications of plant essential oils and extracts in food products are partially limited due to their strong aroma and their compositions' changes according to local climatic and environmental conditions.[8]

Medicinal plants are rich in a numerous variety of secondary metabolites with antimicrobial properties. Examples are tannins, alkaloids, saponine and alkenyl phenols. These compounds are widely used in medicine for their great antimicrobial effects.[9] Guo *et al*. (2018) developed a tannin-gelatin bio-adhesive through a one-step Michael addition reaction. This tissue adhesive exhibited adjustable gelation times, fast degradation, and favorable cytocompatibility, which hold great promises for a number of applications in wound closure and tissue sealant.[10] Roger *et al*. (2017) also reported a tannic acid coated magnetic nanocarrier as a processing aid for food contact surface treatment. This nanocarrier (particle size ~10 nm) was demonstrated to be highly efficient against the growth of *Listeria monocytogenes* with MIC of 200 ppm.[11]

#### 1.1.1.2 Antimicrobial peptides and enzymes

Antimicrobial peptides (AMP) are cationic peptides containing 12-50 amino acids. By causing membrane perturbation, regulating macromolecular synthesis in the cell, they act efficiently against most Gram-negative and Gram-positive bacteria, fungi, virus, and eukaryotic parasites. The antimicrobial ability of AMP is affected by its sequences,

size, structure, and surface charge through altering the interactions between AMP and targets.[12] Nisin, a 34 amino acid cationic peptide produced by certain Gram-positive bacteria, is one of the most widely used AMP. This peptide has gained considerable attentions due to its potent and broad spectrum antimicrobial activity, low likelihood of promoting the development of bacterial resistance, and low cellular cytotoxicity at antimicrobial concentrations.[13]

Enzymes play a critical role in defending living organisms in nature. They possess abilities to directly attack the microorganism and interfere with biofilm formation. A lot of studies have focused on the incorporation of enzymes to polymer materials to prevent microbial colonization. Enzymes with antimicrobial activity can be classified by their antibacterial mechanisms. Proteolytic enzymes are protein hydrolyzing enzymes, and this group of enzyme is widely used on biofilm treatment for some of the enzymes are able to hydrolyze adhesions, cleave cell walls, thus loosen and remove biofilms. Polysaccharide-degrading enzymes can facilitate the hydrolysis of cell walls, and one most commonly used polysaccharide-degrading enzyme is lysozyme.[14] Lysozyme catalyzes the hydrolysis of 1,4-beta-linkages between N-acetylmuramic acid and N-acetyl-D-glucosamine residues in peptidoglycan, which is the major component of Gram-positive bacterial cell wall.[15]

### 1.1.2 Organic acids and derivatives

Many organic acids and derivatives are used as food preservatives, including sorbic acid, propionic acid, acetic acid, and benzoic acids. Most of the organic acids that possessing antimicrobial activity are monoprotic acids. The antimicrobial effectiveness of organic acid are related to the pH of food systems, and the undissociated forms of organic acids are largely responsible for the inhibition of microorganisms. Since most organic acids have $pK_a$ of 3.0-5.0, the use of organic acid as preservatives is limited to food systems with pH less than 5.5. The organic acids inhibit the bioactivity of bacterial by 1) interfering protein synthesis and genetic processes, thus influencing the cell wall synthesis in prokaryotes; 2) acidifying the cell interior environment, and deplete ATP by active proton transport. Rocha et al. incorporated 1.5% sorbic acid into protein films from Argentine anchovy (*Engraulis anchoita*).[16] The incorporated sorbic acid dramatically changed the physical properties of the films by decreasing tensile strength, increasing elongation at break, and increasing water vapor permeability (WVP). Meanwhile, the film with 1.5% sorbic acid exhibited an inhibition effect against *E. coli*, *S. enteritidis* and *L. monocytogenes,* but not *S. aureus*. Park et al. modified vinyl monomers with phenol and benzoic acid as pendant groups. These modified vinyl polymers demonstrated dose dependent antimicrobial effects against several bacteria strains and fungi. However, they reported that the polymerization of the modified monomers significantly decreased their antimicrobial efficiencies by comparing to the monomers.[17]

### 1.1.3 Inorganic antimicrobial nanomaterials

Inorganic antimicrobial agents are reported to be advantageous over organic antimicrobial agents due to their higher stability and greater heat resistance. Recent researches have greatly explored the development and applications of inorganic nanomaterials as antimicrobial agents against bacteria, viruses, and other pathogenic microorganisms. Metal-based nanomaterials have been extensively studied due to their stability, facile synthesis, and efficient biological properties. Varies of nanomaterials have been reported to have efficient antimicrobial activities, such as ZnO, $Fe_2O_3$, $TiO_2$, Ag nanostructures, and so on.[18]

ZnO NPs have drawn lots of attention for their antimicrobial activities, good stability, and UV absorbance properties. They have been intensively studied for applications in both food area and pharmaceutical area. ZnO NPs offer broad-spectrum antimicrobial activity because they can damage cell membranes and generate ROS, and these properties allow ZnO NPs to inhibit the growth of various types of microorganisms. Furthermore, adding ZnO NPs to food packaging materials offered improvements to the mechanical and barrier properties of the packaging materials.[19]

The family of graphene materials (GM) is composed of graphene, graphene oxide (GO), and reduced graphene oxide (rGO). Graphene is a nanomaterial formed by tightly packed $sp^2$ hybridized carbon atoms in a honeycomb lattice. With further

chemical processing of graphene, GO and rGO can be obtained.[20] GO is a graphene sheet with oxygen-containing functional groups such as carboxyl, hydroxyl, and epoxide groups; rGO is synthesized by eliminating functional groups on GO.[21] GMs have excellent barrier properties and are impermeable to most gases and water vapor. They also provide antimicrobial activity through a combination of several mechanisms. Both their barrier properties and antimicrobial capabilities make the GM family materials popular components in food packaging materials.

$TiO_2$ nanoparticles ($TiO_2$ NPs) is one of the most studied metal oxides and can be prepared through several methods. Sol-gel and hydrothermal are the most successful methods because they offer better control of the morphology, particle size, and crystallinity of the products. $TiO_2$ NPs were utilized for broad applications on, e.g., photocatalysis, sensors, solar cell devices, antimicrobial, and batteries. In the antimicrobial applications, $TiO_2$ NPs demonstrated the antimicrobial activity by constantly generating hydroxyl radicals and superoxide ions under nonlethal ultraviolet (UV) exposure, and antimicrobial applications have been reported against various strains of bacteria.[22, 23, 24]

## *1.2 Overview of Ag-based antimicrobial agents and their applications*

Many nanostructures have been studied for their potential applications in the food area, including AgNPs, $TiO_2$ NPs, ZnO nanoparticles (ZnO NPs), and GMs. Among them,

Ag-based nanostructures have drawn a lot of attention for their unique physical properties, including strong surface plasma resonance, large surface-to-volume ratio, efficient catalytic activity, and remarkable broad-spectrum antimicrobial activity against many different strains of bacteria, fungi, and viruses.[25]

### 1.2.1 Commercial available Ag-based antimicrobial products

The majority of the patents filed on Ag-based antimicrobial products is about nanoAg technology, including applications in healthcare products, medical equipment, and food contact surfaces. Medical grade Ag-containing dressing approved by FDA/EPA include: SilverIon (Argentum Medical LLC), Silvadeen (Arion Laboratories), Guard Ag (Beiersdorf AG), and Actisorb 220 (Johnson & Johnson). AgIon (AgIon Technology, Inc.) is made up of Ag ions and zeolites, and this product is approved by FDA as an additive for food contact polymers. PURE Hard Surface/SDC3A is a patented hard surface disinfectant and a sanitizer for food contact surfaces. It offers broad-spectrum efficacy, rapid contact time, and 24-h residual protection. In addition, it is also registered as a no-rinse food-contact surface sanitizer. Examples of Ag-based commercially available active packages are listed in table 1-1.

### 1.2.2 Antimicrobial mechanisms of AgNPs, AgNCs, and Ag ions

The exact antimicrobial mechanisms of Ag-based nanostructures and Ag ions are not fully understood but generally may involve cell membrane damage, protein and DNA

damage, and reactive oxygen species (ROS) generation. The antimicrobial efficacy is decided by several factors: the dissociation of Ag from the nanostructures, the migration of Ag from food packages to the food matrix, and the interactions between target microorganisms and different forms of Ag (e.g., particle, cluster, and ion).

**Table 1-1. Examples of commercially available Ag-based active packages**

| Trade names | Manufacture | Active compounds | Descriptions |
|---|---|---|---|
| Biomaster | Addmaster Ltd., UK | Ag | Masterbatch |
| SilverIon | Life Materials Technology Ltd. | Ag | Masterbatch |
| Surfacine | Surfacine Development Co. LLC., USA | Ag | Masterbatch |
| Ionpure | Solid Spot LLc., US | Ag | Masterbatch |
| Irgaguard | BASF, USA | Ag | Masterbatch |
| D2p | Symphony Environmental Ltd., UK | Ag | Films and trays |
| Bactiblock | NanoBio Master, Spain | Ag | Masterbatch |
| Zeomic | Sinanen Co., Ltd, Japan | Ag | Paperboards, films, cartons, wraps |
| Novaron | Toagosei, Japan | Ag | Paperboards, films, cartons, wraps |
| AgIon | AgIon Technologies, USA | Ag ions & zeolite | Paperboards, films, cartons, wraps |

#### 1.2.2.1 Antimicrobial mechanism of AgNPs

The antimicrobial effect of AgNPs is the combination of the antimicrobial activity from AgNPs and $Ag^+$ released from AgNPs. The cell damage caused by AgNPs starts from the adhesion of AgNPs to bacterial cell membranes. First, the cell wall became circumferential, and electron-dense pits occurred at the sites of binding, followed by the shrinkage of cytoplasm and membrane detachment.[26,27] Transmission electron microscopy (TEM) revealed that a few minutes after the electrostatic interaction between AgNPs and cell membrane, cell wall became circumferential and numerous electron dense pits were observed at sites of the damages induced by AgNPs, followed by the shrinkage of cytoplasm and membrane detachment.[27] Further, the internalized AgNPs and $Ag^+$ that were from AgNPs could react with intercellular contents: they could alter the tertiary structures of proteins, block active binding sites in proteins, interrupt DNA replication and transcription, and finally lead to cell dysfunction.[28] AgNPs could intercalate between purine and pyrimidine base pairs, disrupted the H-bonds and thereby disrupted the double helix structure of DNA. AgNPs also caused DNA molecule to change its state from relaxed to condensed form, and DNA thus loss replication ability. These interactions in result caused cell damages and inhibited cell growth by preventing cell division and reproduction. The production of ROS [e.g., hydrogen peroxide ($H_2O_2$), superoxide anion ($O^{2-}$), hydroxyl radical ($OH\cdot$)] also causes hyperoxidation of lipids, proteins, and DNA in bacterial cells.

#### 1.2.2.2 Antimicrobial mechanism of Ag nanoclusters

Interactions between AgNCs and cells caused damages on cell membrane and intercellular molecules by releasing of $Ag^+$ to cells and generating ROS. Javani et al. (2016) investigated the ROS production of AgNCs synthesized by DNA templates.[29] In their study, a fluorescent probe 2′,7′-dichlorofluorescein diacetate was used to detect the production of multiple ROS in cells, including $H_2O_2$, OH·, and peroxynitrite ($ONOO^-$). *E. coli* and *S. epidermidis* incubated with AgNCs for 14 h in the dark showed remarkable increases in the ROS generation. The authors also reported increased inhibition activity by synthesizing AgNCs in trimer. The AgNCs trimer at 0.75 μM demonstrated comparable antimicrobial activity as 4 μM single AgNCs against *S. epidermidis*. Sharma et al. (2016) constructed a series of poly(vinylidene fluoride) membranes that contained AgNCs and found that the leaching amount of $Ag^+$ from the membrane determined the antimicrobial efficacy.[30] Alahmadi et al. (2018) suggested that the antimicrobial activity of AgNCs was a complex and unpredictable function of the combination of several parameters, such as their size, concentration, stability, and shape.[31] Capping agents could improve the stability of AgNCs and extend the shelf life of AgNCs in solutions; however, they could also inhibit the availability of $Ag^+$ to reach the sites of action and impair their antimicrobial activity.

#### 1.2.2.3 Antimicrobial mechanism of Ag ions

Ibrahim et al. (2001) studied the uptake of Ag ion into bacterial cells by measuring the concentrations of Ag ion on cell membranes at different growth phases.[32] They found

that Ag ion accumulation on the outer membrane of *P. diminuta* reached the maximum during the lag phase and early exponential growth period, then decreased during the mid-exponential and stationary phases. They also found that the accumulation of Ag ion inside of the cell remained greater than that on the cell membrane. Another work also reported that the antimicrobial activity of Ag ion toward biofilms was realized by inducing the production of looser extracellular polymeric substance (EPS) fractions and structural deterioration in protein EPS.[33] High Ag ion concentrations may affect ion exchanges in cells. $Ca^{2+}$ plays important roles in maintaining the lipopolysaccharide assembly on the cell surface and cellular metabolism inside cells. Mohite et al. (2018) demonstrated that the exposure to Ag ion doubled the $Ca^{2+}$ release in pantoea agglomerans cells.[34] Ag ion also bound sulfhydryl- and nitrogen-containing groups and competed for copper sites in bacterial cells.[35] In terms of interactions between Ag ion and proteins, inside *S. aureus* cells, Ag ion interacted with catabolite control protein A through two Cys residues. The protein A was usually involved in gene expression and regulation, and the binding consequently caused protein dysfunction and growth inhibition.[36] Ag ion also impaired the activity of several enzymes, such as succinate dehydrogenase in *R. gelatinosus* and *E. coli*.[37] Increased production of ROS induced by Ag ion was noticed in both HaCaT human cells and bacterial cells, and a high level of ROS caused cell growth inhibition, DNA damage, protein damage, and cell death.[38, 39]

### 1.2.3 Factors contribute to the effectiveness of Ag-based antimicrobial agents

The antimicrobial activities of Ag nanostructures are reported to be highly dependent on their particle size, shape, surface properties and stabilities. Decreased particle size usually contributes to a higher antimicrobial activity because of increased mobility and surface area to volume ratio, resulting in greater interactions with bacteria. For example, Martinez-Castanon et al. (2008) demonstrated that, by reducing the sizes of AgNPs from 89 nm to 7 nm, the minimum inhibitory concentration (MIC) dropped from 11.79 to 6.26 ug/mL for *E. coli* and from 33.17 to 7.5 ug/mL for *S. aureus*.[40]

#### 1.2.3.1 The contribution of stability to the antimicrobial activity

One fundamental problem that limits the antimicrobial activity of AgNPs is the stability of their dispersions. Most AgNPs dispersion is easy to aggregate due to the small sizes, and aggregation can reduce their antimicrobial activity.

To enhance the stability of AgNPs aqueous dispersion, one effective approach is to introduce steric repulsion to the surface of AgNPs by modifying AgNPs with polymers such as polyethylene glycols (PEG), polyacrylamides (PAA), or modifying AgNPs with non-ionic surfactants like Tween and Triton X-100. Another efficient approach is to increase the surface charge and stabilize AgNPs through electrostatic repulsions. The surface charge of the disperse phase can be enhanced by adding ionic surfactants, such

as sodium dodecyl sulfate (SDS),[41] cetyltrimethylammonium chloride or bromide (CTAC, CTAB).[42] A suggested mechanism for the stabilization effect of SDS is that the hydrophilic groups of SDS are absorbed on AgNPs and hydrophobic tails are directed outward to form a first layer. Next, a counter-layer is oriented the opposite way resulting in interpenetration of the surfactant hydrophobic tails between the two layers of hydrophilic groups that headed outward.[43]

#### 1.2.3.2 The contribution of size to the antimicrobial activity

One antimicrobial mechanism of AgNPs is that they can interact with cell membrane, damage the integrity, change the permeability and functionality of bacteria cells. Reducing the size of AgNPs can increase the surface to volume ratio, which allows AgNPs to better interact with bacterial membranes. Recently, Morones and co-workers (2005) have observed the size-dependent interaction between the AgNPs (size range 1–100 nm) and the bacteria using high angel annular dark field (HAADF) scanning transmission electron microscopy (STEM).[44] Agnihotri et al. tested the antimicrobial effects of a series of AgNPs that sized from 5 to 100 nm with same coatings. Results demonstrated that the smallest AgNPs (5 nm in diameter) showed the highest antimicrobial efficiency as well as the shortest bacteria killing time after their interaction with the bacteria.[45] As such, reducing the size of AgNPs could be an efficient way to achieve a higher antimicrobial activity.

#### 1.2.3.3 The contribution of surface property to the antimicrobial activity

The surface property of AgNPs plays critical roles in their interactions with bacteria cells and their stability in solutions. Studies showed that citrate or poly-vinylpyrrolidone capped AgNPs generally presented higher antimicrobial activities for they were more stable in LB and other serum solutions containing proteins.[46] Gnanadhas et al. demonstrated that the uptake of capped AgNPs was significantly higher than that of uncap-AgNPs in the presence of serum. The uptake increased because the interaction among the AgNPs themselves was minimized when capping agents were used.[47] Besides the improvement on the stability by adding capping agent, cationic modification on AgNPs also promoted the adhesion and uptake of AgNPs to bacteria cells, which enhanced the antimicrobial activities of AgNPs.[48]

### 1.2.4 Synergistic effects between Ag-based antimicrobial agents and other compounds

The combination of multiple antimicrobial agents offers a new approach to develop packaging materials with superior antimicrobial activity or multifunctional food packaging systems. The combination usage of multiple agents can effectively reduce the application dose of each agent, lower the potential for inducing drug resistance, and provide new strategies to treat drug-resistant microorganisms. Examples of packaging materials with improved antimicrobial activity through the combination of multiple antimicrobials are listed in Table 1-2. Fayaz et al. (2010) reported a synergistic effect

of AgNPs and antibiotics (e.g., ampicillin, kanamycin, and erythromycin) against Gram positive and Gram negative bacteria.[49] The highest synergistic effect was found in the combination of AgNPs and ampicillin, with an overall 74.89% increase against *E. coli, S. typhi, S. aureus, and M. luteus*. Ruden et al. (2009) studied the synergistic interaction between AgNPs and membrane-permeabilizing antimicrobial peptide polymyxin B and found that the high permeabilization of the outer bacterial membrane by polymyxin B effectively enhanced the intrinsic antibiotic effect of AgNPs; this combination was a promising candidate to treat infection caused by Gram negative pathogens.[50] Akram et al. (2016) demonstrated that a combination of AgNPs, blue light, and antibiotics azithromycin resulted in synergistic effects against methicillin-resistant *S. aureus* (MRSA).[51] The triple combination resulted in a significantly higher killing effect for MRSA with 8.4 log reduction compared to a control group, whereas the double combination of azithromycin and AgNPs resulted 5.2 log reduction. He et al. (2012) also demonstrated that a combination of Ag species [AgNPs or Ag ion] with Chattonella marina exerted a synergistic effect on the viability of fish gill cells.[52] These cells lost minimal viability when exposed to AgNPs or Ag ion at concentrations between 0.02 and 0.2 ppm; moreover, additional Chattonella marina to the treatment significantly decreased cell viability by 10% and 16% for AgNPs and Ag(I), respectively. Lotfi et al. (2019) prepared a series of antimicrobial PE films containing AgNPs and $TiO_2$ NPs in different proportions and found that an equal concentration of 5% AgNPs and 5% $TiO_2$ NPs showed the strongest antimicrobial activity and longest shelf-life extension when the films were used as plastic wraps for chicken.[53]

The combination of multiple functional nanostructures is a promising way to construct multifunctional packaging materials (e.g., AgNPs, ZnO NPs, $TiO_2$ NPs, and GMs provide antimicrobial properties; nanoclays improve barrier properties; and microorganism sensors monitor freshness). Meanwhile, the combination of several antimicrobial agents may reduce the dose and exposure time of individual compounds and increase the antimicrobial efficiency. However, potential disadvantages of combination applications are also present. The combination may increase the risk of contamination by resistance bacteria as well as potential toxicity by utilizing several antimicrobials together. The biological effect and safety need more understanding and evaluation. Furthermore, different microorganisms may require different formulations of combined antimicrobials to maximize the antimicrobial activity, which increases the difficulty of applying combined antimicrobials in food packaging systems.

**Table 1-2. Synergistic effects of combining different antimicrobial agents**

| Function | Effective agents | Type | Characteristics | Matrix | Bacteria | Conclusion | Ref |
|---|---|---|---|---|---|---|---|
| Antimicrobial<br>Antioxidant | Liposome-encapsulated laurel essential oil | Coating | Diameter ~200 nm | Chitosan | Staphylococcus aureus<br>Escherichia coli | Extension of shelf life from 9 days by regular PE to 15 days with developed film at 4°C | 54 |
| Antimicrobial | AgNPs Cellulose nanofibril<br>AgNPs | Fiber | AgNPs ~11 nm | NA | E. coli<br>L. monocytogenes | Greater inhibitory effect on E. coli over L. monocytogenes without significant cytotoxicity on human cell growth | 55 |
| Antimicrobial<br>Barrier<br>Adhesion | Carrageenan<br>AgNPs<br>Laponite | Coating | Coated on PP 24-$\mu$m thick film | Oxygen plasma surface modified PP film | S. aureus<br>E. coli | Decrease in barrier properties with increased Laponite concentration<br>Enhanced adhesion between coating and PP films following oxygen plasma treatment<br>Excellent antimicrobial activity provided by AgNPs | 56 |
| Antimicrobial | Alginate microbeads containing AgNPs | Film | AgNPs ~10–21 nm<br>Microbeads ~190 $\mu$m | PLA | S. aureus | Sustained release of Ag over 10 days<br>Inhibitory effects against S. aureus | 57 |
| Antimicrobial | AgNPs synthesized by Nigella sativa extract | Film | AgNPs ~8 nm | Chitosan | Bacillus subtilis<br>S. aureus<br>E. coli<br>Pseudomonas aeruginosa | Antimicrobial efficacy: B. subtilis > S. aureus > E. coli > P. aeruginosa | 58 |

### 1.2.5 Migration of Ag from packaging materials to food matrix

Migration is defined as the mass transfer of a component from a food-contact material to the food matrix. It is a crucial factor regarding risk assessment and food safety evaluations. The migration of nanostructures to the food matrix involves a few submicroscopic processes: the desorption or detachment of nanostructures from the packaging materials; the dissolution and dispersion of the nanostructures in the surrounding environment; the degradation of polymer materials that induce the release of nanostructures from the polymer; and the sorption and interaction of nanostructures with foodstuffs.[59]

The migration of nanostructures from packaging material to the food matrix is largely determined by their size, structure, chemical composition, and temperature as well as the acidity of the surrounding environment. Particle size is the dominant parameter that determines the release rate for particles smaller than 10 nm, and the diffusion coefficient decreases exponentially with increased particle size.[60] As a result of an increased surface-to-volume ratio in smaller particles, 4 nm AgNPs released approximately 100× more Ag mass than the AgNPs larger than 10 nm.[61] The desorption rate was also found to be temperature dependent in the example of polyvinylpyrrolidone-AgNPs coated with polystyrene (AgNPs ~78.9 nm). The desorption rate of Ag increased with the temperature increase in a linear relationship up to 40°C. Afterward, the desorption rate continually increased with the temperature

increase at an increased pseudo-second order until 70°C. The nonlinear relationship at higher temperatures suggested that the Ag might be reabsorbed by free carbonyl groups on the coated polystyrene surface and thus limited the desorption rate. A more comprehensive analysis of the parameters that affect the desorption rate in this study further indicated that temperature was the prominent contributor, followed by time and pH values.[62] Acidic food products were reported to accelerate the migration rate. The amount of Ag released from AgNPs in 3% acetic acid was 2.4-fold higher than Ag released from 95% EtOH.[63]

Types of polymer materials and surface treatments also play important roles in determining the migration rate of components from the polymer matrix. Different polymers present different compatibilities for nanostructures and thus influence the migration rate in different ways. Chen & Hu (2018) examined the migration rate of zinc from ZnO NPs/PP composite films into 3% acetic acid by using three types of PP: homopolymer of PP (PPH), block copolymer of PP (PPB), and random copolymer of PP (PPR).[64] The results demonstrated that the migration of zinc from PP followed the order of PPH > PPB > PPR. This is because the side chains on PPB and PPR protected well-embedded ZnO NPs, whereas a notable phase separation was observed in ZnO NPs embedded PPH because of the high crystallinity and compact structure of PPH. Regarding the surface treatment for the polymer matrix, an increase in the interaction between the nanostructure and polymer matrix could effectively decrease the migration rate by not only decreasing the desorption but also increasing the reattachment between

diffused nanostructures and the polymer matrix. For example, an increased amount of carbonyl and carboxyl groups by UV, ozone, and Pluronic treatments strengthened the attachment of AgNPs to PE and inhibited the release of Ag from the polymer matrix.[65] Comparisons of the nanostructures' migration were carried out between different nanomaterials. When nanostructures were incorporated into PE and biblock copolymer, copper nanoparticles (CuNPs) and titanium nanoparticles (TiNPs) demonstrated higher migration rates than AgNPs and the desorption of Ag from AgNP coating on polystyrene could be predicted by a pseudo-second-order kinetic sorption model with $R^2_{Prediction} = 0.90$.[62, 63, 66, 67]

The release and migration of Ag from packaging materials or coating materials to food products is the major concern regarding the safety of applying Ag-based material in the food packaging systems. Studies showed that the migration activity of Ag from nano-Ag impregnated polymer containers was different from nano-Ag based coating materials. Higher levels of migration had been observed for samples exposed to nano-Ag coating materials.[68] Also, for AgNPs, the main mechanism for migration is dissolution of AgNPs from the packaging coating, or particle desorption and dissolution in acidic food simulants.[67] Overall, the migration of Ag from packages is case by case, the migration activity is determined by the physical property of the coating matrix, the incorporation methods of Ag nanostructures to matrix, the form and stability of Ag nanostructures and so on. Detailed migration activity and safety

evaluation should be performed based on the specific characteristics of the Ag contained packaging material.

### 1.2.6 Antimicrobial efficacy comparison between $AgNO_3$, AgCl, AgNPs, and AgNCs

Jo et al. (2009) studied the antifungal activity of AgNPs (20–30 nm), $AgNO_3$, AgCl, and electrochemical Ag generated by electrolysis. All forms of Ag inhibited the colony formation of plant-pathogenic fungi *Bipolaris sorokiniana*, and their antifungal activity was weakened in the following order: $AgNO_3$ > electrochemical Ag > AgNPs > AgCl.[69] To further elucidate how the antimicrobial efficacy changed depending on which form of Ag was present during the synthesis of AgNPs, $Ag^+$ was loaded in potassium hexaniobate crystals and exposed to UV irradiation to form AgNCs and then AgNPs by extending irradiation time. With increased irradiation time, the inhibition zone of Ag-loaded hexaniobate crystals first increased slightly, which corresponded to the formation of AgNCs; the inhibition zone then decreased over irradiation time, which was the result of forming AgNPs with increased particle size through irradiation.[70] AgNCs with particle sizes under 2nm also demonstrated stronger antimicrobial activity over AgNPs with size of 100 nm. The AgNCs were reported to have an MIC of 11.8 mg/L against *P. aeruginosa*, whereas the MIC of AgNPs in 100 nm were reported to be 83.8 mM (~9000 mg/L).[71] Mosselhy et al. (2015) reported that all tested bacterial strains (*A. hydrophila, Ps. putida, E. coli, B. subtilis*, and *S. aureus*) showed no

response to AgNPs, except *S. aureus* was inhibited at $3 \times 10^5$ colony-forming units (CFU)/mL by 10 μg/mL AgNPs, whereas 10 μg/mL $AgNO_3$ inhibited all bacterial strains.[72] Table 1-3 summarizes the antimicrobial efficacy of $Ag^+$, AgNPs, and AgNCs based on their MIC and minimum bactericidal concentration (MBC) values. Overall, the antimicrobial activities of Ag-based antimicrobial agents decrease with increased sizes, and the Ag ions generally demonstrated the best antimicrobial activity, followed by AgNCs, which offered comparable antimicrobial effects to Ag ions with a lower toxicity. However, the antimicrobial activity of AgNPs was limited comparing to the other two forms.

**Table 1-3 Antimicrobial efficacy comparison between different Ag-based nanostructures**

| Ag type | Material | Diameter | Bacterial strains | Minimum inhibitory concentration | Minimum bactericidal concentration | Ref |
|---|---|---|---|---|---|---|
| Ag | Chitosan/Ag-coated $\gamma Fe_2O_3$ NPs | 6.9 nm | E. coli | 1.1 μg/mL Ag eq. | 4.2 μg/mL Ag eq. | 73 |
| | Ag exchanged zeolite Y | NR | E. coli | NR | 25 μg/mL Ag eq. | 74 |
| AgNPs | AgNPs | 60 nm<br>85 nm | Bacillus subtilis | 30–40 μg/mL<br>30–40 μg/mL | 30–50 μg/mL<br>40–60 μg/mL | 75 |
| | AgNPs | 7.39 nm | E. coli (DH5α) | >5 μg/mL | NR | 76 |
| | Glutathione-stabilized AgNPs | 10–50 nm | Multidrug-resistant Campylobacter | 4.92–39.4 μg/mL | 9.85–39.4 μg/mL | 77 |
| | β-cyclodextrin-thiol–stabilized AgNPs | 4 nm | Staphylococcus aureus<br>E. coli | 1.8 μg/mL<br>0.9 μg/mL | NR | 78 |
| | Catechol-conjugated chitosan-coated AgNPs | 43.0±3.8 nm | S. aureus<br>E. coli | 10 μg/mL<br>5 μg/mL | NR | 79 |
| | AgNPs loaded with wrinkled mesoporous silica | ~3–5 nm | S. aureus<br>E. coli | 3.04 μg/mL Ag eq.<br>4.04 μg/mL Ag eq. | 6.08 μg/mL Ag eq.<br>8.08 μg/mL Ag eq. | 80 |
| | AgNPs | 89.86 nm | Candida albicans | 5.244 μg/mL | NR | 81 |
| AgNCs | AgNCs | 1 nm | S. aureus<br>E. coli | 9±1 μg/mL<br>14±2 μg/mL | NR | 82 |
| | AgNCs | 2.2–2.4 nm | E. coli | 1.05 μg/mL | NR | 83 |

### 1.2.7 Applications of Ag-based nanostructures as antimicrobial packaging materials

Ag were incorporated into some commonly used packaging materials to realize antimicrobial activity. Packaging materials used for food products can be grouped into non-degradable polymeric films and biodegradable polymeric films.

Among the non-degradable polymers, polyethylene (PE), polyvinyl chloride, polyvinylpyrrolidone, and ethylene vinyl alcohol are the most commonly used to host AgNPs for food packaging.[84] Low-density PE (LDPE) is largely used as a covering film for fresh food products and has been intensively studied as the matrix for Ag-based nanostructures. Low-temperature plasma–treated LDPE films had increased numbers of hydrophilic groups such as C–O and C=O, which increased the hydrophilicity and reactivity of the films. Thus, more AgNPs could be coated on the film surface, which intensified the antimicrobial activity against MRSA and *E. coli*.[85] Zhao et al. (2007) reported that the surface free energy of metal-polymer composites changed based on the ratios and types of metal and polymer. Surfaces with less energy exhibited a reduced microbial adhesion and were more sensitive to cleaning agents because of a weak binding affinity.[86]

Biodegradable polymeric films represent an alternative option in food packaging because they may be obtained from renewable sources with no contribution to

environmental pollution. The most commonly used are polysaccharides such as cellulose, pullulan, agarose, starch, agar, polylactic acid (PLA), and CS. Besides introducing an antimicrobial effect, adding AgNPs to the biodegradable polymers could cause a slight decrease in the mechanical resistance and thermal stability.[87] Agar films have been prepared by the solvent casting method, and a blend of agar with banana powder and AgNPs endows the film with antioxidant, antimicrobial, and UV screening properties.[88]

### 1.2.8 Current challenges for Ag-based antimicrobial agents

Though the development of Ag-based antimicrobial packaging materials have made a great advancement in the past decades, many challenges remain to be addressed: 1) uncontrolled release of Ag could not ensure long time antimicrobial efficacy; 2) high application dose of Ag might cause the diffusion of Ag to food systems and are toxic to humans; 3) Ag cores in many Ag-based antimicrobial agents might become environment hazards after usage. To meet these challenges, major strategies are undertaken, including 1) development of coreless Ag composite that has robust antimicrobial efficacy and are environmental friendly for its small particles size, 2) decrease of the application dose of Ag to reduce potential toxicity and, 3) controlled release of Ag to restrict the diffusion of Ag to food systems.

## *1.3 Overview of AgNCs*

Ag nanoclusters (AgNCs) with sizes between 1-3 nm have drawn a lot of attention recently for their unique properties form bulk materials. Their synthesis, structures, fluorescence properties, as well as potential applications will be discussed in this part.

### 1.3.1 Structure of AgNCs

AgNCs consisting of dozens of atoms, have a diameter smaller than 2 nm, which is closed to the Fermi wavelength (~0.5 nm for Ag). With such a small size, the band structures of AgNCs are discontinuous and broken down into discrete energy levels. Thus AgNCs endow unique physical and chemical properties (such as tunable fluorescence with great photostability and quantized charging property), which are different from AgNPs with larger particle sizes (Figure 1-1).[71]

The structure of AgNCs generally includes an Ag core that is surrounded by stabilizers. The core is composited of dozens of Ag atoms, and the amount of stabilizers used to stabilize one AgNC varies by different stabilizers. Figure 1-2 is a structural illustration of AgNCs stabilized by different stabilizers.

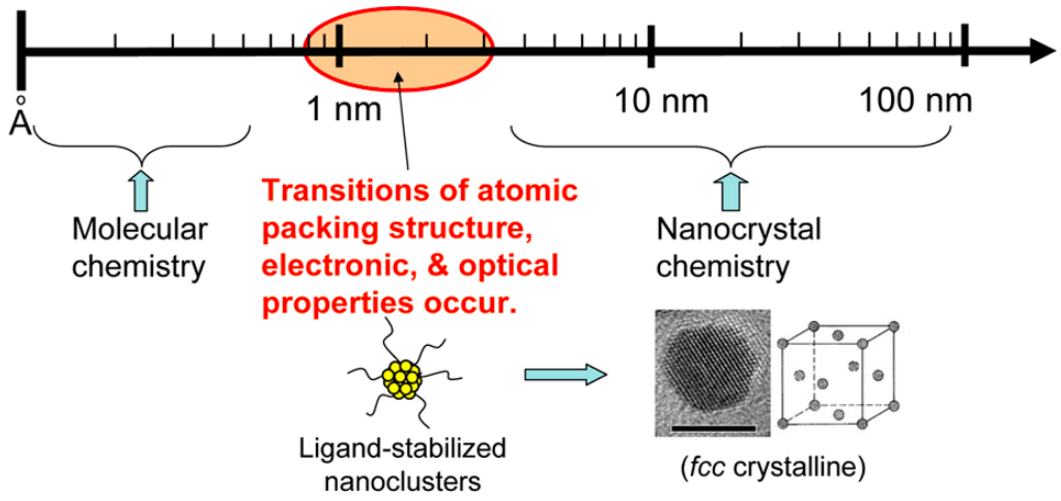


**Figure 1-1**. Metal nanoclusters bridge between organometallic complexes and plasmonic nanoparticles. Reproduced from Ref [89].

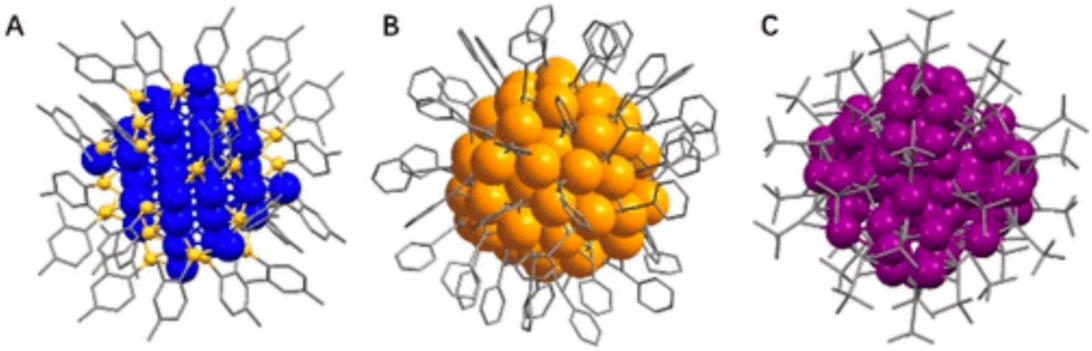


**Figure 1-2**. Total structures of (A) $Ag_{46}S_7(SPhMe_2)_{24}$, (B) $Ag_{74}(C{\equiv}CPh)_{44}$, and (C) $Ag_{51}(tBuC{\equiv}C)_{32}$. Reprinted from Ref [90].

### 1.3.2 Optical properties of AgNCs

#### 1.3.2.1 UV-vis absorption of AgNCs

Surface plasmon resonance (SPR) is a major feature for the UV-vis absorption of AgNPs, and their absorptions are typically around 400 nm. AgNCs, on the contrary, have several different absorption peaks from AgNPs in the UV-vis region. The location of absorption peaks of AgNCs is also related to the size and composition of AgNCs.[91] For example, the absorption peaks of thiol-protected AgNCs presented a red shift with increased particle sizes (Figure 1-3). Such a change could be used to confirm the synthesis of AgNCs and monitor the transformation from small AgNCs to large AgNPs.

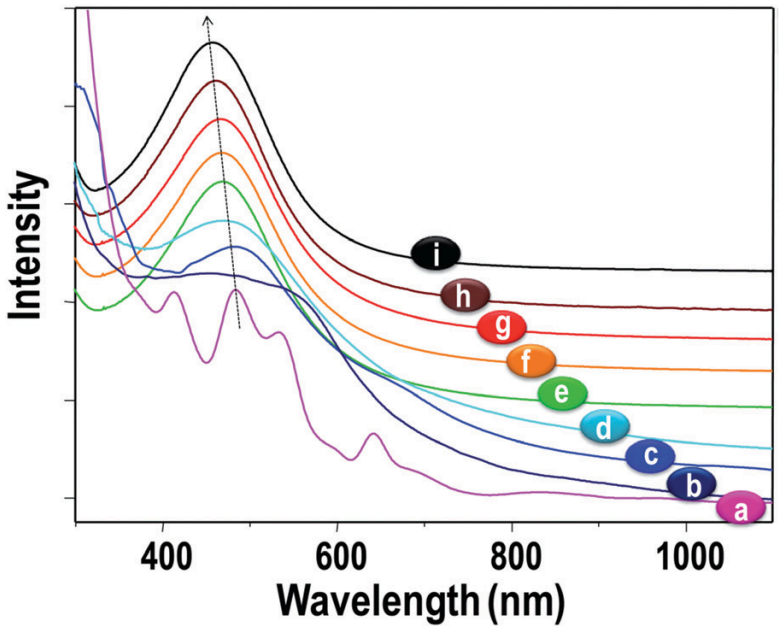


**Figure 1-3**. UV-vis absorption spectra of thiol-protected Ag44 [a], Ag55 [b], Ag~75 [c], Ag~114 [d], Ag152 [e], Ag~202 [f], Ag~423 [g], Ag~530 [h] and Ag NPs [i]. Reproduced from Ref [92].

#### 1.3.2.2 Relationship between material energy levels and optical properties

The fluorescence properties of a material is closely related to its energy levels (Figure 1-4). The energy levels of the electrons in bulk metals are continuous, and electrons' movement is highly free in the bulk materials. Once the size is reduced to the nano level, the motion of electrons is restricted because of the small size of the nanoparticles. Since interactions are limited to only happen within the surface of nanoparticles, metal nanoparticles could display intense colors due to their SPR effect. In addition, in this situation, the optical properties are determined by the a series of interactions between electrons and light. Generally, metal nanoparticles absorb light strongly, but they do not or only show weak luminescence.

With further reducing on the size to metal NCs, the energy levels become discrete, in which NCs are not conductive any more. In this situation, the collective oscillation of electrons is obstructed and NCs do not subject to the SPR effect. Instead, they will follow quantum mechanical rules. Once they absorbed light, electronic transitions happened between their discontinued energy levels, and thus shown bright luminescence.

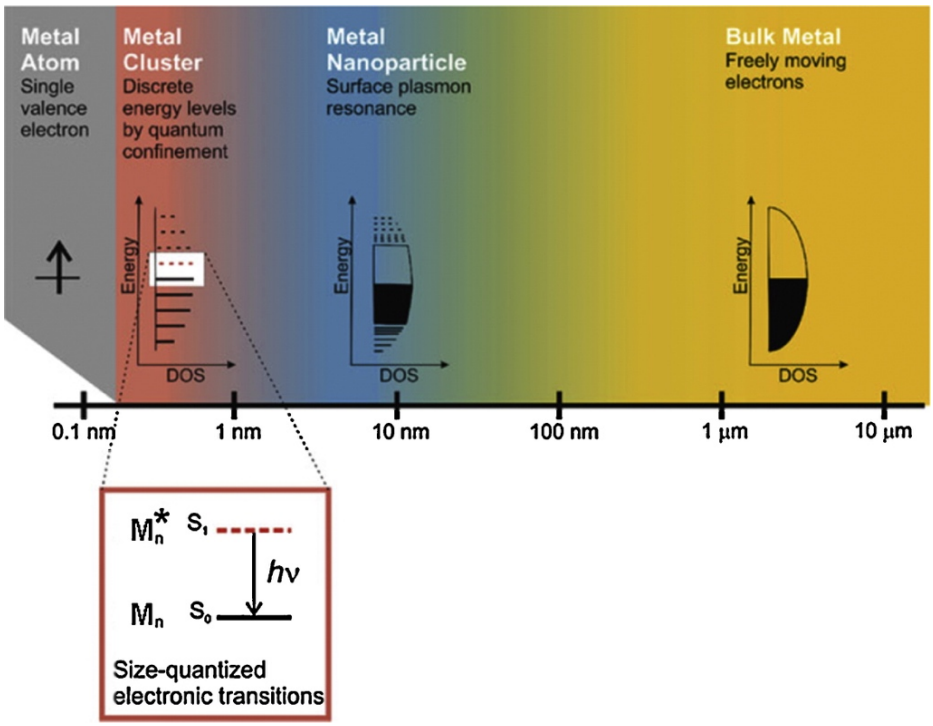


**Figure 1-4**. The effect of size on metals. Whereas bulk metal and metal nanoparticles have a continuous band of energy levels, the limited number of atoms in metal nanoclusters results in discrete energy levels, allowing interaction with light by electronic transitions between energy levels. Metal nanoclusters bridge the gap between single atoms and nanoparticles. Reprinted from Ref. [93]

### 1.3.2.3 Fluorescent properties of AgNCs

AgNCs emit bright fluorescence by returning from the excited state to the ground state, but some mechanism of fluorescent properties of AgNCs remains unclear. Factors contribute to the fluorescent properties of AgNCs include cluster size, protecting ligand, crystal structure, pH, temperature et al. Though many types of fluorescent AgNCs are reported and studied, the quantum yield of AgNCs is considered low comparing to most small-molecule fluorescent probes.[94]

### 1.3.3 Formation and stabilization of AgNCs

The formation and stabilization of AgNCs in solution have been accomplished in various ways. To successfully synthesize AgNCs, multiple parameters should be considered, including temperature, reducing methods, stabilizers, and the concentration ratios of Ag to stabilizer. Small changes on the synthetic formulation and procedure may cause the formation of large AgNPs with no fluorescence property.[95] Choosing stabilizers is also crucial for the synthesis of AgNCs, since the stability of AgNCs is limited and they could aggregate irreversibly as to reduce their surface energy. Thus, a proper stabilizer is thus indispensable.

Conventionally, AgNCs are synthesized by reducing $Ag^+$ using chemical reductants or light irradiation. Since AgNCs tend to interact with each other and aggregate to reduce surface energy, stabilizers or templates (e.g. DNA, polymers, et al.) are added to stabilize AgNCs.[96] AgNCs enabled various applications. For example, Wang et al. (2005) reported the use of core-shell structured nanoparticles with hydrophilic surfaces and hydrophobic cores as a template to synthesize AgNCs, in which the template greatly enhanced the stability and fluorescence intensity of AgNCs.[18] Previously, AgNCs have been extensively investigated for applications for biosensing, bioimaging, and disease diagnosis. However, the exploration of the antimicrobial application of AgNCs, though highly promising, has been limited, especially for food packaging applications. Compared to large AgNPs, the ultra-small size of AgNCs impart unique

advantages such as large surface to volume ratio, high local surface Ag concentration, and high mobility. These advantages may enhance the antimicrobial potency of AgNCs, and enable the achievement of superior antimicrobial capacity using much lower amounts of AgNCs than that of AgNPs.

### 1.3.4 Applications of AgNCs

#### 1.3.4.1 The application of AgNCs as antimicrobial agents

AgNCs with high surface to volume ratios are expected to perform high antimicrobial activity over a variety of microorganisms by damaging their membrane, impairing DNA, and increasing oxidative stress in cells. Studies suggests that GSH-protected AgNCs demonstrated stronger antimicrobial effect than AgNPs against *E. coli* and *S. aureus*.[97] Similar results were also proved on a multi-drug resistant bacteria strain *P. aeruginosa*.[71]

#### 1.3.4.2 The application of AgNCs as biosensors

AgNCs have been exclusively studied as luminescent probes for the detection of DNA, RNA, protein, enzyme activity, small molecules and ions.[98] AgNCs is generally highly sensitive to the surrounding environment, and the change of pH, temperature, composition could all effect the optical performance of AgNCs. Moreover, the fluorescence of some AgNCs located at long wavelength can readily penetrate cell membrane. These properties demonstrated AgNCs a great candidate in the applications of biosensing and bioimaging.

## *1.4 Alkynyl Ag*

Alkynyl Ag, also called Ag acetylide, is among the first organometallics ever produced. Traditionally, the alkynyl Ag is prepared by the treatment of an alkyne in ammoniacal Ag nitrate solution to give the alkynyl Ag as a precipitate, which may be easily collected by filtration and stored in the absence of light. Recently, Zhang *et al*. (2015) developed biocompatible and degradable polyphosphoester-based nanoparticles that could release Ag in a controllable manner over 5 days.[99] The alkynyl Ag was obtained by a reversible reaction between Ag acetate and alkynes, and it was promising for the treatment of lung infections.[100] In the form of alkynyl Ag, Ag are directly substituted to the alkynyl group, where Ag and Ag ion would later be released through the reversible reaction. Also, the extreme mild and facile synthesis procedure of alkynyl Ag makes it possible to be modified on other biopolymers. Additionally, there was no Ag core in this structure, which could decrease the dose of Ag for antimicrobial applications.

Researches about applications of alkynyl Ag on the area of antimicrobial are very limited. To the best of our knowledge, there is no reported study about the antimicrobial activity of alkynyl Ag and any applications in the food area. However, the coreless structure of alkynyl Ag together with its sustained Ag releasing property make it a potential candidate as an antimicrobial agent.

## *1.5 Matrix used in antimicrobial coating material*

### 1.5.1 CS and its derivatives

CS is a polysaccharide prepared by deacetylation of chitin, which is one of the most abundant natural polymers in living organism such as crustacea, insects and fungi. CS has been proved to be nontoxic, biodegradable, and biocompatible, and it has widely been used in the food industry as a safe and natural fat digestion and lip trapping compound. Studies also approved that CS and modified CS had some antibacterial and antifungal activities. The antimicrobial activity was reported to be correlated to the molecular weight and solubility of CS. CS with lower molecular weight promised better solubility, which directly contributes to a higher antimicrobial efficacy.[101, 102]

### 1.5.2 Zein

Zein, a group of prolamins from corn, is a GRAS (generally recognized as safe) food-grade ingredient. Zein films have low WVP compared to many other bio-based films, because three quarters of the amino acid residues in zein are hydrophobic. Zein films have previously been developed as antimicrobial food packaging materials by incorporating antimicrobial lysozyme and thymol.[103] For it is not soluble in pure water, zein serves as great candidates for natural food packaging materials.

## *1.6 Research objectives of the dissertation*

In this dissertation, two types of novel Ag-based antimicrobial agents, AgNCs and Ag-CS were developed and evaluated in terms of their antimicrobial efficiencies, toxicity, safety, and potential applications. AgNCs were embedded in zein film to form an antimicrobial coatings that have great antimicrobial effects with a low application dose, which are comparable with Ag nitrate. Also, the AgNCs with ultra-small particle sizes are environmental friendly and low toxic. To further decrease the application dose by avoid using Ag cores in the antimicrobial agents, Ag-CS was developed to form an antimicrobial agents with a coreless structure. The Ag-CS demonstrated a great antimicrobial property and have great potentials to be used in the food area.

# Chapter 2: Ag nanocluster-embedded zein films as antimicrobial coating materials for food packaging

*Adapted from Mei, L.; Teng, Z.; Zhu, G.; Liu, Y.; Zhang, F.; Zhang, J.; Li, Y.; Guan, Y.; Luo, Y.; Chen, X.; Wang, Q. Silver Nanocluster-Embedded Zein Films as Antimicrobial Coating Materials for Food Packaging. ACS Appl. Mater. Interfaces* ***2017****, 9 (40), 35297–35304. https://doi.org/10.1021/acsami.7b08152.*

## *2.1 Abstract*

Highly efficient antimicrobial agents with low toxicity and resistance have been enthusiastically pursued to address public concerns on microbial contamination in food. Ag nanoclusters (AgNCs) are known for their ultra-small sizes and unique optical as well as chemical properties. Despite extensive studies of AgNCs for biomedical applications, previous research on their application as antimicrobials for food applications is very limited. Here, for the first time, by incorporating AgNCs (~ 2 nm in diameter) into zein films, we developed a novel coating material with potent antimicrobial activity, low toxicity to human cells, and low potential to harm the environment. In addition, we systematically evaluated the antimicrobial activities and cytotoxicity of AgNCs-embedded zein films and compared them with zein films embedded with $AgNO_3$ or AgNPs with diameters of 10 nm and 60 nm (AgNP10 and AgNP60, respectively). At equivalent Ag concentrations, AgNCs and $AgNO_3$

solutions exhibited considerably higher antimicrobial activities than those of AgNP10 and AgNP60 solutions. Moreover, AgNCs had less cytotoxicity to human cells than $AgNO_3$, with half maximal inhibitory concentration ($IC_{50}$) of 34.68 μg/mL for AgNCs compared to 9.14 μg/mL for $AgNO_3$. Overall, the novel AgNCs coating developed in this research has great potential for antimicrobial applications in food packaging materials due to its high antimicrobial efficacy, ultra-small size and low cytotoxicity.

## *2.2 Introduction*

Microbial contamination reduces the shelf life of food products, increases the risk of foodborne illness, and causes huge economic losses to the food industry. One approach to combating microbial contamination in the food supply is to develop antimicrobial food packaging systems and coating materials, which incorporate antimicrobial agents that can interact with food or headspace in the package to extend the shelf life of food products and enhance food safety without affecting food quality.[104]

Ag and Ag-based compounds have been used as broad-spectrum antimicrobial agents for centuries. They are known to have antimicrobial activity against many different strains of bacteria, fungi, and viruses and are stable due to their low volatility. Among them, AgNPs have attracted much attention for their unique physical properties, including strong surface plasma resonance, large surface to volume ratio, efficient catalytic activity, and remarkable antimicrobial activity.[105] The antimicrobial activities

of AgNPs are reported to be highly dependent on the particle size.7 Decreased particle size contributing to higher antimicrobial activity as a result of increased mobility and surface area to volume ratio, resulting in greater interaction with bacteria. For example, Martinez-Castanon *et al*. demonstrated that, by reducing the sizes of AgNPs from 89 nm to 7 nm, the minimum inhibitory concentration (MIC) dropped from 11.79 to 6.26 μg/mL for *E. coli* and from 33.17 to 7.5 μg/mL for *S. aureus*.[40] Small AgNPs could attach to and penetrate the cell membrane, altering the permeability and cellular respiration and causing further damage to intracellular biomolecules such as genomic DNA.[44] Although the development of Ag-based antimicrobial packaging materials has advanced greatly in the past decades, many challenges remain to be addressed: 1) creating sustained-release delivery systems of antimicrobials to ensure prolonged antimicrobial efficacy;[106, 107] 2) minimizing antimicrobial agents' toxicity to human; 3) reducing the residual antimicrobial agents or antimicrobial packaging materials in order to reduce environmental hazard.[108-110] In this study, we have addressed these challenges by incorporating AgNCs as antimicrobial agents for their broad antimicrobial spectrum, ultrasmall particle size, low cytotoxicity and highly efficient antimicrobial effects.

AgNCs, consisting of dozens of atoms, have a diameter about 2 nm, which is closed to the Fermi wavelength (~0.5 nm for Ag). With such small sizes, the band structures of AgNCs are discontinuous and break down into discrete energy levels, and AgNCs thus endow unique physical and chemical properties (such as tunable fluorescence with

great photostability and quantized charging property), which are different from AgNPs with larger particle sizes.[71, 111] Conventionally, AgNCs are synthesized by reducing $Ag^+$ using chemical reductants or light irradiation. Since AgNCs tend to interact with each other and aggregate to reduce their surface energy, stabilizers or templates (e.g. DNA, polymers, *et. al.*) are critical for the stability of AgNCs.[96] AgNCs enabled various applications. For example, Wang *et. al.* reported the use of core-shell structured nanoparticles with hydrophilic surfaces and hydrophobic cores as templates to synthesize AgNCs, in which the templates greatly enhanced the stability and fluorescence intensity of AgNCs.[95] Previously, AgNCs have been extensively investigated for applications of biosensing,[112] bioimaging,[113] and disease diagnosis;[114] however, the exploration of the antimicrobial application of AgNCs, though highly promising, has been limited, especially for food packaging applications. Compared to AgNPs larger than 10 nm, the ultrasmall size of AgNCs impart unique advantages such as large surface to volume ratio, high local surface Ag concentration, and high mobility. These advantages enhance the antimicrobial potency of AgNCs, enabling the achievement of superior antimicrobial capacity using much smaller amounts of AgNCs than is possible with AgNPs.[29,115,116] However, the antimicrobial activity of AgNCs remains to be systematically studied and compared with AgNPs and $AgNO_3$ solution.

Zein, a group of prolamins from corn, is a Generally Recognized As Safe (GRAS) food-grade ingredient.[117] Zein films have low water vapor permeability compared to many other bio-based films, because three quarters of the amino acid residues in zein are

hydrophobic.[118] Zein films have previously been developed as antimicrobial food packaging materials by incorporating antimicrobial lysozyme and thymol.[118] Compared with these biological based antimicrobials, zein films embedded with inorganic and highly potent AgNCs may offer unique advantages such as high efficacy and low volatility.

In this work, we aim to develop a novel antimicrobial coating material for food packaging. We optimized the synthesis of ultrasmall AgNCs in water using poly methacrylic acid (PMAA) as a stabilizer and characterized the AgNC-embedded zein films. Further, we systematically evaluated the antimicrobial activities and cytotoxicity of the resulting AgNC-embedded zein films by comparing them with zein films that were incorporated with $AgNO_3$ and AgNPs. The developed films showed potent antimicrobial activity and low toxicity to human cells. We envision that, by a simple dry-cast process, this material can be coated and combined with other packaging materials to further enhance antimicrobial potency and broaden the spectra of antimicrobial activity.

## *2.3 Material and Methods*

### 2.3.1 Materials

Ag nitrate was purchased from VWR International, Radnor, Pennsylvinia, USA. PMAA was obtained from Polysciences, Inc, Warrington, USA. AgNPs of 10 nm and 60 nm in diameter were purchased from Alfa Aesar (Haverhill, Massachusetts, USA). Zein was purchased from MP Biomedicals (Santa Ana, California, USA), and Ethyl Alcohol (ACS grade) was purchased from Pharmco-Aaper (Shelbyville, Kentuchy, USA).

### 2.3.2 Synthesis of fluorescent AgNCs by UVA lamp light

AgNCs were synthesized using modifications to a previously reported method.24 Briefly, a mixture of $AgNO_3$ and PMAA in deionized water was reduced by ultraviolet-A irradiation at wavelengths ranging from 315 to 400nm (UVA Lamp, Sankyo Denki, Japan). To optimize the synthesis conditions to achieve maximum florescence emission in minimum time, $AgNO_3$ and PMAA were dissolved in deionized water with concentration ratios varying from 2:1 to 20:1, followed by exposure to UVA for a series of times. The fluorescence emission of the reducing product was measured every 15 min with excitation at 512 nm for a maximum of 7.5-h UVA exposure.

Synthesis of AgNCs for the Ag release profile, toxicity, and antimicrobial studies, proceeded by reducing 60 mg/mL AgNO3 and 10 mg/mL PMAA with 60 min UVA

exposure, according to the optimal conditions determined in preliminary experiments. After 60 min exposure to UVA light, the solution acquired a pink color, which indicated the formation of AgNCs. The synthesized AgNC solution was then filtered with dialysis bags (MWCO 1KDa, Spectrum Laboratories, INC, US) to remove unreacted Ag ions, and stored in a refrigerator for future use. The yield of AgNCs was 10%, which was estimated from Inductively Coupled Plasma (ICP) measurements (ICPE-9000, Shimadzu, Kanagawa, Japan). Briefly, 1 mL stock solution of AgNCs was diluted 10 times with 5% (v/v) aqueous nitrous acid, and $AgNO_3$ are dissolved by 5% (v/v) aqueous nitrous acid at concentrations of 0.01, 0.1, 1, 10, 100 mg/mL with final volume of 10 mL. $AgNO_3$ solution samples were first tested by ICP to generate the standard curve, and then AgNCs samples was tested.

Synthesis of AgNC-embedded zein film was achieved by dissolving 100 mg zein protein in 1 mL of 70% (v/v) aqueous ethanol, and adding AgNC solution to the ethanol in a 3:7 (v/v) ratio. The zein solution and AgNCs in ethanol were later mixed with ratio of 1:1 (v/v). The mixture was later coated on disk paper or agar for further experiments through a dry-cast process.

### 2.3.3 Synthesis of AgNCs by sunlight and lamp light.

AgNCs were synthesized by reducing $AgNO_3$ under UVA radiation with a stabilizer PMAA. Briefly, 60 mg/mL $AgNO_3$ and 10 mg/mL PMAA were mixed and exposed to sunlight for 40 h or to lamp light for 30 h.

### 2.3.4 Synthesis of AgNPs.

AgNPs with diameter of 550 nm (AgNP550) were synthesized by reducing $AgNO_3$ with sodium borohydride. To be specific, 0.01mM $NaBH_4$ were dropped into 0.25mM $AgNO_3$ followed by vigorous shake. The mixture was then heated up to boiling temperature for 1h to remove unreacted $NaBH_4$. The synthesized AgNP550 were then dialyzed and refrigerated.

### 2.3.5 Characterization of AgNCs

After synthesis, AgNCs were characterized for their fluorescence, morphology, and surface charges. The fluorescence of AgNCs was measured using a microplate reader (SpectraMax, Molecular Devices, LLC, California, USA) with the emission range of 560-700 nm with excitation at 510 nm. The morphology of AgNCs was observed via scanning transmission electron microscopy (STEM). Samples were prepared for microscopy as follows. The purified stock solution of AgNCs was diluted 50 times with deionized water, and 5 $\mu$L of the diluted solution was dried on a microscopy grid (400 mesh ultrathin carbon film on lacey carbon support film, Ted Pella, INC, US) under the hood for 1 h. The sample AgNC and zein mixture was prepared for STEM by mixing 0.5$\mu$L AgNCs stock solution with 4.5 □L 0.01% zein in 70% ethanol, and then dropping 5 $\mu$L of the mixture on a carbon grid and drying under the hood for 1 h. These grids were later imaged using STEM (JEM 2100 FEG TEM/STEM, JEOL, Tokyo, Japan), and the size distribution was measured and

analyzed using the software Image J (National Institutes of Health, USA). Zeta potential was measured on a Zetasizer Nano (Malvern Instruments Ltd, Worcestershire, UK), using 1 mL each of AgNC solution, AgNC and zein mixture, AgNP10 and zein mixture, AgNP60 and zein mixture, as well as zein mixture in 70% ethanol.

### 2.3.6 Assessment of antimicrobial activity

The agar diffusion test and growth curve measurement were applied to a pathogenic strain of E. Coli O157:H7 to examine the antimicrobial efficacy of different Ag composites.

#### 2.3.6.1 Agar diffusion assay

For the agar diffusion assay, AgNCs, $AgNO_3$, AgNP10, and AgNP60 were dissolved in deionized water (DI water) with concentrations of 2 mg/mL and 0.4 mg/mL Ag equivalents, respectively. Then, 5 $\mu$L of each sample was spread and allowed to dry on diffusion disks (VWR International, Radnor, Pennsylvinia, USA) with diameters of 7 mm, thus, each disk contained 10 $\mu$g or 2 $\mu$g Ag equivalents. The diffusion disks were further dried under the hood, followed by loading an additional 5 $\mu$L of 10% zein solution and drying. One colony of E. Coli O157:H7 was dispersed and incubated in tryptic soy broth (TSB, VWR International, Radnor, Pennsylvinia, USA) at 37 °C for 16 h, and 100 $\mu$L of bacteria suspension (absorbance at OD600: 1) was spread evenly on tryptic soy agar (25mL tryptic soy agar per dish, Sigma-Aldrich, St. Louis, Missouri,

USA). The dried disks were then placed on the plates. Diffusion disks loaded with 5 $\mu$L TSB, 5 $\mu$L 10% zein solution, and 3.4 $\mu$L 0.05% PMAA solution (equivalent to the amount of PMAA in AgNCs with 10 $\mu$g Ag equivalents) were used in the control group. After incubating the plates at 37 °C for 24 h or 72 h, the width of the inhibition rings surrounding the disks were measured with a ruler.[119]

#### 2.3.6.2 Growth curve measurement

The antimicrobial activity of bare AgNCs, $AgNO_3$, AgNP10 and AgNP60 (without zein coating) was also studied by measuring the growth curves of E. Coli O157:H7 exposed to the different treatments. E. Coli were cultured in TSB for 16 h and diluted with TSB to an optical density (OD) at 600 nm of 0.05. The diluted bacteria were then incubated with AgNCs, $AgNO_3$, AgNP10, and AgNP60 with final concentrations of 1 $\mu$g/mL, 5 $\mu$g/mL, or 10 $\mu$g/mL Ag equivalents, respectively, for 9 h in a 37 °C incubator. The absorbance or OD of each sample at 600 nm was then measured every half hour with a UV/Vis Spectrophotometer (Beckman Coulter, Brea, CA, USA).

#### 2.3.6.3 MIC determination

To test the MIC of AgNCs, AgNO3, AgNP10 and AgNP60. Mueller-Hinton agar were coated by AgNCs, $AgNO_3$, AgNP10 and AgNP60 embedded films with Ag concentrations of 0.525, 1.05, 2.1, 4.2, 8.4, 16.8, 33.6, 67.2, 134.4, 168, 201.6, and 235.2 $\mu$g/cm2. Agars coated with plain zein film were used as control. Then, 100 $\mu$L bacteria suspension (OD600 = 1.0) were evenly spread on the pretreated agar and

incubated at 37 °C for 24 h. The lowest Ag concentrations that resulted in no visible growth of microorganisms were determined as the MIC.

### 2.3.7 Cell viability

The cytotoxicity test of AgNCs, AgNP10, AgNP60, and $AgNO_3$ was performed on human cell line HCT116 (ATCC, Manassas, VA). Briefly, the cells were seeded on 96-well plates and incubated overnight for adhesion, followed by adding 0.2, 0.4, 0.8, 1.6, 3.2, 6.4, 12.8, 25.6, 51.2, or 102.4 μg/mL of AgNCs, AgNP10, AgNP60, or $AgNO_3$ dissolved in Dulbecco's Modified Eagle Medium (Thermo Fisher Scientific, Waltham, Massachusetts, USA), respectively. After incubating for 48 h, the cell viability was measured by the cell counting kit-8 (Dojindo Molecular Technologies, Maryland, USA). Specifically, 10 μL of cck-8 solution was added to each well of cells and incubated for around 2 h. The absorbance at 450nm was recorded by a plater reader (SpectraMax, Molecular Devices, Sunnyvale, California, USA), and cell viability was calculated according to the manufacturer's guidance. Results were analyzed in GraphPad Prism 7 (GraphPad Software, Inc., La Jolla, California, USA).

### 2.3.8 Release profile of Ag from zein film

AgNCs was synthesized by reducing 60 mg/mL $AgNO_3$ and 10 mg/mL PMAA with UVA light for 60 min, and then mixed with ethanol in ratio of 3:7 (v/v). Zein

protein was dissolved in 70% ethanol. Zein solution at concentration of 10% were then mixed with 100 μg/mL AgNCs, AgNP10, AgNP60, and $AgNO_3$. Later, 1 mL of each mixture were casted and dried into film. The casted films were then immersed in 20 mL water in dark for 3 days, and every half day 1 mL of surrounding solution was collected. The collected solution samples were diluted with 5% nitric acid and measured for Ag concentration by ICP (5000 ICP-OES, Agilent Technologies, Santa Clara, California, USA).

### 2.3.9 Statistics

The experimental results were analyzed using GraphPad Prism 7 (GraphPad Software, Inc., La Jolla, California, USA) with significance level $p < 0.05$. Two-way ANOVA and Tukey's multiple comparisons test were conducted for the agar diffusion test data. One-way ANOVA and Bonferroni post-test were conducted for the cell viability data.

## *2.4 Results and discussion*

### 2.4.1 Synthesis, optimization, and characterization of AgNCs

AgNCs were synthesized by reducing Ag ions via UVA irradiation with PMAA as a stabilizer. The effects of irradiation time, concentration of $AgNO_3$ and PMAA, ratio of $AgNO_3$ to PMAA, and light sources (e. g. UVA lamp, linear light bulb, and sun light) on the formation and fluorescence intensity of AgNCs were systematically

investigated. The fluorescence emission results for different UVA irradiation times are shown in Figure 2-2A. The fluorescence intensity increased rapidly at the beginning of the reduction due to continuous formation of AgNCs, and after 60 min of UVA exposure, the fluorescence intensity reached a plateau, which indicated the saturation of the AgNC formation. Further UVA irradiation did not cause a decrease in fluorescence, which verified the great photostability of the AgNCs. The wavelength of maximum emission underwent a red shift at the beginning of the AgNC formation and then became stable, which corresponded to the formation and saturation of AgNCs.

The synthesis of AgNCs was further acheived using other light sources, such as 18 Watt linear light bulb and sunlight. The results indicated that the light bulb and sunlight could also reduce the Ag+ and form AgNCs, but they were less effective than UVA irradiation (Figure 2-1).

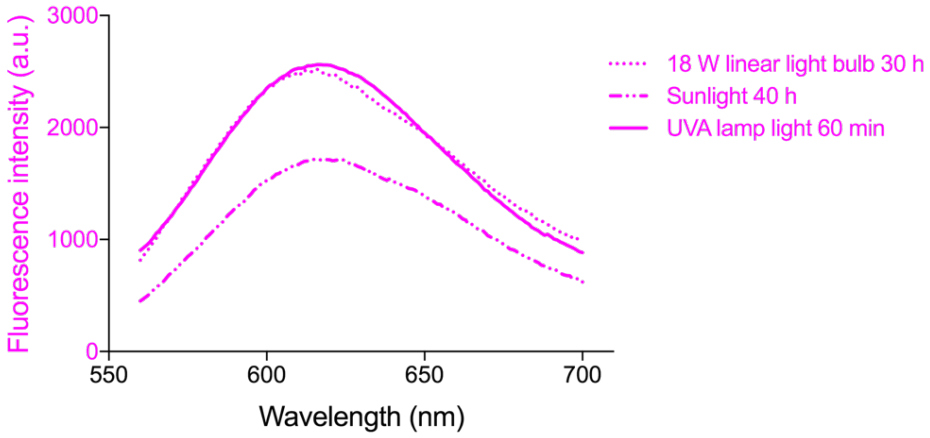


**Figure 2-1.** AgNCs synthesized by 40 h sunlight, 30 h linear light bulb light and 60 min UVA lamp light.

PMAA plays a critical role in the synthesis of AgNCs. It carried carboxylic acid groups that are capable to coordinate with Ag+, and the hydrophobic regions in PMAA facilitated the formation of AgNCs. Further, the spatial structure prevented the aggregation of AgNCs.17, 24 Thus, different concentration ratios of $AgNO_3$ to PMAA ($AgNO_3$-to-PMAA ratios) were then tested with 60 min of UVA irradiation to optimize the conditions for synthesis of AgNCs. Holding PMAA at 10 mg/ml and increasing $AgNO_3$-to-PMAA ratios initially enhanced the fluorescence intensity of AgNCs. However, a plateau was reached between ratios of 8:1 to 12:1, followed by a slight decrease (Figure 2-2B). This phenomenon indicated the non-linear relationship between the $AgNO_3$ to PMAA ratio and the fluorescence intensity of AgNCs. A similar trend was also observed when the PMAA concentration was fixed at 40 mg/mL, fluorescence intensity of AgNCs increased and reached a maximum at 240 mg/mL , followed by slight decrease (Figure 2-3).

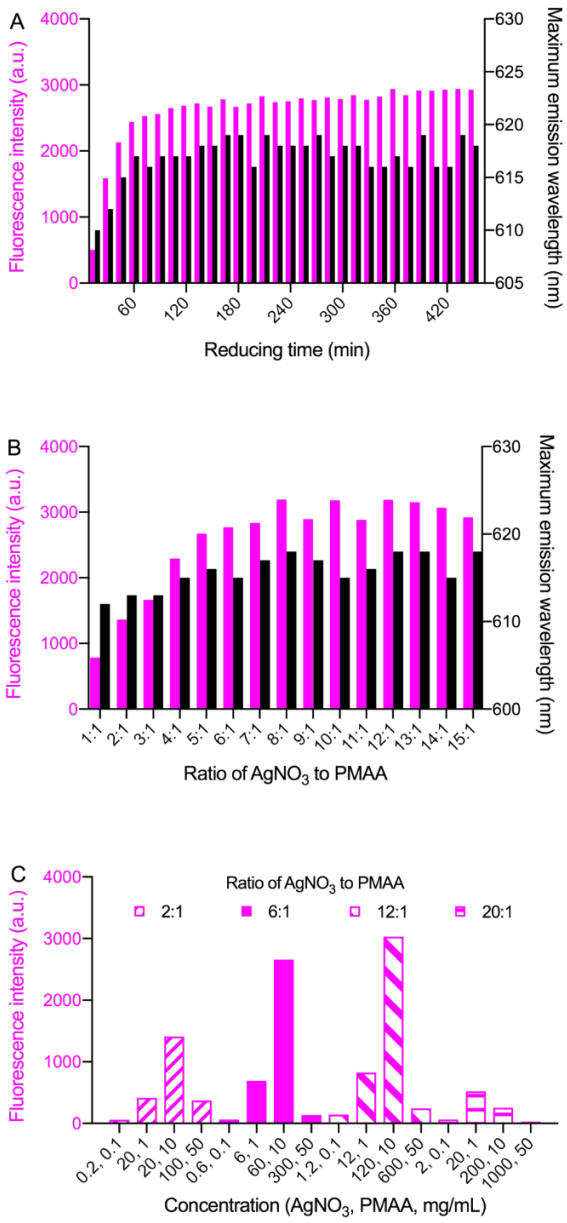


**Figure 2-2.** Optimization of AgNC synthesis by varying UVA irradiation time, the $AgNO_3$-to-PMAA ratios, and absolute concentrations of $AgNO_3$ and PMAA. A) Fluorescence intensity and the maximum emission wavelength of AgNCs formed with different UVA irradiation times. B) Fluorescence intensity and maximum emission wavelength of AgNCs that were synthesized using $AgNO_3$-to-PMAA ratios ranging from 1:1 to 15:1 ($AgNO_3$: PMAA). C) Fluorescence intensities of AgNCs that were synthesized with different absolute concentrations of $AgNO_3$ and PMAA at $AgNO_3$-to-PMAA ratios of 2:1, 6:1, 12:1, and 20:1 ($AgNO_3$ : PMAA).

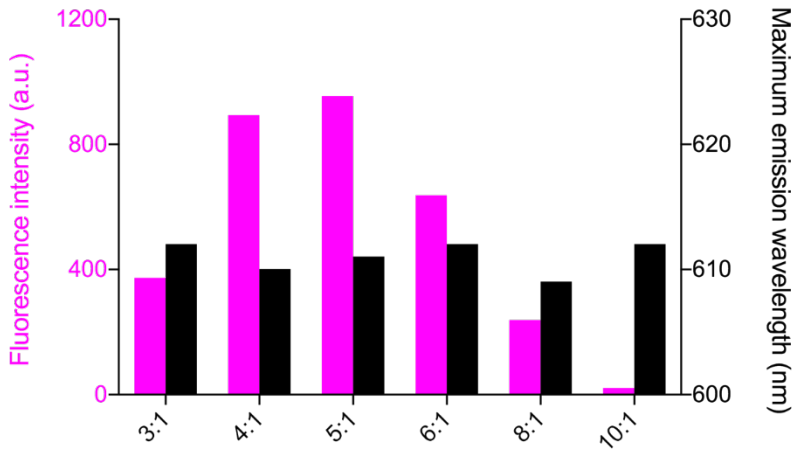


**Figure 2-3.** Fluorescence intensity of AgNCs synthesized with different concentration ratios of $AgNO_3$ to PMAA with fixed PMAA concentration of 40 mg/mL.

In addition to the changes in $AgNO_3$-to-PMAA ratios, changes of absolute concentrations of $AgNO_3$ and PMAA were also found to affect the fluorescence properties of AgNCs. Thus, AgNCs were synthesized using a series of absolute concentrations of $AgNO_3$and PMAA under $AgNO_3$-to-PMAA ratios of 2:1, 6:1, 12:1, and 20:1 (Figure 2-2C). Generally, with the same $AgNO_3$-to-PMAA ratio, higher concentration of these substrates produced larger amount of AgNCs, resulting in higher fluorescence intensity. However, when the Ag and PMAA concentration exceeded a threshold, the fluorescence intensity decreased significantly, indicating that very high $AgNO_3$ concentration may inhibit the formation of AgNCs. The concentrations of $AgNO_3$ for optimal formation of AgNCs varied depending on the different $AgNO_3$-to-PMAA ratios. Furthermore, AgNCs formed by the series of concentrations of $AgNO_3$

and PMAA: 12, 1; 120, 10; 20, 1; and 200, 10 ($AgNO_3$, PMAA; mg/mL) developed a small amount of pink floccule likely containing AgNCs and PMAA, which was presumably caused by the high ratio of, AgNCs, $AgNO_3$, AgNP10, and AgNP60 to PMAA, as well as the gel formation ability of PMAA. At very high concentrations of $AgNO_3$ and PMAA, i.e. 600, 50 and 1000, 50 ($AgNO_3$, PMAA; mg/mL), the $AgNO_3$, was supersaturated and not well dissolved; no dramatic fluorescence emission was observed.

Based on the results of the synthesis method optimization, we determined to synthesize AgNCs by reducing 60 mg/mL AgNO3 and 10 mg/mL PMAA with 60 min UVA exposure for further study.

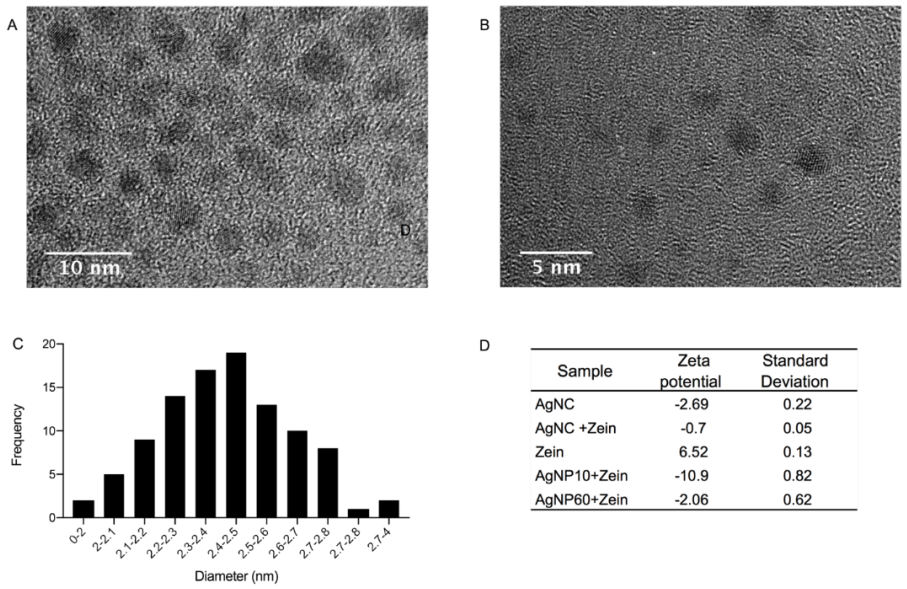


| Sample | Zeta potential | Standard Deviation |
|---|---|---|
| AgNC | -2.69 | 0.22 |
| AgNC +Zein | -0.7 | 0.05 |
| Zein | 6.52 | 0.13 |
| AgNP10+Zein | -10.9 | 0.82 |
| AgNP60+Zein | -2.06 | 0.62 |

**Figure 2-4.** Characterization of AgNCs. A) STEM images of AgNCs and B) AgNCs in 0.1% zein and 70% ethanol solution. C) Size distribution of AgNCs ($n$ = 100). D) Zeta potential of AgNCs, zein, and mixtures of zein and AgNCs, zein and AgNP10, and zein and AgNP60.

The characterization of AgNCs was performed by observing their morphology and surface charge. Under scanning transmission electron microscopy (STEM), AgNCs showed a narrow size distribution around 2.2-2.4 nm (Figures 2-4A, C) and were well dispersed (Figure 2-5A). After mixing AgNCs with zein in 70% ethanol, no significant changes in the size and dispersion of AgNCs were observed, which indicated that AgNCs were highly stable in the zein-containing 70% ethanol solution (Figures 4B, 5B). The zeta potential of AgNCs was -2.69 mV and -0.70 mV before and after mixing with zein solution, respectively. The mixture of zein and AgNP10, AgNP60 in 70% ethanol presented zeta potentials of -10.9 mV and -2.06 mV, respectively (Figure 2-4D).

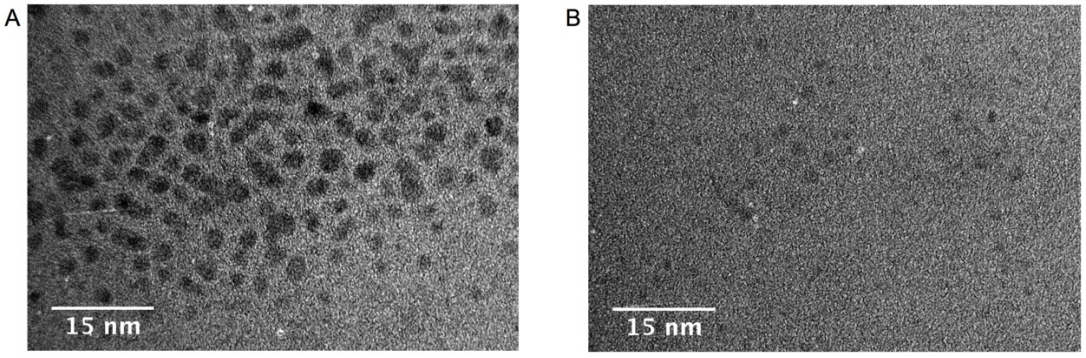


**Figure 2-5.** STEM images of AgNCs before (A) and after (B) mixing with zein.

### 2.4.2 Potent antimicrobial activity exhibited by AgNCs-embedded zein film

The antimicrobial activity of AgNCs–embedded zein film was tested on pathogenic *E. Coli O157:H7* using both an agar diffusion test and a growth curve measurement.

$AgNO_3$, AgNP10, and AgNP60 were included as comparisons (Figure 2-6). In the agar diffusion test, Ag composites of each kind (Ag equivalents: 2 $\mu$g and 10 $\mu$g, respectively) and zein (2.5 mg) were loaded on diffusion disks to test their antimicrobial activities. Diffusion disks loaded with 5 $\mu$L TSB, 1.7 $\mu$g PMAA, and 2.5 mg zein were used as control.

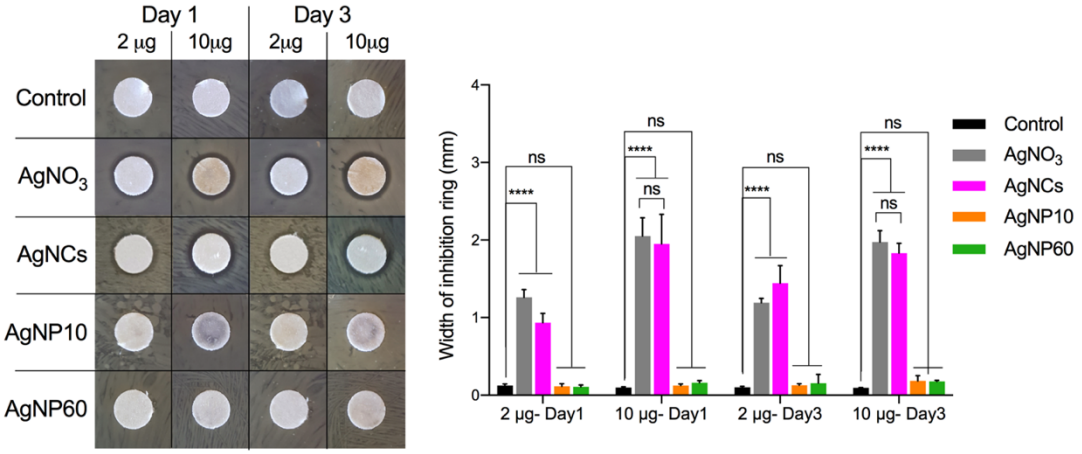


**Figure 2-6.** Agar diffusion test of different Ag nanocomposite-embedded zein films. Left: Inhibition zone of *E. coli* O157:H7 treated by $AgNO_3$, AgNCs, AgNP10, and AgNP60 with 2 µg and 10 µg Ag equivalents, respectively, for 1 and 3 days. Right: the width of inhibition zone. (****$p < 0.0001$, $ns > 0.9999$, $n = 3$)

After 1-day and 3-day treatments, no inhibition rings were observed in the control group, and some bacterial colonies were present on the agar plate on day 3. After treating bacteria with 2 µg Ag equivalents of AgNCs or $AgNO_3$ for 1 day, clear inhibition zones of 0.93 mm and 1.26 mm widths were observed around the AgNC and $AgNO_3$ saturated disks, respectively. When bacteria were treated with 10 µg Ag equivalents of AgNCs and $AgNO_3$ greater antimicrobial effects were observed, as indicated by inhibition zones of 1.95 mm and 2.05 mm, respectively. There was no

significant difference between the width of inhibition rings after 1-day or 3-day treatments of $AgNO_3$ and AgNCs with 10 μg Ag equivalents, which verified the comparable antimicrobial activities of $AgNO_3$ and AgNCs. Moreover, as expected, the inhibition activities of both $AgNO_3$ and AgNCs were concentration-dependent. However, no clear inhibition rings were observed in bacteria treated by AgNP10 or AgNP60 of 2 μg or 10 μg Ag equivalents, and there was no significant difference in inhibition zones between AgNP10 or AgNP60 treated groups and the control group.

These results can be explained by both the high surface to volume ratio and high mobility of AgNCs relative to those of AgNPs. The higher surface to volume ratio of AgNCs results in greater surface contact with bacteria and consequently higher antimicrobial activity. The greater mobility of Ag nanocomposites is another key factor that contributes to improved antimicrobial activity. Specifically, the antimicrobial activity can be influenced by the release rate of Ag from different Ag nanocomposites that were embedded in zein films. Thus we studied the release rate of Ag from these films by submerging different Ag nanocomposite- embedded zein films in water and testing Ag concentrations in the surrounding water every half day. We observed that AgNP10 and AgNP60 embedded zein films released Ag at the slowest rate, whereas both AgNC-embedded zein film and $AgNO_3$ steadily released Ag at a much faster rate (Figure 2-7). This result corresponded to the weak antimicrobial activity of AgNP10 and AgNP60 and the potent antimicrobial activity of AgNCs and $AgNO_3$. To determine whether zein films inhibited the mobility of AgNP10 and AgNP60, we performed agar

diffusion tests for bare AgNCs, AgNP10, AgNP60, $AgNO_3$ (no zein coating) at 10 μg Ag equivalents. The antimicrobial efficacies were similar to those with zein coatings, and no clear antimicrobial activity was observed for AgNP10 or AgNP60 (Data not shown). We also examined the agar diffusion test for large AgNPs with diameters of 550 nm (AgNP550) (Figure 2-8). Again, no clear bacteria inhibition zone was observed with 50 $\mu$g AgNP550 treated for 1 day.

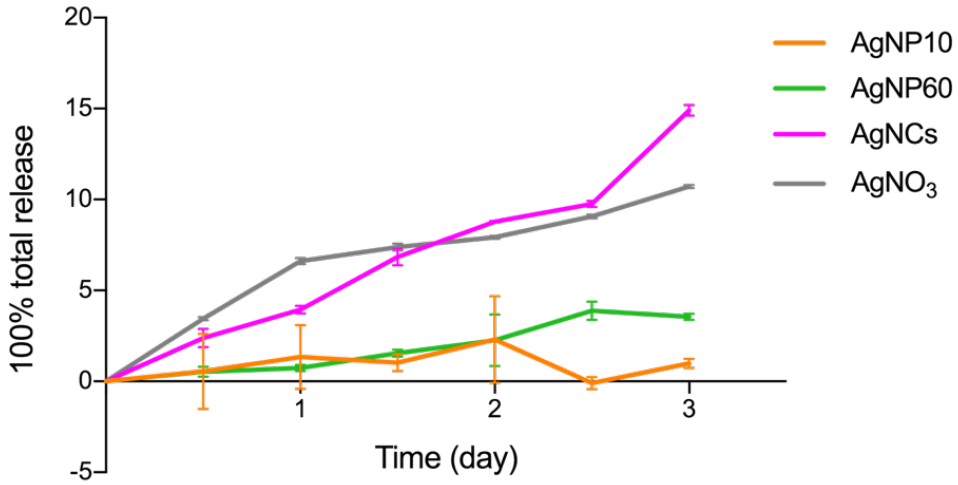


**Figure 2-7.** Releasing profile of AgNCs, $AgNO_3$, AgNP10, and AgNP50 embedded zein films submerged in water.

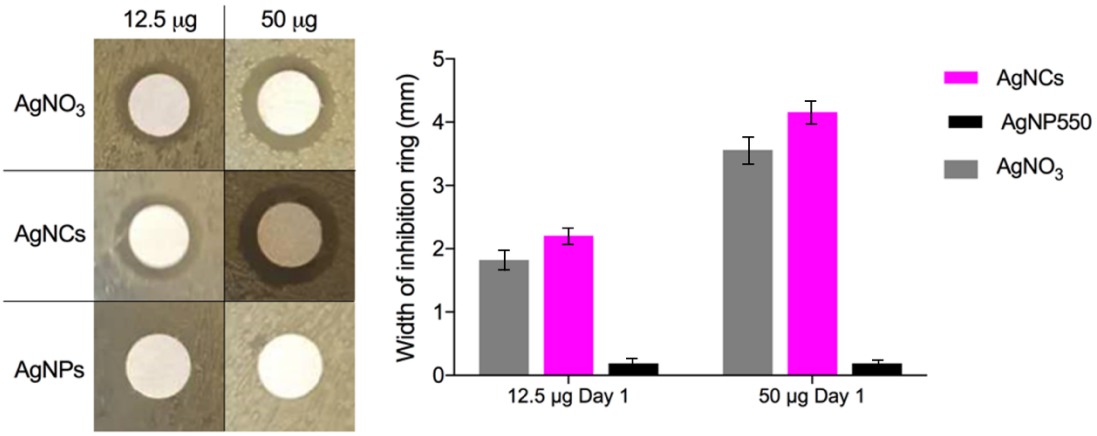


**Figure 2-8.** Inhibition ring of zein film embedding AgNCs, $AgNO_3$, and AgNP550. Left: Inhibition zone of E. coli treated by 12.5 μg and 50 μg AgNCs, $AgNO_3$, and AgNP550 for 1 day. Right: the width of inhibition rings.

Figure 2-9 shows the effect of UVA irradiation time (40 minutes; AgNC40 and 100 minutes; AgNC100) during AgNC synthesis on antimicrobial activity assessed by agar diffusion tests at 2 μg and 10 μg Ag equivalents. After 1-day bacterial treatment, AgNC100 (2 μg Ag equivalents) showed clear inhibition zone of 1.98 mm width, which was comparable to that observed for AgNCs with 10 μg Ag equivalents synthesized using 60 minutes UVA irradiation (1.95 mm). The widest inhibition zone, measuring 2.62 mm was observed for AgNC40 with 10 μg Ag equivalents, which was significantly larger than that for AgNC100 (10 μg Ag equivalents). However, no significant difference was observed between the inhibition rings treated by AgNC40 and AgNC100 with 10 μg Ag equivalents after 5 days (Figure 2-10). Nor was there any significant difference observed between the inhibition rings for AgNC40 and

AgNC100 at 2 µg Ag equivalents for either 1-day or 5-day treatments. These results indicate that the reducing time is not an important factor contributing to the antimicrobial effect of AgNCs.

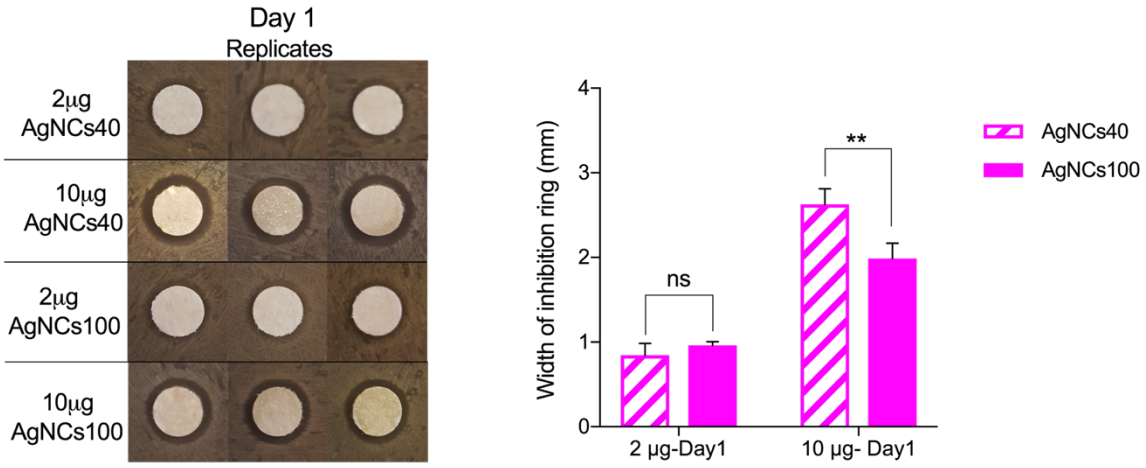


**Figure 2-9**. Agar diffusion test of zein films embedding AgNCs synthesized by 40 minutes (AgNC40) and 100 minutes (AgNC100) UVA irradiation. Left: Inhibition zone of *E. coli* O157:H7 treated with AgNC40 and AgNC100 at 2 µg and 10 µg Ag equivalents, respectively. Right: the width of inhibition rings (**$p < 0.01$, ns>0.9999, $n$=3).

The growth curves showing the absorbance at 600 nm for *E. coli* O157:H7 cultures treated with bare AgNCs, $AgNO_3$, AgNP10 and AgNP60 at 1, 5, and 10 µg/mL Ag equivalents, respectively are shown in Figure 2-11. At concentrations of 1 µg/mL and 5 µg/mL Ag equivalents, AgNCs exhibited comparable antimicrobial activity to $AgNO_3$. At the concentration of 10 µg/mL Ag equivalent, a longer lag phase (5.5 h) was observed for $AgNO_3$-treated *E. coli* than for AgNCs-treated *E. coli* (4 h). However,

after 8h growth, both $AgNO_3$-treated and AgNCs-treated *E. coli* reached stationary phase, and the maximum cell densities of two treatments were comparable. In addition, longer generation time and lower maximum cell density were observed for *E. coli* O157:H7 treated by $AgNO_3$ and AgNCs at 5 μg/mL and 10 μg/mL Ag than for *E. coli* cells treated with AgNP10 and AgNP60. While $AgNO_3$ and AgNCs showed concentration-dependent antimicrobial activity, AgNP10 and AgNP60 showed no antimicrobial efficacy even at a concentration as high as 10 μg/mL Ag. This result was consistent with the agar diffusion test results and release profiles of zein films embedding different Ag nanocomposites (Figure 2-12).

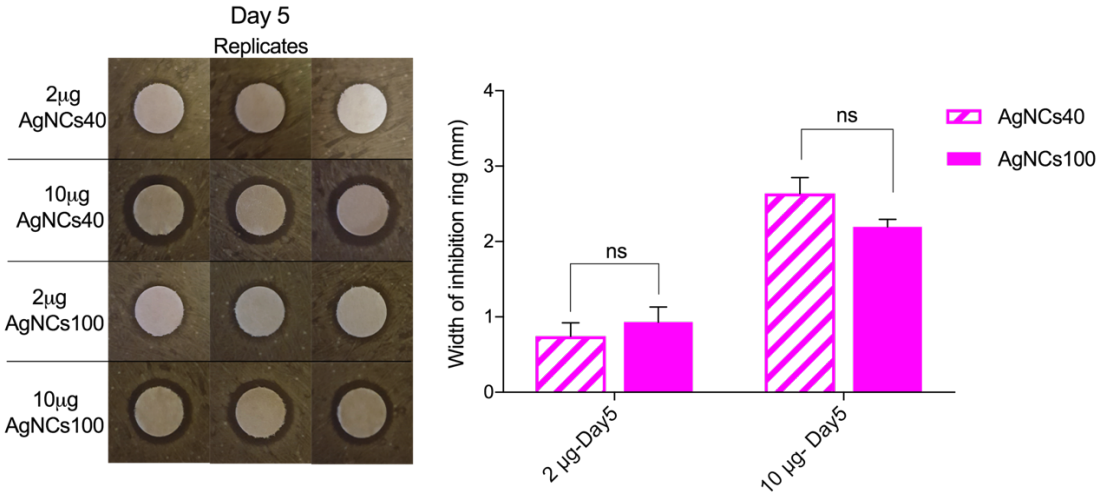


**Figure 2-10.** Inhibition ring of zein film embedding Ag nanolcusters synthesized by 40 minutes (AgNCs40) and 100 minutes (AgNCs100) UVA radiation. Left: Inhibition zone of E. coli treated by 2 μg and 10 μg AgNCs40 and AgNCs100 for 5 days. Right: the width of inhibition rings (ns>0.9999, $n$=3).

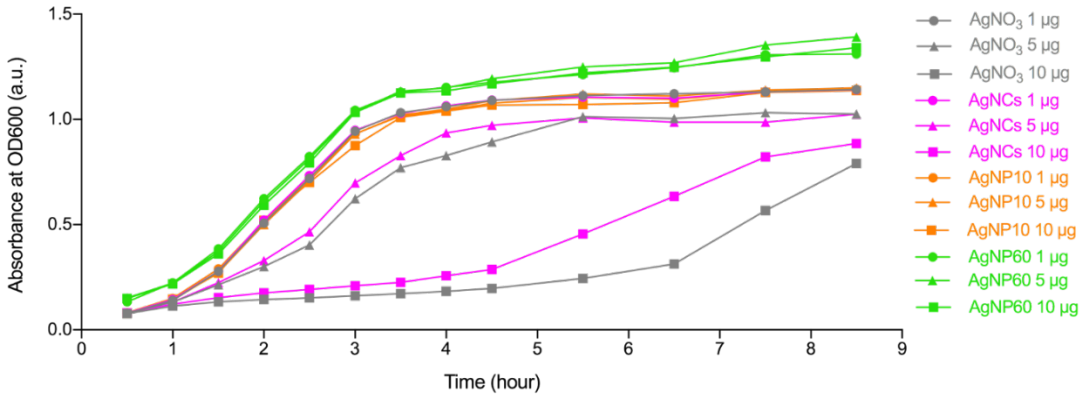


**Figure 2-11**. Growth curve of *E. coli* O157:H7 treated with different Ag nanocomposites. E coli were incubated in tryptic soy broth with $AgNO_3$ (gray), AgNCs (pink), AgNP10 (orange), and AgNP60 (green) at concentrations of 1 (•), 5 (▲), and 10 (■)µg/mL Ag equivalents, respectively.

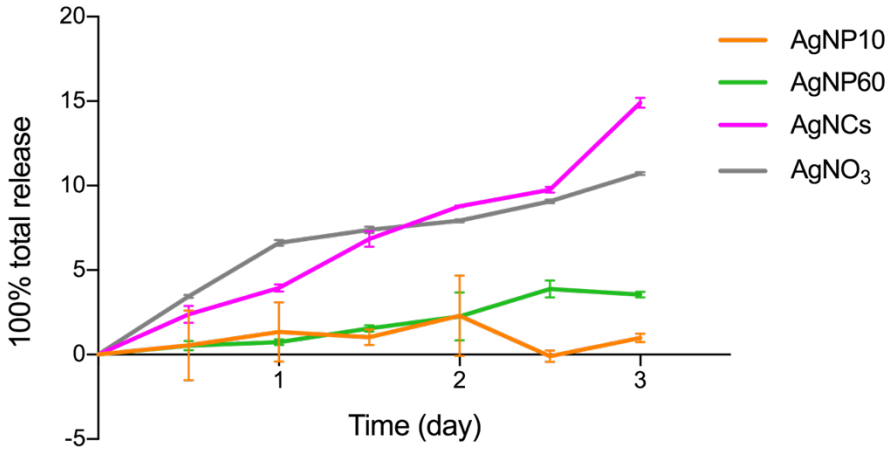


**Figure 2-12**. Releasing profile of AgNCs, $AgNO_3$, AgNP10, and AgNP50 embedded zein films submerged in water.

Moreover, to mimic the actual antimicrobial performance of this coating, different Ag nanocomposites embedded zein films were coated on the nutrient agar, followed by inoculating bacteria to test the MIC. The MICs of Ag for AgNCs, AgNO3, AgNP10,

and AgNP60 were 1.05, 0.525, 134.4, and 201.6 ug/cm$^2$, respectively. In consistence with the previous assay, these results further supported our findings on the antimicrobial efficacies of these Ag nanocomposites.

### 2.4.3 Low cytotoxicity of AgNCs to human cells

The viability of human colon cancer cells of cell line HCT116 after treatment with different Ag nanocomposites for 48 h at 37 °C is shown in Figure 2-13. The results of the cytotoxicity study indicate that AgNCs are significantly less cytotoxic than $AgNO_3$. At a Ag concentration of 10 μg/mL, AgNC treated cells showed 80% viability, whereas the survival rate for $AgNO_3$ treated cells was only 20%. The $IC_{50}$ for AgNCs was 34.68 μg/mL, in contrast to 9.14 μg/mL for $AgNO_3$. AgNP10 and AgNP60 showed less toxicity than both AgNCs and $AgNO_3$, and this was possibly caused by same reasons as their lower antimicrobial efficacy; namely, the lower mobility, slower cell membrane penetration, and inefficient Ag release of Ag nanoparticles.

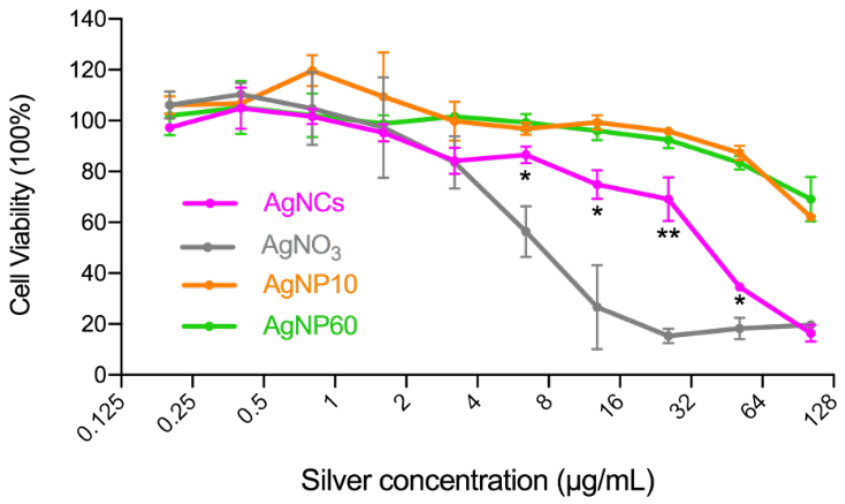


**Figure 2-13**. Cell viability of HCT116 human colon cancer cells treated with AgNCs (pink), $AgNO_3$ (grey), AgNP10 (orange) and AgNP60 (green). Asterisks represent the significant differences between the cell viabilites for AgNC and $AgNO_3$ treatments at the same Ag concentration. (**$p < 0.01$, *$p < 0.05$, $n$=3)

## *2.5 Conclusion*

In summary, we developed a novel antimicrobial coating material by embedding antimicrobial AgNCs into zein films. The fluorescence of AgNCs depended on the UVA irradiation time, light sources, concentration ratio of $AgNO_3$ to PMAA, and absolute concentrations of $AgNO_3$ and PMAA. The antimicrobial efficacy and toxicity of AgNCs were systematically evaluated and compared with those of $AgNO_3$, AgNP10, and AgNP60. AgNCs presented comparable dose-dependent antimicrobial efficacy to $AgNO_3$, but with significantly lower toxicity towards human cells than $AgNO_3$. Further, AgNCs presented much greater antimicrobial capacity than AgNP10 and AgNP60, which indicates that the administration dose of AgNCs for antimicrobial

applications could be dramatically reduced compared to that of AgNPs. Overall, the study indicated that the low toxicity, low volatilization, and ultrasmall size of AgNCs enhanced their antimicrobial properties and that AgNC-embedded zein film is promising antimicrobial coating material for food packaging.

# Chapter 3: Preparation and Characterization of Alkynyl Ag Modified Chitosan

## *3.1 Abstract*

CS was modified by substituting alkynyl Ag on CS through chemical reactions to form a potential antimicrobial coating material. The synthesis of Ag-CS was carefully investigated and Ag-CS with three alkynyl Ag substitution degrees were prepared . All prepared Ag-CS were characterized for their chemical composition, morphology, and physical properties. The Ag-CS also demonstrated a controlled release of Ag for over 5 days, whereas AgOAc infused CS released over 90% Ag within 4 h. The Ag-CS were also proved to induce ROS generations in human cancer cells, and presented comparable cytotoxicity as AgOAc.

## *3.2 Introduction*

The growth of spoilage and pathogenic microorganisms on food products results in significant economic loss and public health consequences. Smart packages with controlled release of antimicrobial agents present a great opportunity to inhibit microbial growth and thus improve food product safety and shelf life.[120] By releasing antimicrobial agents to either the food matrix or the surrounding spaces, the growth of microorganisms can be inhibited or eliminated (Mousavi Khaneghah et al., 2018).

However, the sustained release manner of antimicrobial agents is crucial to provide an effective inhibition and maintain food quality and safety over storage time. [2]

Ag (Ag) has long been used as an effective antimicrobial agent in medical areas including wound infection control and healing.[121] It is known for its broad-spectrum antimicrobial activity with great efficacy against many different strains of bacteria, fungi, and viruses with little risk of inducing resistance.[26,122] Although many Ag-based nanostructures have been developed over the past decade,[83,88] there remain unsolved challenges of Ag-based antimicrobial packaging materials or coating materials: 1) uncontrolled release of Ag does not necessarily ensure a long-term antimicrobial efficacy, 2) high application levels of Ag might cause Ag diffuse into food matrices and may be toxic to human,[59,65,67] and 3) after usage, Ag cores might become environmental hazards.[60,108] To meet these challenges, major strategies have been undertaken, including 1) development of coreless Ag composites, 2) decreased application levels to reduce potential toxicity, and 3) controlled release of Ag to minimize the diffusion of Ag into food matrices.

Alkynyl Ag is obtained by a reversible reaction between Ag acetate (AgOAc) and alkynes.[123] The Ag in alkynyl Ag is directly bonded to the alkynyl group, where Ag elements and Ag ions can later be released through a reversible reaction.[99] Meanwhile, the extremely mild and facile synthesis procedure of alkynyl Ag makes it possible to be incorporated into other biopolymers through chemical reactions.

CS is a polysaccharide prepared by the deacetylation of chitin. CS has been proved to be nontoxic, biodegradable, and biocompatible, and it has been widely used in the food industry as a food additive and film forming agent.[124] Studies have also shown that CS and its modified derivatives have some antibacterial and antifungal activity. CS with lower molecular weight showed better solubility and higher antimicrobial efficacy.[125] All of these properties suggest CS is a promising matrix material for construction of antimicrobial coatings.[126]

Here, we report for the first time an alkynyl Ag based antimicrobial coating material synthesized by grafting alkynyl Ag to CS. In this structure, Ag can be released through a reversible chemical reaction to inhibit microorganism growth and provides extended release of Ag for over 5 days, which assures its potential as an effective antimicrobial coating material for food packaging.

## *3.3 Material and Methods*

### 3.3.1 Materials

CS (molecular weight of 15,000 Da, with minimum 85% degree of deacetylation) was purchased from Polysciences, Inc. (Pennsylvania, USA). EDC (1-ethyl-3-(3-dimethylaminopropyl) carbodiimide hydrochloride), 4-Pentynoic acid, AgOAc, and trichloroacetic acid were purchased from Sigma Aldrich (Massachusetts, USA).

### 3.3.2 Synthesis of alkynyl group substituted CS (CC-CS) and alkynyl Ag substituted CS (Ag-CS)

Ag-CS was synthesized through two steps of chemical reactions (Scheme 1). CS (with a viscosity of 4.5 mP·S for 1mg/mL CS aqueous solution at pH 5) was first substituted by alkynyl groups to form CC-CS, then the alkynyl groups reacted with AgOAc to form alkynyl Ag on CS, which was defined as Ag-CS (Möhler et al., 2018). To synthesize CC-CS, 4-pentynoic acid and CS were dissolved in 15 mL DI water, and pH was adjusted to 5 by acetic acid. This solution was stirred for 1h at room temperature to fully dissolve CS, and EDC dissolved in 5mL DI water were slowly added into the solution, and stirred overnight. The synthesized CC-CS solution was then dialyzed in water for 24 h, followed by store at 4°C. In the synthesis of CC-CS, three substitution degrees were adopted by varying the reaction molar ratios of alkynyl group on 4-pentynoic acid to the amino group on CS, and the molar ratios of 1:10, 1:4, and 1:2 were used for low substituted CC-CS (L-CC-CS), medium substituted CC-CS (M-CC-CS), and high substituted CC-CS (H-CC-CS). Then, the amount of EDC was determined using a reaction molar ratio of EDC to 4-pentynoic acid of 1:1. The molar amount of amino group on CS was estimated by the following equation:

Molar concentration of amino group for 1% CS solution (mole / L)

= 10 g (mass of CS in 1 L 1% CS solution)/ 167.3 (estimated molecular weight of CS repeated monomer)

Specifically, the formulation used to synthesize 20 mL CC-CS are: L-CC-CS: 200mg CS, 13.8 mg 4-pentynoic acid, and 107.2 mg EDC; M-CC-CS: 200mg CS, 34.4 mg 4-pentynoic acid, and 268 mg EDC; H-CC-CS: 200mg CS, 68.8 mg 4-pentynoic acid, and 536 mg EDC.

To synthesize Ag-CS, CC-CS reacted with AgOAc to form L-Ag-CS, M-Ag-CS, and H-Ag-CS depending on which CC-CS was used. AgOAc were dissolved in DI water, and added into CC-CS solution dropwise. The mixture was stirred at room temperature overnight, followed by a dialysis in water. Synthesized Ag-CS was stored in the refrigerator for further experiments. Specifically, the formulation used to synthesize 100 mL Ag-CS solutions are: L-Ag-CS: 64.5 mg AgOAc and 44.3 mg L-CC-CS; M-Ag-CS: 64.5 mg AgOAc and 48 mg M-CC-CS; and H-Ag-CS: 64.5 mg AgOAc and 54.3 mg H-CC-CS.

### 3.3.3 Characterization of Ag-CS

#### 3.3.3.1 Fourier Transform Infrared (FTIR) and Nuclear Magnetic Resonance (NMR) spectra of CC-CS and Ag-CS

H-CC-CS and H-Ag-CS samples were prepared by freeze drying. FTIR spectra were then collected on a Thermo Nicolet NEXUS 670 FTIR (ThermoFisher Scientific, Massachusetts, USA).

The $^{1}H$ NMR spectra were recorded using a Bruker AV600 spectrometer (Bruker, Massachusetts, US). Stock solutions of L-Ag-CS, M-Ag-CS and H-Ag-CS with added DMSO were directly subjected to NMR test.

#### 3.3.3.2 The morphology and elements distribution of Ag-CS

Scanning electron microscopy (SEM) samples were prepared by adhering freeze drying all CS, CC-CS and Ag-CS solutions. In the control group, original CS powder is the original CS powder we purchased, and the sample of CS were prepared by following the synthesis steps of CC-CS without adding 4-Pentynoic acid (the reagent that offers alkynyl groups). Freeze dried samples were adhered directly to the carbon conductive tape, and coated by a layer of carbon with a thickness of around 50 nm. SEM images were collected on a field emission SEM (Hitachi SU-70, Hitachi Ltd., Japan) while operating at 2 kV. Element distribution of Ag in the Ag-CS was examined by an energy dispersive spectroscopy on the SEM. An FIB/SEM (GAIA FIB/SEM, Tescan, Czech Republic, operation at 2 kV) was adopted for M-Ag-CS and H-Ag-CS samples.

#### 3.3.3.3 The viscosity of CC-CS and Ag-CS

All modified CC-CS and Ag-CS were diluted to 1 mg/mL, and measured by a viscometer (Model KU-3, AMETEK Brookfield, Massachusetts, USA) at room temperature, and the viscosity was calculated according to the following equation provided by the manufacture.

$$\text{Viscosity in cP (mPa·S)} = \text{Dial reading } (\alpha i) \times \text{Factor}$$

Where

Factor = given values provided by the manufacture, variated based on the spindle and speed used during test

Dial reading = dial reading obtained during the test

### 3.3.3.4 Ag concentration determination in the Ag-CS

The content of Ag in each Ag-CS sample was determined by an Inductively Coupled Plasma (ICP) instrument (ICPE-9000, Shimadzu, Kanagawa, Japan). Briefly, 7 mL of synthesized Ag-CS solutions was diluted 2 times with 3% (v/v) aqueous nitrous acid and measured by ICP. The Ag concentration of Ag-CS samples was determined according to a standard curve.

### 3.3.3.5 Release profile of Ag from Ag-CS

Ten mL of Ag-CS with different substitution degrees at a concentration of 150 $\mu$g/mL Ag equivalents were retained in a dialysis bag with a molecular weight cut off at 10 KDa. The dialysis bags were immersed in 100 mL DI water and the surrounding solution was collected every 12 h for 5 days. The collected samples were then diluted 2 times with 3% (v/v) aqueous nitrous acid and measured for Ag concentration by ICP. The released amounts of Ag were converted to percentages of the initial Ag concentration.

### 3.3.3.6 Cytotoxicity of Ag-CS

The cytotoxicity test of Ag-CS was performed on a human cell line HCT116 (ATCC, Manassas, VA). Briefly, the cells were seeded in 96-well plates and incubated overnight for adhesion, followed by adding Dulbecco's Modified Eagle Medium (DMEM, Thermo Fisher Scientific, Waltham, Massachusetts, USA) dispersed Ag-CS with Ag concentrations of 0.4, 0.8, 1.6, 3.2, 6.4, 12.8, 25.6, 51.2 and 102.4 μg/mL Ag equivalents. AgOAc was included as a positive control. After 48 h incubation, cell viability was measured by the cell counting kit-8 (Dojindo Molecular Technologies, Maryland, USA). Specifically, 10 μL of cck-8 solution was added to each well of cells and incubated for 2 h. The absorbance at 450 nm was recorded by a plate reader (SpectraMax, Molecular Devices, Sunnyvale, California, USA), and cell viability was calculated according to the manufacturer's guidance.

### 3.3.3.7 Ag-CS induced reactive oxygen species (ROS) generation in human colon cancer cells HCT116

The ROS generation was measured using a fluorescent probe H2DCFDA. HCT116 cells were seeded in 24-well plates and incubated 16 h for adhesion. Treatment solutions were prepared by diluting CC-CS and Ag-CS in DMEM and achieved a final concentration of 100 $\mu$g/mL for CC-CS and 10 $\mu$g/mL Ag equivalent for Ag-CS. Cells were then treated by 1 mL of each prepared treatment solution and incubated for 2 h at 37 $^{o}$C. After treatment, all cells were washed 3 times by PBS and treated with H2DCFDA probe for 1 h. Finally, cells were washed and monodispersed for flow

cytometry, and the fluorescence intensity at 525 nm were recorded to indicate the ROS amount inside of cells.

#### 3.3.3.8 Statistics

All experiments were conducted in triplicate with data reported as mean ± standard error. Statistical analyses were performed using Prism 8 (GraphPad Software, Inc., California, USA) with significance level $p < 0.05$. One-way ANOVA and Bonferroni post-test were conducted for the cell viability data.

## *3.4 Results and discussion*

### 3.4.1 Synthesis of CC-CS and Ag-CS

To synthesize Ag-CS, a facile two-step modification was carried out. CS was first grafted by an alkynyl group to form CC-CS, then AgOAc reacted with the alkynyl group and formed Ag-CS (Scheme 1). We found that the introducing of alkynyl Ag affected the viscosity of CS. Moreover, as reported in literatures, the antimicrobial activity of CS was partially depended on its solubility and mobility.[16] Therefore, we synthesized a series of CC-CS and Ag-CS with different substitution degrees in order to understand the correlation between the substitution degree and the antimicrobial. CC-CS with different substitution degrees were obtained by varying the reaction molar ratios of carboxyl group on 4-Pentynoic acid to amino group on CS from 10% to 90%.

When the molar ratio exceed 75%, the reaction product CC-CS formed gel and lost mobility, which was not suitable for further modification and antimicrobial applications. Therefore, CC-CS synthesized by molar ratios of 10, 25, and 50% were chosen for future experiments and named as L-CC-CS, M-CC-CS, and H-CC-CS, respectively. To further synthesize Ag-CS, different CC-CS and AgOAc were reacted with a molar ratio of 1:1, and corresponded Ag-CS were named as L-Ag-CS, M-Ag-CS, and H-Ag-CS respectively depending on which CC-CS was used. The Ag contents were determined to be 2.79, 5.15, and 17.22% respectively for L-Ag-CS, M-Ag-CS, and H-Ag-CS.

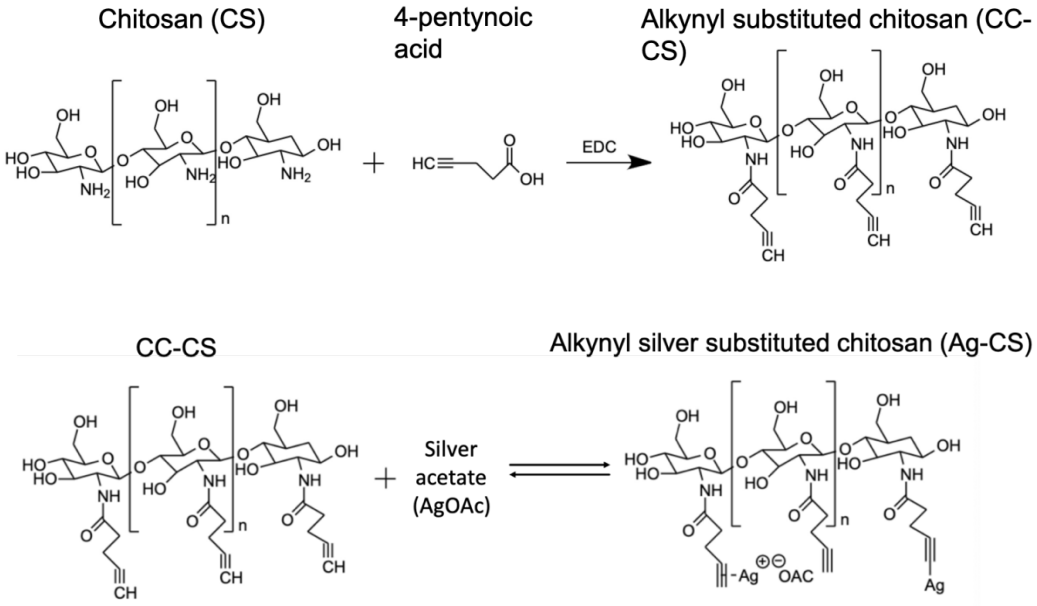


**Scheme 3-1**. The synthesis route of CC-CS (top: the addition of alkynyl group to CS) and Ag-CS (bottom: the substitution of Ag to CC-CS).

### 3.4.2 Characterization of Ag-CS

FTIR spectra was used to characterize CS, H-CC-CS, and H-Ag-CS to confirm the chemical structures (Figure 3-1). As a result, the C≡C stretching at 2105 $cm^{-1}$ was observed for H-CC-CS and H-Ag-CS, which confirmed the successful substitution of alkynyl group to CS. Moreover, the C-H stretching for terminal alkyne at 3251 $cm^{-1}$ is significantly reduced after the addition of Ag to alkynyl group. Moreover, the C-H stretching for a terminal alkyne at 3251 $cm^{-1}$ was observed on H-CC-CS and H-Ag-CS, and this peak significantly reduced after the addition of Ag to alkynyl group. In the FTIR of all Ag-CS (Figure 3-2), C=O stretching, N-H bending, and C-N stretching for amide group was confirmed by the presents of bands on 1650 $cm^{-1}$, 1556 $cm^{-1}$, and 1320 $cm^{-1}$, respectively (Mauricio-Sánchez et al, 2017). The C-H stretching on alkyl chain was confirmed by peaks around 2887 $cm^{-1}$, and C-O-C bridge was confirmed by bands at 1054 $cm^{-1}$, and 1017 $cm^{-1}$.[127] Liquid state $^{1}H$ NMR were recorded for L-Ag-CS, M-Ag-CS, and H-Ag-CS. As shown in Figure 3-3, the peaks at 1.90 ppm corresponded to the hydrogen on alkynyl group, and the peak at 8.12 ppm corresponded to the NH, peaks from 4.57 to 3.85 ppm correlated with four hydrogens on glucose skeleton of CS.[128]

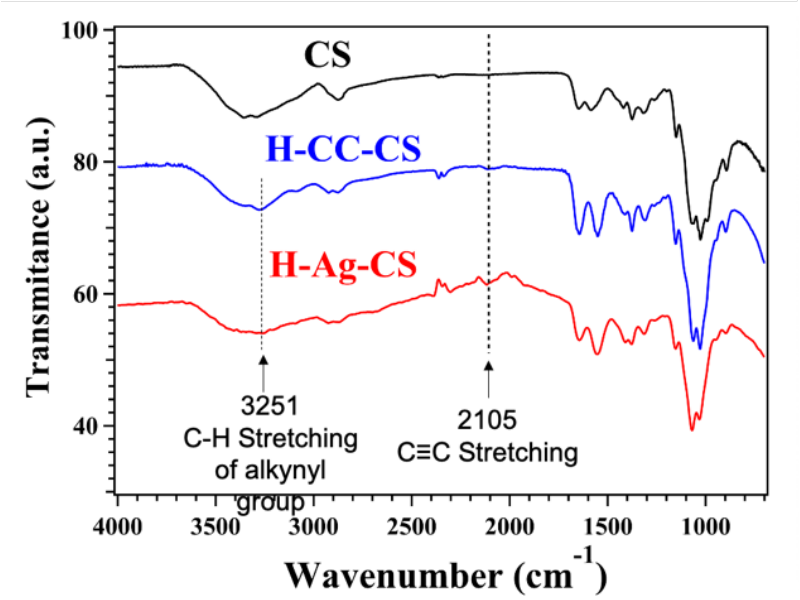


**Figure 3-1**. FTIR of CS (black), H-CC-CS (blue) and H-Ag-CS (red). Two mL of fresh prepared CS, H-CC-CS, and H-Ag-CS were freeze dried, and the dried samples were tested for FTIR spectra from 700 $cm^{-1}$ to 4000 $cm^{-1}$.

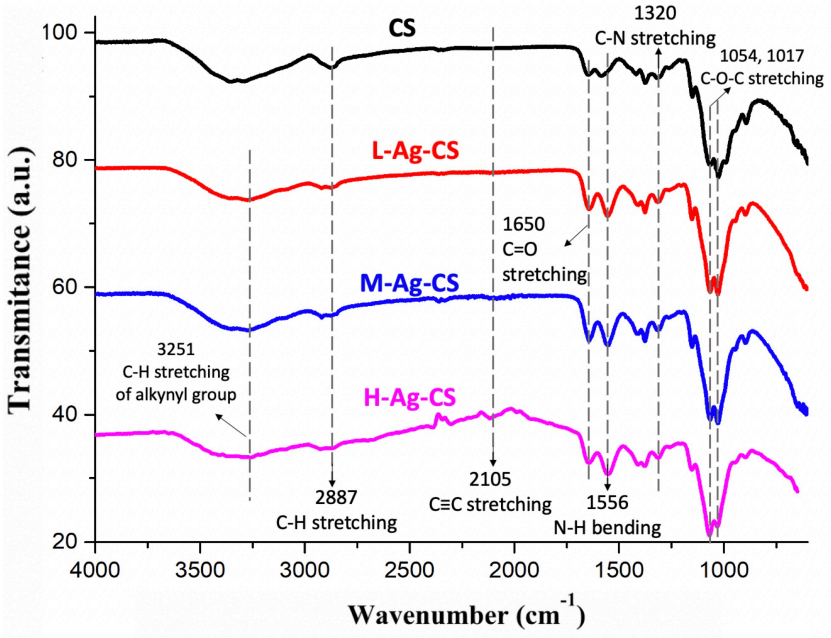


**Figure 3-2**. FTIR of L-Ag-CS, M-Ag-CS, and H-Ag-CS. All Ag-CS were freeze dried before subjecting to FTIR test.

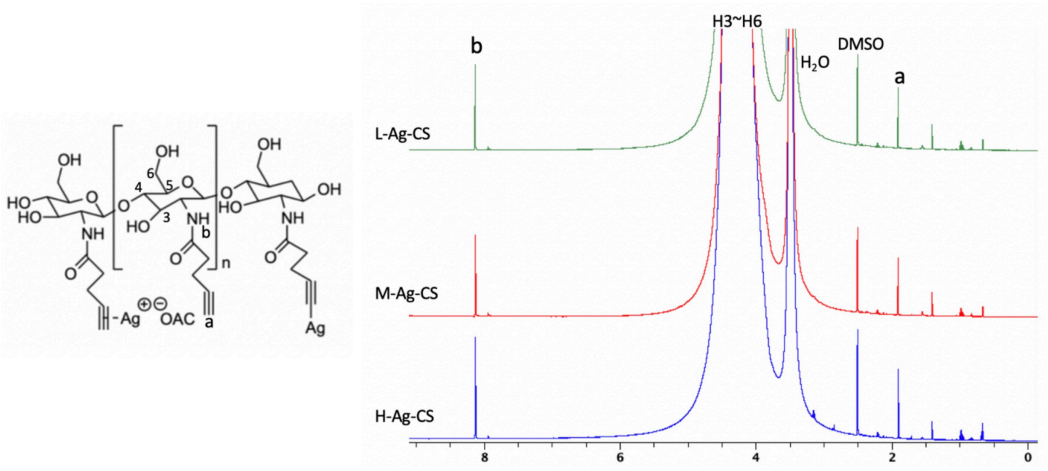


**Figure 3-3**. $^1$H NMR spectra of L-Ag-CS, M-Ag-CS, and H-Ag-CS in water-DMSO solution.

SEM images were taken to study morphology, and all dried CC-CS samples with different substitution degrees presented sheet structures (Figure 3-4). Unlike the untreated CS with obvious roughness, all CC-CS showed a smooth surface under SEM, and none of them showed obvious pores under the current magnification. The introducing of Ag to CC-CS did not cause significant morphological changes. Further, to study the Ag distribution on modified CS, energy dispersive X-ray spectroscopy (EDS) analysis was performed on the L-Ag-CS sample (Figure 3-5). EDS results showed that the distribution of Ag and O were highly overlaid at the location of samples, and the scattered Ag signal indicated that Ag was evenly distributed in the L-Ag-CS. Additional EDS element spectra results on M-Ag-CS and H-Ag-CS showed clear peaks of Ag, C, O, and N. Meanwhile, the weight percentage of Ag in the selected area is 7.83% for M-Ag-CS, and 14.8% for H-Ag-CS, which corresponded well with the medium and high substitution degrees (Figure 3-6).

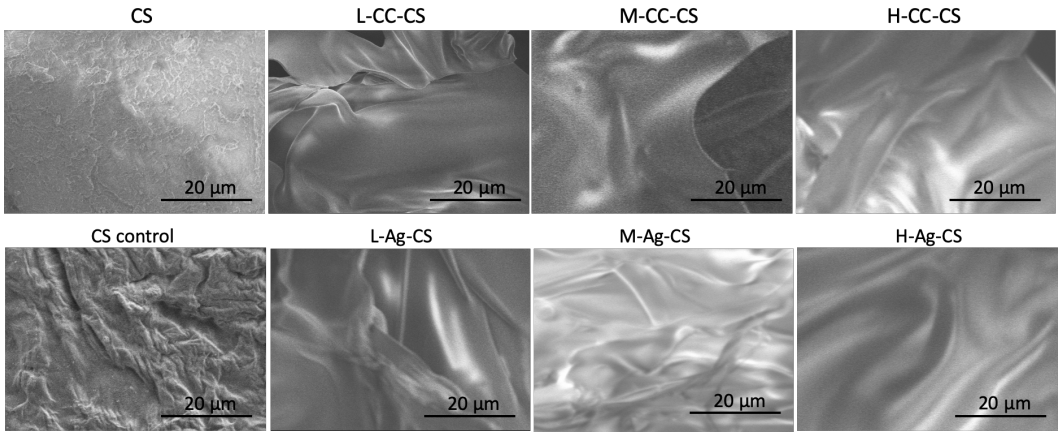


**Figure 3-4**. SEM images of CS, CC-CS, and Ag-CS with different degrees of substitution. Fresh prepared CS, CC-CS, and Ag-CS with different degrees of substitution were freeze dried, and the dried samples were mounted on SEM conductive adhesive tapes for SEM imaging. Images were captured under low voltage of 2kV with scale bar of 20 $\mu$m.

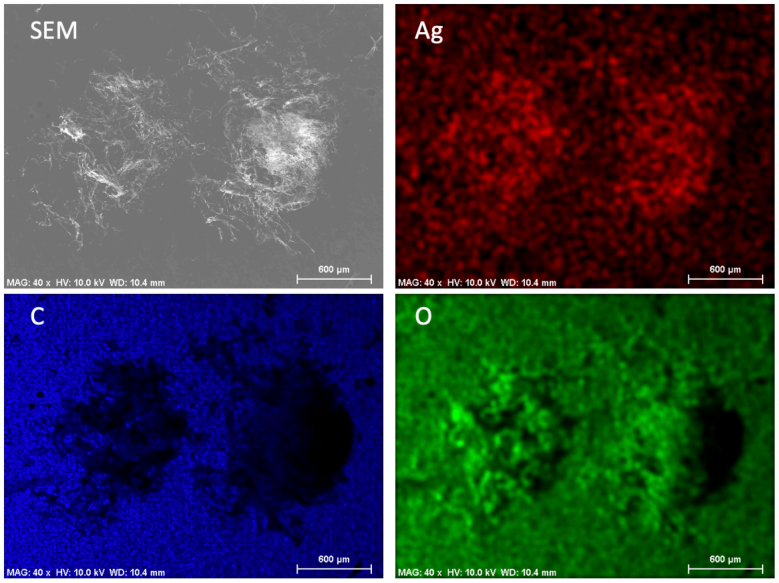


**Figure 3-5**. SEM-EDS analysis results of L-Ag-CS. L-Ag-CS were freeze dried and mounted on SEM conductive adhesive tapes. EDS mapping of elements Ag, C, and O were recorded at a voltage of 10 kV with scale bar of 600 $\mu$m.

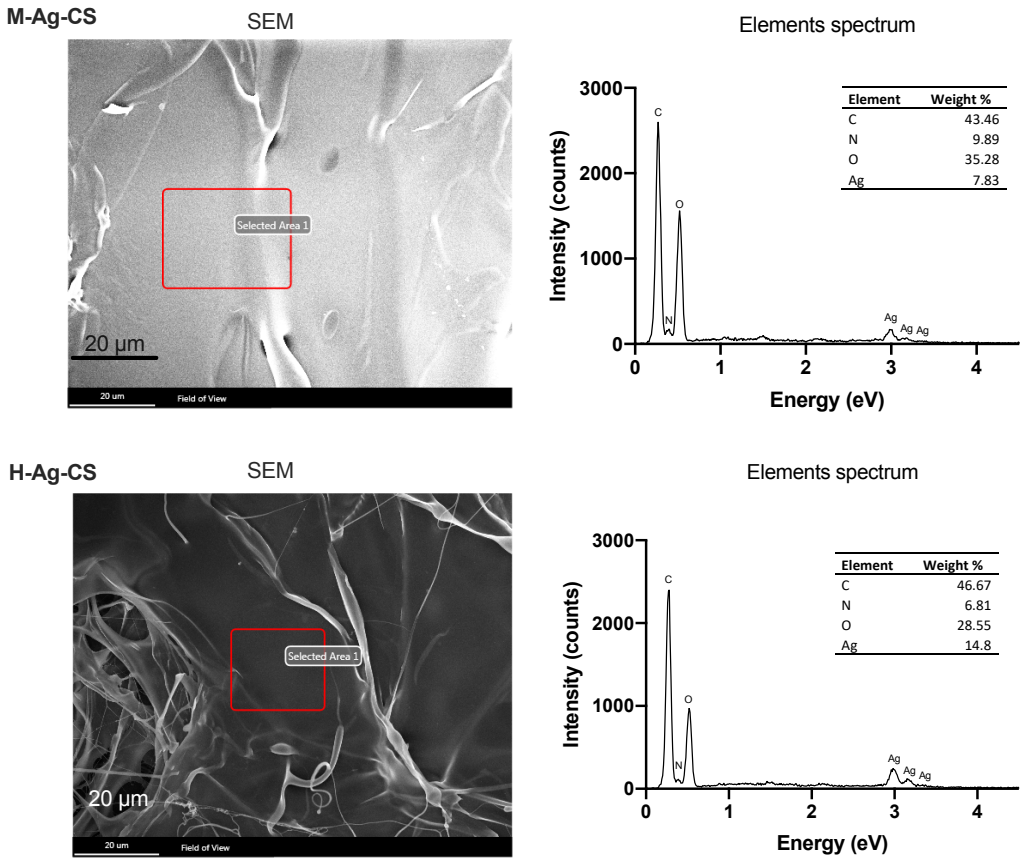


**Figure 3-6**. SEM images and EDS element spectra of M-Ag-CS and H-Ag CS. SEM Images were captured under low voltage of 2kV with scale bar of 20 $\mu$m. EDS element spectra of selected area in the SEM images were recorded at a voltage of 10 kV.

The viscosity of CS significantly increased by introducing alkynyl group and Ag alkynyl group to CS. (Figure 3-7) Addition of alkynyl group to CS at the lowest substitution degree slightly increase the viscosity from 4.5 mP·S (CS) to 5.0 mP·S (L-CC-CS), and viscosity increased again along with substitution degree from 6.0 mP·S (M-CC-CS) to 16.0 mP·S (H-CC-CS). The increase of molecular weight was the major reason for the increased viscosity. Higher molecular weight normally leads to larger

excluded volume that promotes intermolecular interaction of polysaccharide and suppress its solubility.[19] Addition of Ag to the structure further increased the viscosity of Ag-CS from 24.0 mP·S of L-Ag-CS to 136.5 mP·S of H-Ag-CS. The increasing of viscosity maybe caused by 1) forming of metal-ligand coordination bonds between Ag and amino group and hydroxyl group, and 2) solubility decreased from CC-CS to Ag-CS.[14, 20] The solubility of CS at 1 mg/mL before and after modification showed no obvious difference when observed by eyes. The Ag-CS solutions at a concentration of 1 mg/mL present slight yellow color, whereas CS solutions was clear (Figure 3-8).

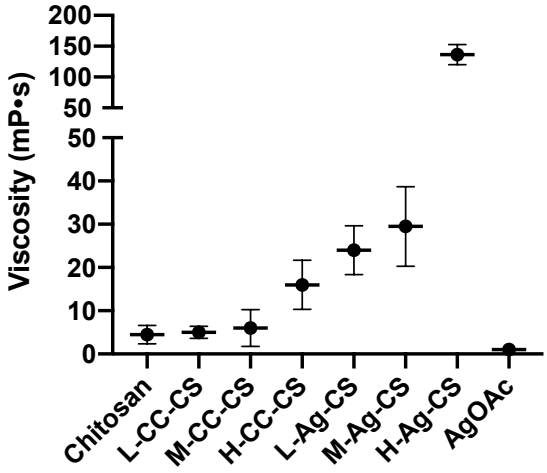


**Figure 3-7 .** Viscosity of CS, CC-CS, and Ag-CS with different degrees of substitution. Round: zeta potential of different materials in DI water at pH 6.5; Rectangular: viscosity of different materials in DI water with concentrations of 1 mg/mL CS equivalents at $20^0$C.

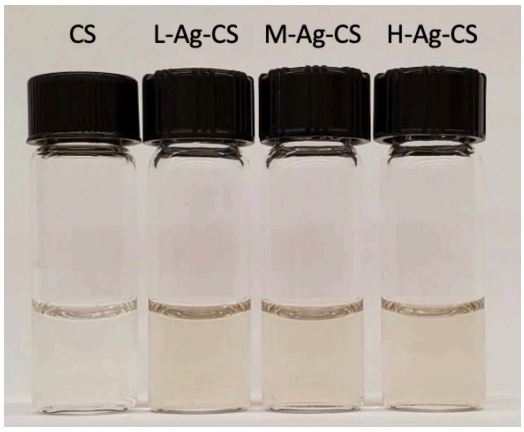


**Figure 3-8**. Images of CS and Ag-CS solutions at the concentration of 1 mg/mL CS equivalent.

### 3.4.3 The release of Ag from Ag-CS and the toxicity of Ag-CS

The sustained releasing of antimicrobial agents is currently a major challenge for antimicrobial coating materials, and the release rate of Ag directly affects the antimicrobial activity of the coating material. Therefore, we studied the Ag release profile of Ag-CS with different substitution levels, using AgOAc as a control (Figure 3-9). Unlike AgOAc, which released 91.18±2.07% Ag within 4 h, all Ag-CS preparations showed sustained release for more than 5 days. By 5 days, 85.15±1.77%, 86.17±1.42%, and 68.29±1.93% of the bound Ag was released from L-Ag-CS, M-Ag-CS, and H-Ag-CS, respectively. This result indicates that Ag-CS has a significant advantage as an antimicrobial coating material for food packaging systems due to its prolonged release and high release rate.

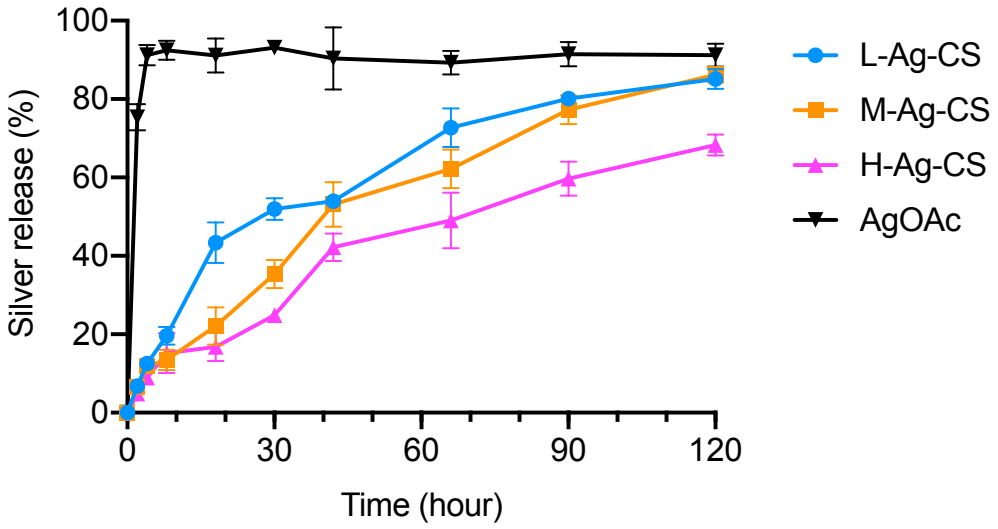


**Figure 3-9.** Release profile of L-Ag-CS, M-Ag-CS, H-Ag-CS and AgOAc in DI water. L-Ag-CS, M-Ag-CS, and H-Ag-CS samples with initial concentrations of 150 $\mu$g/mL Ag equivalent were dialyzed with 10K dialysis bags. The surrounding solution was sampled every 2 h in the first 8 h and then every 12 h, Ag concentration was measured by ICP test.

The cytotoxicity of Ag-CS was not significantly different from AgOAc (Figure 3-10). H-Ag-CS and AgOAc exhibited slightly lower $IC_{50}$ of 5.6 and 6.4 $\mu$g/mL Ag equivalent than L-Ag-CS and M-Ag-CS with $IC_{50}$ of 8.5 and 9.1 $\mu$g/mL Ag equivalent. One possible mechanism of Ag-CS induced cell injury is generating ROS in cells. Cells were treated by CC-CS (100 $\mu$g/mL) and Ag-CS (10 $\mu$g/mL Ag equivalent) in DMEM for 2 h. The ROS amount inside of cells were then tested using a fluorescence probe H2DCFDA. The results showed that CS, and all CC-CS only slightly increased the ROS levels in cells; however, 2 h treatment with Ag-CS significantly increased the ROS levels in cancer cells. The ROS generation is expected to be one mechanism that caused cell damage by Ag-CS (Figure 3-11). Although Ag-CS showed similar

cytotoxicity to the AgOAc, the antimicrobial activity of Ag-CS with 1 μg/mL Ag was remarkably higher than AgOAc at a concentration of 5 μg/mL. The potent antimicrobial activity of Ag-CS relative to AgOAc and $AgNO_3$ is foreseen to greatly decrease the effective application dose of Ag, and thus improve the efficacy and safety of applying Ag-CS as an antimicrobial coating material.

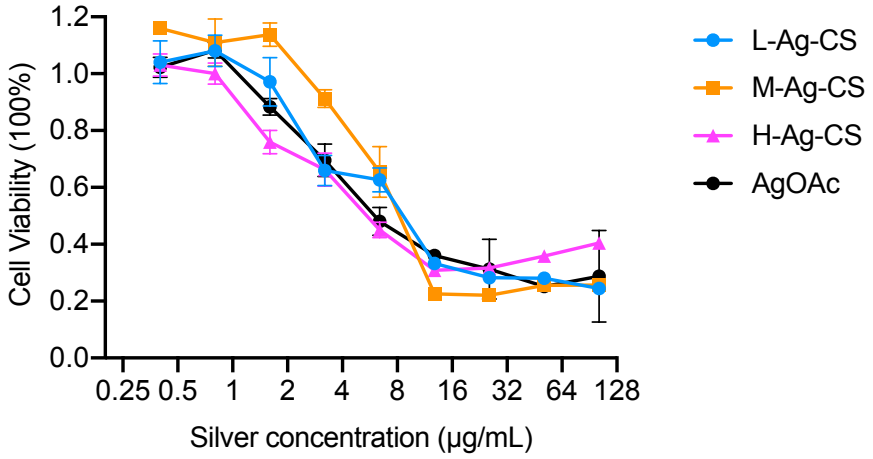


**Figure 3-10**. Cell viability of HCT116 human colon cancer cells treated by Ag-CS and AgOAc. HCT116 cells were treated by L-Ag-CS (blue), M-Ag-CS (orange), H-Ag-CS (Pink), AgOAc (grey) in varied concentrations from 0.4 to 102.4 $\mu$g/mL Ag equivalents. Cell viability was tested by cck-8 kit after 48 h treatment.

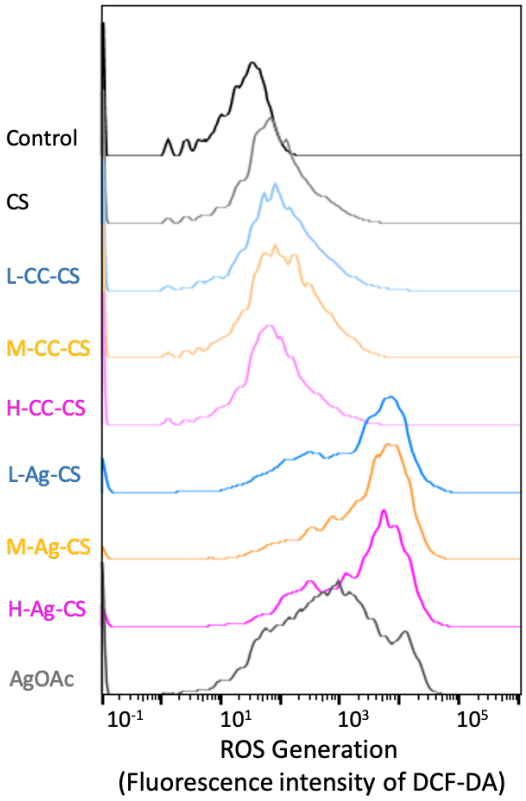


**Figure 3-11**. Effect of CS, CC-CS and Ag-CS on the ROS generation in cancer cells after 2 h treatment. The concentration of CS, and all CC-CS was 100 $\mu$g/mL. For Ag-CS and AgOAc, 10 $\mu$g/mL Ag equivalents were used in the treatment.

## *3.5 Conclusion*

In this work, Ag-CS with different substitution degrees were prepared. Multiple techniques were adopted to characterize Ag-CS. The chemical structures of Ag-CS were confirmed by FTIR and $^{1}$H NMR, and the Ag content in Ag-CS were determined by ICP and SEM-EDS with 2.65, 7.83, 14.8% for L-Ag-CS, M-Ag-CS, and H-Ag-CS, respectively. The modification of alkynyl group and the formation of alkynyl Ag group gradually increased the viscosity of CS, but all Ag-CS presented a smooth surface

under SEM and Ag was evenly distributed over the surface. Ag-CS demonstrated controlled release of Ag for over 5 days, whereas Ag infused CS released over 90% Ag within 4 h. The Ag-CS were also proved to induce ROS generations in human cancer cells, which offered the basis of their cytotoxicity.

# Chapter 4: Bacteria Inhibition and Inactivation Properties of Ag-CS and Its Applications in Food Area

## *4.1 Abstract*

Ag-CS was formed by substituting alkynyl Ag to CS through chemical reactions. The antimicrobial properties of Ag-CS was carefully studied through several tests including: bacteria inactivation test, bacteria growth curve measurements, minimum inhibitory concentration determination, inhibition ring test. Ag-CS presented stronger antimicrobial effects over $AgNO_3$ against both Gram negative bacteria *E. coli* and Gram positive bacteria *L. monocytogenes* at same concentration of Ag equivalents. Ag-CS also demonstrated stronger bacteria inactivation activity over $AgNO_3$ against two bacteria strains. Both antimicrobial and bactericidal activities of Ag-CS are dose dependent.

## *4.2 Introduction*

Microbial contamination reduces the shelf life of food products, increases the risk of foodborne illness, and causes huge economic losses to the food industry.[129] One approach to combat microbial contamination in the food supply is to develop antimicrobial food packaging systems and coating materials, which incorporate antimicrobial agents that can interact with food or headspace in the package to extend the shelf life of food products and enhance food safety without affecting food quality.[1]

The antimicrobial packaging market size is estimated to grow from USD 7.28 billion in 2015 to USD 10 billion by 2021.[130]

Ag and Ag-based composites are brilliant antimicrobial agents for their broad antimicrobial activities to Gram positive and Gram negative bacteria strains, fungi, and viruses.[26] They have been applied as antimicrobial agents in wound dressing, medical equipment coatings, paints, and food packaging materials to prevent contaminations and infections.[83] Unlike other antimicrobial agents that can potentially cause drug resistance, Ag and Ag-based composites are known for their feature of not causing drug resistance while providing high antimicrobial efficacy by disturbing bacterial cell membrane and causing intracellular damage to DNA, RNA, enzymes and so on.[1] Among which, Ag-based nanostructures (e. g. AgNPs and AgNCs) have been intensively studied. However, their applications are limited for their heavy metal core that can be left to the environment after usage and causes pollution.[108] Moreover, the potential toxicity of Ag to human beings also prevent it from adding to many food systems. Thus, to apply Ag-based composites in food systems and food packaging systems, a Ag-based composite should have strong antimicrobial effect, and it should be environmental friendly and present low toxicity to humans. To meet these needs, we came up with a new Ag-based antimicrobial coating material, Ag-CS.

In the structure of Ag-CS, Alkynyl Ag are modified on CS through covalent bonds, and Ag is well distributed in CS in the form of ion, which is highly active as an

antimicrobial agent. In our design, comparing to commonly used AgNPs, the adoption of alkynyl Ag can greatly decrease the application dose, avoid potential environment pollution by eliminating metal cores, and increase antimicrobial efficacy by using the form of Ag ion. In this work, we systematically discussed the bacteria inhibition and inactivation properties, and explored the potential applications of Ag-CS as antimicrobial coatings on shrimps and strawberries during cold storages. The Ag-CS demonstrated superior bacteria inhibition and inactivation efficiency over AgOAc or $AgNO_3$ at same concentrations of Ag equivalents. By coating on shrimps and strawberries, Ag-CS dramatically decreased their spoilage rates. Overall, these results indicated Ag-CS as a potent antimicrobial agent with great potentials to be used in food area.

## *4.3 Materials and methods*

### 4.3.1 Synthesis of Ag-CS

Ag-CS was synthesized through two steps of chemical reactions (Scheme 1). CS (with a viscosity of 4.5 mP·S for 1mg/mL CS aqueous solution at pH 5) was first substituted by alkynyl groups to form CC-CS, then the alkynyl groups reacted with AgOAc to form alkynyl Ag on CS, which was defined as Ag-CS (Möhler et al., 2018). To synthesize CC-CS, 4-pentynoic acid and CS were dissolved in 15 mL DI water, and pH was adjusted to 5 by acetic acid. This solution was stirred for 1h at room temperature to

fully dissolve CS, and EDC dissolved in 5mL DI water were slowly added into the solution, and stirred overnight. The synthesized CC-CS solution was then dialyzed in water for 24 h, followed by store at 4 °C. In the synthesis of CC-CS, three substitution degrees were adopted by varying the reaction molar ratios of alkynyl group on 4-pentynoic acid to the amino group on CS, and the molar ratios of 1:10, 1:4, and 1:2 were used for low substituted CC-CS (L-CC-CS), medium substituted CC-CS (M-CC-CS), and high substituted CC-CS (H-CC-CS). Then, the amount of EDC was determined using a reaction molar ratio of EDC to 4-pentynoic acid of 1:1. The molar amount of amino group on CS was estimated by the following equation:

Molar concentration of amino group for 1% CS solution (mole / L)

= 10 g (mass of CS in 1 L 1% CS solution)/ 167.3 (estimated molecular weight of CS repeated monomer)

Specifically, the formulation used to synthesize 20 mL CC-CS are: L-CC-CS: 200mg CS, 13.8 mg 4-pentynoic acid, and 107.2 mg EDC; M-CC-CS: 200mg CS, 34.4 mg 4-pentynoic acid, and 268 mg EDC; H-CC-CS: 200mg CS, 68.8 mg 4-pentynoic acid, and 536 mg EDC.

To synthesize Ag-CS, CC-CS reacted with AgOAc to form L-Ag-CS, M-Ag-CS, and H-Ag-CS depending on which CC-CS was used. AgOAc were dissolved in DI water, and added into CC-CS solution dropwise. The mixture was stirred at room temperature overnight, followed by a dialysis in water. Synthesized Ag-CS was stored in the refrigerator for further experiments. Specifically, the formulation used to synthesize

100 mL Ag-CS solutions are: L-Ag-CS: 64.5 mg AgOAc and 44.3 mg L-CC-CS; M-Ag-CS: 64.5 mg AgOAc and 48 mg M-CC-CS; and H-Ag-CS: 64.5 mg AgOAc and 54.3 mg H-CC-CS.

### 4.3.2 Bacteria inhibition properties of Ag-CS

The bacteria inhibition activities of Ag-CS was evaluated by growth curve measurement, inhibition zone test, and MIC determination, and two bacteria strains were included in the study: a Gram negative strain *E. coli* O157:H7, and a Gram postive strain *L. innocua*.

#### 4.3.2.1 Inhibition zone test on *E. coli* O157:H7

The inhibition zone test was performed on a three-strain cocktail of *E. coli* O157:H7 (RM4406, ATCC 43895, and ATCC 700728). Specifically, 1, 2, 5 and 10 μg Ag equivalents of different Ag-CS preparations were loaded onto filter paper discs with a diameter of 7 mm and dried in a fume hood. One colony of *E. coli* was inoculated to trypticase soy broth (TSB) and cultured overnight, followed by spreading 100 $\mu$L bacteria culture to trypticase soy agars (TSA). The Ag-CS loaded discs were then placed on the center of bacteria inoculated agar plates, and the widths of the inhibition rings were measured by a ruler after 24 h and 48 h.

#### 4.3.2.2 Growth curve measurement

*E. coli O157:H7* was cultured in a Mueller-Hinton broth for 16 h and diluted with the same broth to an optical density (OD) at 600 nm of 0.01. The diluted bacteria were then treated with Ag-CS, CC-CS, or AgOAc with final concentrations of 1 μg/mL, 5 μg/mL, and 10 μg/mL Ag equivalents. The bacteria were incubated at 37°C and the OD of each sample at 600 nm was measured every half hour with a UV/Vis spectrophotometer (Beckman Coulter, California, USA) for 11 h.

#### 4.3.2.3 Minimum inhibition concentration (MIC)

MIC was obtained by the broth dilution method (Wiegand et al., 2008). Specifically, *E. coli O157:H7* was incubated in the Mueller-Hinton broth until reaching the exponential growth stage. Bacteria cells at a concentration of $10^5$ CFU/mL were then incubated with different concentrations of Ag-CS, CC-CS, CS, AgOAc, or $AgNO_3$ for 18-20 h at 37°C. The MIC was designated as the lowest Ag concentration for which samples showed no visible growth of microorganisms.

### 4.3.3 Bacteria inactivation properties of Ag-CS

#### 4.3.3.1 Bacteria culture preparation.

One Gram negative strain *E. coli O 157:H7* (a mixture of RM4406, ATCC 43895, and ATCC 700728) and one Gram positive strain *L. monocytogenes* (ATCC 43256) were adopted to evaluate the antimicrobial efficiency of Ag-CS in this work. Bacteria from

stock culture was recovered and inoculated onto TSA plates. Before each experiment, a single colony of bacteria was inoculated and incubated in TSB for 20 h at 37°C to reach the stationary phase.

#### 4.3.3.2 Bacteria inactivation test.

The bacteria inactivation ability of Ag-CS was tested on both *E. coli* and *L. monocytogenes*. One colony of *E. coli* were incubated in 10 mL TSB for 20 h to reach stationary phase with cell density of approximately log9 ($10^9$ CFU/mL), and one colony of *L. monocytogenes* were incubated in 10 mL TSB for 20 h to reach stationary phase with a cell density of approximately log7 ($10^7$ CFU/mL), followed by 10 min centrifuge at 4000 g to collect cells. The cell pellets were then resuspended in fresh TSB and treated by Ag-CS with final concentrations of 1, 2, 5, 10, 20, 30 $\mu$g/mL Ag equivalent under 37°C. TSB were used for the control group. At time points of 0, 1.5, 4, 7, 10, 24 h, 100$\mu$L of each samples were collected and serial diluted with fresh TSB, and 100$\mu$L of each dilution were plated onto TSA. All plates were enumerated after 24 h incubation at 37°C. All treatment are triplicated.

### 4.3.4 Effects of Ag-CS coatings on the freshness of shrimps and strawberries during cold storage

#### 4.3.4.1 Effects of Ag-CS coatings on the freshness of shrimps during cold storage

Fresh head-on shrimps were obtained from local seafood market, and they were refrigerated prior to the study. Stock solutions of Ag-CS at different substitution degrees were diluted to reach a final concentration of 10 $\mu$g/mL Ag equivalent. Shrimps were dipped in DI water (control) or Ag-CS solutions for 3 s, then the shrimps were picked up and directly transferred to zip lock bags and stored in a refrigerator at 4°C for 12 days. After storage, the appearance of shrimps were recorded by pictures, and total volatile basic nitrogen (TVB-N) was determined for chopped shrimp meat. TVB-N was carried out with the Conway micro-diffusion method. Briefly, 10 g shrimp meat was blended in 40 mL of 4% TCA (Trichloroacetic acid) solution and sit for 30 min, and the mixture was then centrifuged for 15 min at a relative centrifuge force of 10,000 g. One mL of the supernatant was mixed with 1 mL saturated $K_2CO_3$ solution in one slot inside of the Conway diffusion cells (Bel-Art Conway diffusion cell, Millipore Sigma, US) to produce ammonia, which in turn was absorbed into 1 mL 2% $H_3BO_3$ (boric acid) solution in another slot inside of the Conway diffusion cell. After 2 h, the $H_3BO_3$ solutions were titrated using 0.01 N HCl to determine the TVB-N level in the shrimp.

To estimate the safety of the Ag-CS coating, the Ag residual level in shrimps and the distribution of Ag residual in shrimps after storage was measured. Briefly, shrimps

were dipped in M-Ag-CS solutions with a concentration of 15 $\mu$g/mL Ag equivalent for 3 s at room temperature and stored at 4°C for 15 days. After storage, shrimps were washed under running water for 10 s, followed by peeling shrimps into two groups: group of shrimp meat and group of shrimp heads & shell mix. All samples were minced in a food processor, and send to the AGQ Labs & Technological Services (California, US) for quantification of the Ag content.

#### 4.3.4.2 Effects of Ag-CS coatings on the freshness of strawberries during cold storage

To better evaluate the effectiveness of Ag-CS as an antimicrobial coating material, we also performed a shelf-life test on strawberries. Fresh organic strawberries were dipped in the M-Ag-CS solutions at a total concentration of 10 $\mu$g/mL Ag equivalents. The strawberries were then dried in air and refrigerated at 4°C for 8 days, photos of strawberries were collected every other day.

### 4.3.5 Statistics

All experiments were conducted in triplicate with data reported as mean ± standard error. Statistical analyses were performed using Prism 8 (GraphPad Software, Inc., California, USA) with significance level $p < 0.05$. One-way ANOVA and Tukey's multiple comparisons test were conducted for the inhibition zone test data.

## *4.4 Results and discussion*

### 4.4.1 Growth curve measurement of Ag-CS treated *E. coli* and *L. monocytogenes*

The antimicrobial activity of Ag-CS was evaluated by growth curve measurement, inhibition zone test, and MIC determination, with two bacteria strains: a Gram negative strain *E. coli* O157:H7, and a Gram positive strain *L. monocytogenes*.

The antimicrobial effect of Ag-CS was first tested by growth curve measurement to understand the impact of Ag-CS on the proliferation of bacteria in liquid media. Bacteria were cultured with Ag-CS at concentrations of 1, 5, and 10 $\mu$g/mL Ag equivalents in the medium and their OD at 600 nm was measured every half hour. To determine the roles of CC-CS and Ag-CS on the antimicrobial activity, for each Ag-CS sample tested, a parallel CC-CS sample with an equal CS concentration was tested as a negative control (Figure 4-1).

The results (Figure 4-1) showed that all Ag-CS treatments presented distinct inhibition activity against bacteria even at the lowest concentration of 1 $\mu$g/mL Ag equivalent, whereas AgOAc at this concentration showed no significant difference from the negative control group. The inhibition activity was also proved to be dose-dependent for different Ag-CS treatments, where higher Ag concentrations resulted in greater inhibition of bacteria growth. At 1 $\mu$g/mL Ag equivalent, all Ag-CS preparations

suppressed the growth of *E. coli* below our detection limit for about 3 h. By increasing the concentration from 1 to 5 $\mu$g/mL Ag equivalents, *E. coli* was suppressed under the detection limit for 10, 5, and 6 h for L-Ag-CS, M-Ag-CS, and H-Ag-CS respectively, whereas AgOAc only provided 2 h suppression. This result suggested that the bacteria had been injured in this stage and took time to adapt to the environment and proliferate. Further increasing of Ag equivalent concentration in Ag-CS to 10 $\mu$g/mL extended the suppression to 10 h or longer, whereas AgOAc kept bacterial growth below the detection limit for 7 h. All these results indicated the superior antimicrobial efficacy of Ag-CS over AgOAc at equivalent Ag concentrations. In addition, the bacteria that underwent suppressed growth presented longer generation time and lower maximum bacteria cell densities when they reached the stationary phases than the control group. This indicated the bacteria had been injured permanently and their response to the environment as well as their proliferation ability had been affected. The results also suggested that Ag-CS with low levels of substitution might be preferred as the antimicrobial agent in bacteria suspensions since L-Ag-CS at 5 $\mu$g/mL demonstrated a significantly stronger inhibition against *E. coli*.

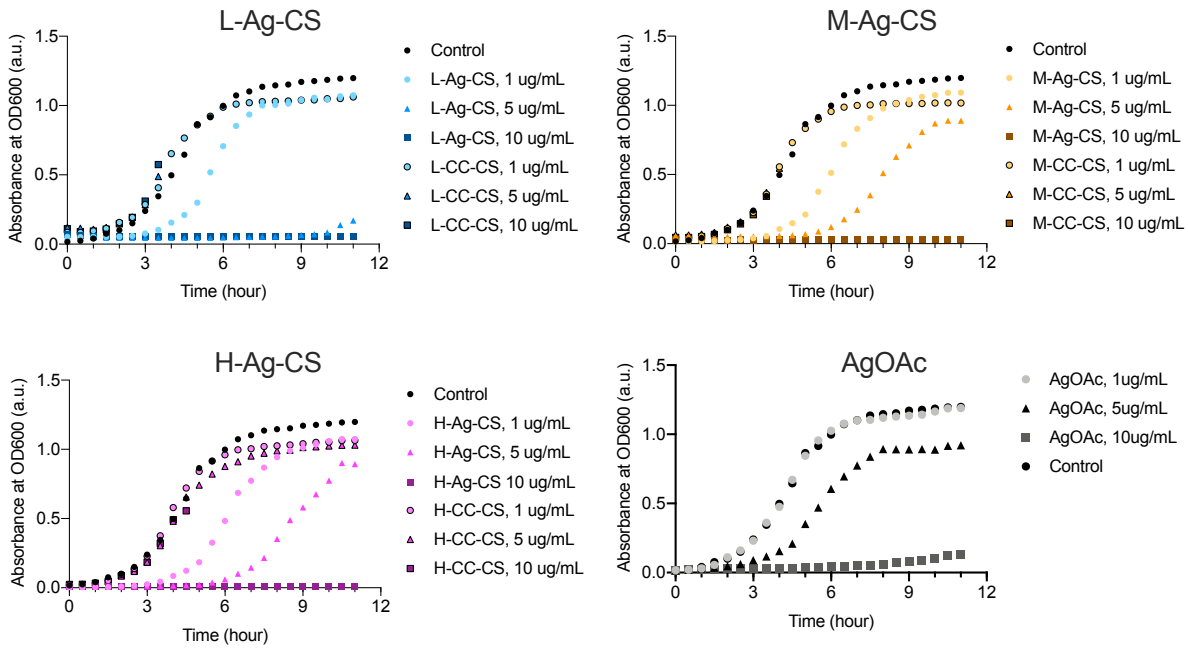


**Figure 4-1.** Growth curve of *E. coli* O157:H7 treated by Ag-CS and CC-CS with three levels of substitution. *E. coli* were incubated with L-CC-CS (outlined blue), M-CC-CS (outlined orange), H-CC-CS (outlined Pink), L-Ag-CS (blue), M-Ag-CS (orange), H-Ag-CS (Pink), and AgOAc as positive control (grey) at concentrations of 1 (●), 5 (▲), and 10 (■) μg/mL Ag equivalents, respectively.

To investigate the contribution of the CS matrix to the antimicrobial effect of Ag-CS, CC-CS treatments were included in the growth curve measurement. Since Ag-CS was obtained by substituting an alkynyl group H with Ag, we ran parallel trials with equal amounts of CC-CS that had been used to synthesize the Ag-CS samples as controls in the growth curve measurement. Moreover, since all Ag-CS samples have different Ag content, there were significant differences in the amount of CC-CS in control groups. For instance, as stated previously, the Ag contents in L-Ag-CS, M-Ag-CS, and H-Ag-CS were 2.79, 5.15, and 17.22% respectively. Thus, with the 1 $\mu$g/mL Ag equivalency,

the final concentration of Ag-CS in the testing samples are 35.84, 19.42, and 5.81 $\mu$g/mL respectively for L-Ag-CS, M-Ag-CS, and H-Ag-CS. In this situation, the amount of CC-CS used to synthesize L-Ag-CS, M-Ag-CS, and H-Ag-CS with 1 $\mu$g/mL Ag equivalency significantly varied and decreased from L-Ag-CS to H-Ag-CS. This variation in the amount of CC-CS with different substitution degrees was also found to affect the microbial growth significantly. Results demonstrated that all CC-CS trials corresponding to Ag-CS with 1 $\mu$g/mL Ag equivalent and H-CC-CS corresponding to H-Ag-CS with 5 $\mu$g/mL Ag equivalent presented no significant antimicrobial activity compared to the control treatment. However, all other CC-CS samples caused co-coagulation of bacteria within 3 to 5 h after mixing. A similar phenomenon was observed in the original CS without any modification. The proliferation and suspension of bacteria were affected by CS based on its concentration and amounts. At concentrations below 50 $\mu$g/mL, it did not have any significant effect on the growth of bacteria. However, at a higher concentration of 100 $\mu$g/mL CS, the bacteria was co-coagulated after 7 h incubation. At 150 $\mu$g/mL and above, the co-coagulation occurred within 5 h. More interestingly, this phenomenon disappeared when a smaller culture volume of 150 $\mu$L (instead of a volume of 2 mL in the growth curve measurement) was used, and no co-coagulation was observed in Ag-CS samples. L-Ag-CS exhibited the strongest antimicrobial activity, likely due to having the highest CS content in the sample, which causing the co-coagulation precipitation of bacteria cells. Overall, the growth curve measurement results show that all Ag-CS preparations provided a

stronger inhibition to the growth of bacteria than AgOAc in a dose dependent manner, and L-Ag-CS had the strongest antimicrobial efficacy in liquid medium.

To study the difference of antimicrobial activity of Ag-CS against different bacteria strains. *L. monocytogenes* and *E. coli* were treated by M-Ag-CS at a series concentrations of Ag equivalents: 1, 2, 5, 10, 20 and 30 $\mu$g/mL. $AgNO_3$ and M-CC-CS were included as positive and negative controls, respectively (Figure 4-2). For *L. monocytogenes*, 1 and 2 $\mu$g/mL $AgNO_3$ showed no antimicrobial effects by comparing to the control group, 5 $\mu$g/mL $AgNO_3$ slightly inhibited the growth of *L. monocytogenes*. Started from 10 $\mu$g/mL $AgNO_3$, the growth of *L. monocytogenes* was completely inhibited below detection limit for 9 h. Unlike $AgNO_3$ only started showing antimicrobial effects from 10 $\mu$g/mL, M-Ag-CS significantly inhibited the growth of *L. monocytogenes* as low as 1 $\mu$g/mL Ag equivalent. 1 $\mu$g/mL M-Ag-CS significant slowed down the proliferation rate of *L. monocytogenes* with a decreased cell density at the stationary phase than control group, 2 $\mu$g/mL M-Ag-CS further suppressed the proliferation of *L. monocytogenes* at log phase and cell density at stationary phase. With over 5 $\mu$g/mL M-Ag-CS, the growth of *L. monocytogenes* was completely inhibited below detection limit. These results indicated that M-Ag-CS performed stronger antimicrobial effects than $AgNO_3$ against *L. monocytogenes* at all concentrations of Ag equivalents. Similar results were observed on *E. coli*. *E. coli* revealed to be more sensitive to $AgNO_3$ than *L. monocytogenes* , its growth started to be effect from 2 $\mu$g/mL $AgNO_3$, but the inhibition efficacy of 2 $\mu$g/mL $AgNO_3$ was

weaker than M-Ag-CS at 1 $\mu$g/mL Ag equivalent. The growth of *E. coli* was suppressed below detection limits by 10 $\mu$g/mL $AgNO_3$ and 10 $\mu$g/mL M-Ag-CS. Both results on *E. coli* and *L. monocytogenes* indicated that M-Ag-CS performed stronger antimicrobial effects than $AgNO_3$ at same concentrations of Ag equivalents.

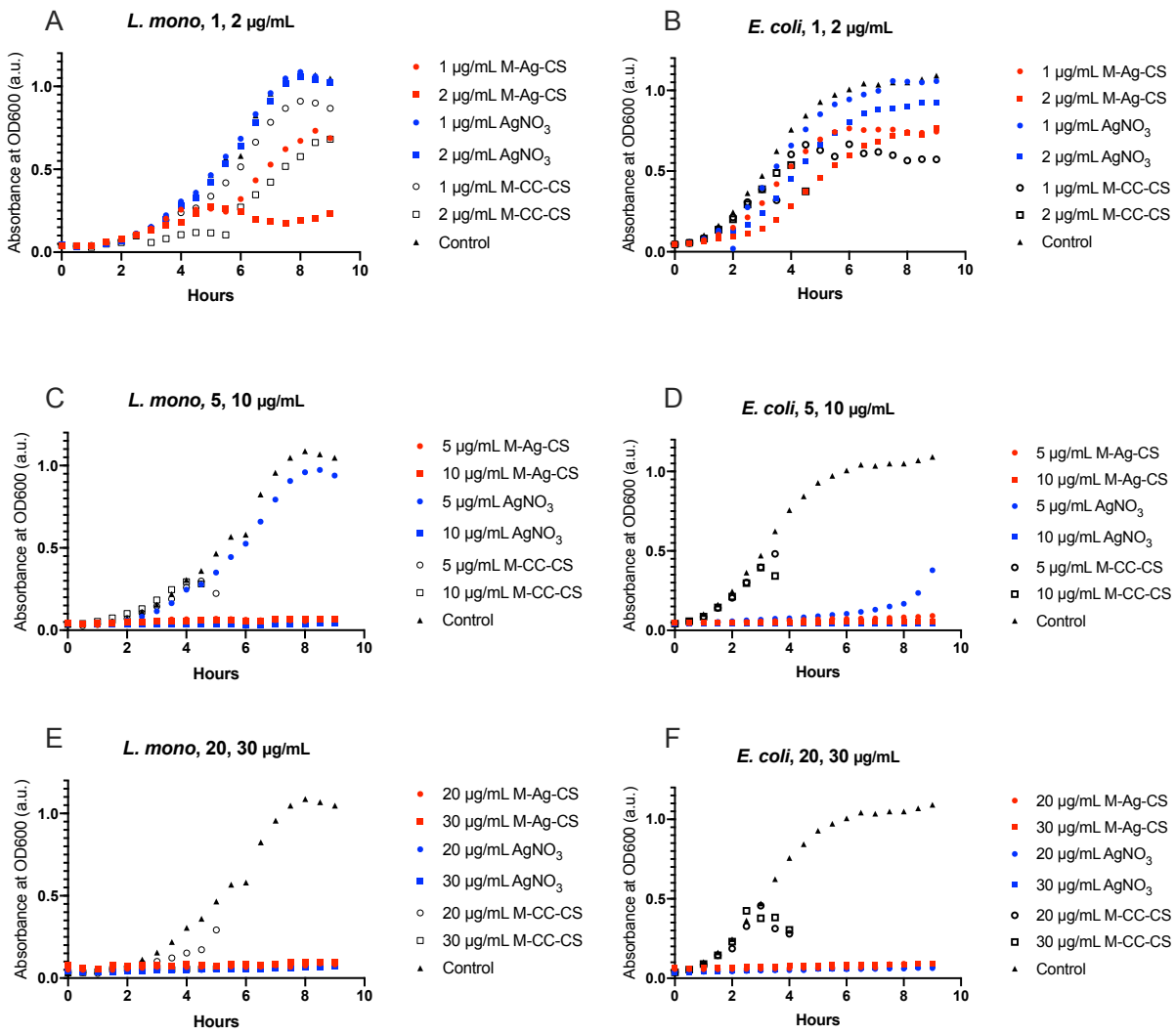


**Figure 4-2**. Growth curve of M-Ag-CS treated *L. monocytogenes* and *E. coli* at a series concentrations of Ag equivalents: 1, 2, 5, 10, 20 and 30 $\mu$g/mL.

### 4.4.2 Inhibition zone test of Ag-CS against *E. coli* and *L. innocua*

Inhibition zone tests were carried out to test the antimicrobial activity of Ag-CS, including the release and dispersal of Ag from the coating material. All Ag-CS exhibited potent antimicrobial activity, significantly more than the control treatment (i.e. AgOAc). By increasing the amount of Ag equivalent from 1 $\mu$g to 2 $\mu$g, the inhibition ring widened from 1.33±0.20 to 1.51±0.04 mm for L-Ag-CS, 1.20±0.13 to 1.69±0.05 mm for M-Ag-CS, and 1.60±0.15 to 2.13±0.21 mm for H-Ag-CS after 48 h treatment, respectively (Figure 4-3). In this concentration range, H-Ag-CS presented the highest antimicrobial activity among all Ag-CS treatments, which contrasted with our results from the growth curve measurements (in which L-Ag-CS presented the highest antimicrobial activity). This difference is likely attributed by the differing Ag releasing profile in two methods. In the growth curve measurement, CS-induced co-precipitation of Ag-CS and bacteria cells was the primary factor contributing to the antimicrobial activity, thus L-Ag-CS that contained the highest concentration of CS demonstrated the best antimicrobial activity. In the inhibition zone test, however, the antimicrobial activity was largely determined by the diffusion of Ag from Ag-CS and the Ag-bacteria cell interactions. In this situation, H-Ag-CS was able to release more Ag than other treatments, owing to its having the highest level of substitution. The Ag concentration dependent antimicrobial activity was also observed in the inhibition zone tests of Ag-CS with the Gram positive bacteria strain *L. innocua* (Figure 4-4).

The increase in the Ag-CS amount to 5 and 10 $\mu$g Ag equivalent in the inhibition zone test did not increase the antimicrobial activity, we think it may be due to an experimental error. While preparing the Ag-CS loaded disks, higher Ag concentrations required higher loading volumes, and oxidation and aggregation of Ag ions likely occurred during the extended preparation procedure, compromising the antimicrobial activity of the Ag-CS.

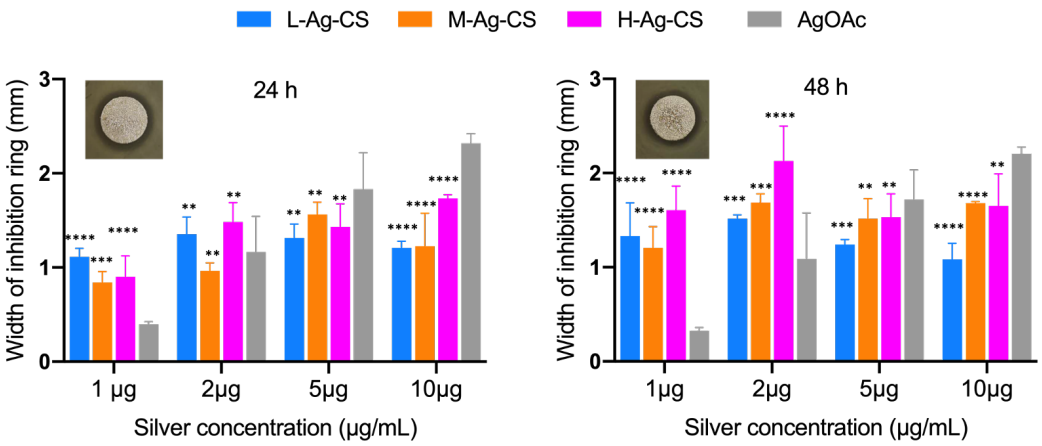


**Figure 4-3.** Inhibition zone test of Ag-CS with different degree of substitution. *E. coli* was treated by L-Ag-CS (blue), M-Ag-CS (orange), H-Ag-CS (pink), and AgOAc (gray) for 24 h and 48 h with 1 µg, 2 µg, 5 µg, and 10 µg Ag equivalents, respectively. The width of the inhibition ring was measured by a ruler. The inserts were the photos of inhibition ring of H-Ag-CS with 5$\mu$g/mL Ag equivalents at 24 h (left) and 48 h (right). (All groups were compared with AgOAc group at same concentration of Ag equivalents. Statistical significance determined from one-way ANOVA followed by multiple comparison test. ***$p < 0.001$, **$p < 0.01$, *$p < 0.1$, $n = 3$)

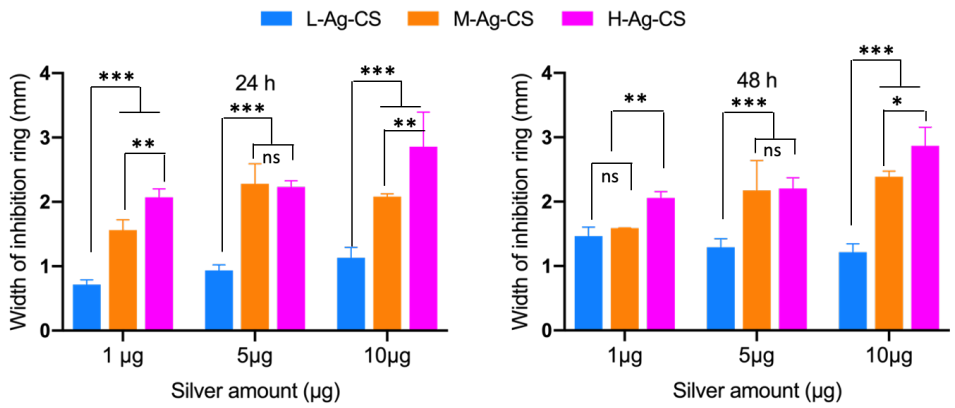


**Figure 4-4.** The antimicrobial effect of Ag-CS against Gram positive bacteria *L. innocua*. Different amount (1, 5, and 10 $\mu$g Ag equivalent) of Ag-CS were loaded on diffusion disks and placed in the center of *L. innocua* inoculated plates. The width of inhibition ring around the diffusion disk were recorded after 24 h (left) and 48 h (right) incubation at 37°C. Statistic analysis was performed by one-way ANOVA. $***p < 0.001$, $**p < 0.01$, $*p < 0.1$, $ns > 0.9999$, $n = 3$.

### 4.4.3 MIC determination.

The MIC of CC-CS and Ag-CS preparations were determined by the dilution method with a volume of 150 $\mu$L. H-Ag-CS was found to have the lowest MIC (6.2 $\mu$g/mL), where the MIC for M-Ag-CS and L-Ag-CS was 6.4 and 10.4 $\mu$g/mL, respectively (Table 4-1). The MIC test was also performed on CC-CS with concentrations from 0 to 300 $\mu$g/mL, and no MIC was found within this concentration range. AgOAc and $AgNO_3$ were tested for MIC as positive controls, and they exhibited MIC values of 13.4 and 12.8 $\mu$g/mL respectively. The MIC of all Ag-CS samples were lower than those of AgOAc and $AgNO_3$. This might be the result of sustained release of Ag from Ag-CS, whereas AgOAc and $AgNO_3$ released Ag rapidly within 4 h. This result demonstrates

the potent and prolonged antimicrobial activity of Ag-CS relative to AgOAc and $AgNO_3$.

**Table 4-1. MIC of Ag-CS and CC-CS with different levels of substitution. MIC of L-Ag-CS, M-Ag-CS, and H-Ag-CS determined by broth a dilution method. AgOAc and AgNO3 were included as positive controls.**

| MIC | Ag equivalent ($\mu$g/mL) |
|---|---|
| L-Ag-CS | 10.4 |
| M-Ag-CS | 6.4 |
| H-Ag-CS | 6.2 |
| All CC-CS | Up to 300ug/mL, no MIC observed |
| AgOAc | 13.4 |
| $AgNO_3$ | 12.8 |

### 4.4.4 Bacteria inactivation property of M-Ag-CS against *E. coli* and *L. monocytogenes*

The bacteria inactivation property of M-Ag-CS was studied on two bacteria strains: Gram positive *L. monocytogenes* and Gram negative *E. coli* (Figure 4-5). The growth

of *L. monocytogenes* was not effected with the existence of up to 5 $\mu$g/mL $AgNO_3$ in TSB. Whereas Ag-CS with 1 ppm Ag equivalent achieved 0.75 log reduction with 1.5 h treatment and reached 0.97 log reduction with 7 h treatment, however, the growth of *L. monocytogenes* recovered by 10 h and reached a cell density close to that of the control group. Significant log reduction of $AgNO_3$ treated *L. monocytogenes* was observed when Ag equivalent concentration was over 20 $\mu$g/mL, while M-Ag-CS 5 with concentrations over 5 $\mu$g/mL Ag equivalent showed significant inactivation properties. Meanwhile, the bacteria inactivation activity of 5 $\mu$g/mL M-Ag-CS (4.49 log at 10 h) was revealed to be stronger than 20 $\mu$g/mL $AgNO_3$ (4.14 log at 10 h), and M-Ag-CS demonstrated a higher bacteria inactivation efficacy against *L. monocytogenes* than $AgNO_3$ at same concentrations of Ag equivalents (Figure 4-5, A and C).

*E. coli* were found to be less sensitive to M-Ag-CS when Ag concentrations were lower than 5 $\mu$g/mL, and no significant inactivation activity were observed within this concentration range (Figure 4-5, B and D). However, with concentrations higher than 10 $\mu$g/mL, M-Ag-CS resulted a better inactivation activity against *E. coli* over *L. monocytogenes*. Besides, *E. coli* treated by 20 $\mu$g/mL and 30 $\mu$g/mL M-Ag-CS showed a sharp log reduction in 1.5 h and decreased the log number of *E. coli* below the detection limit ($10^2$ CFU/mL), whereas this phenomenon was observed with a higher concentration of $AgNO_3$ (30 $\mu$g/mL Ag equivalent).

Based on the results obtained after 24 h treatment, 1, 5, 10 $\mu$g/mL $AgNO_3$ treated *L. monocytogenes* and 1, 5, 10, 20 $\mu$g/mL $AgNO_3$ treated *E. coli* presented a similar cell density comparing to their control groups. With higher Ag concentration, 20 and 30 $\mu$g/mL $AgNO_3$ treatment slightly inactivated *L. monocytogenes* while 30 $\mu$g/mL $AgNO_3$ strongly inactivated *E. coli* (Figure 4-5, E and F). M-Ag-CS presented a much stronger inactivation activity than $AgNO_3$. 5 and 10 $\mu$g/mL M-Ag-CS caused about 5 log reduction on *L. monocytogenes*, and M-Ag-CS at 20 and 30 $\mu$g/mL resulted over 7 log reduction on *L. monocytogenes*. In M-Ag-CS treated *E. coli*, over 7 log deduction was observed with concentrations higher than 10 $\mu$g/mL Ag equivalents.

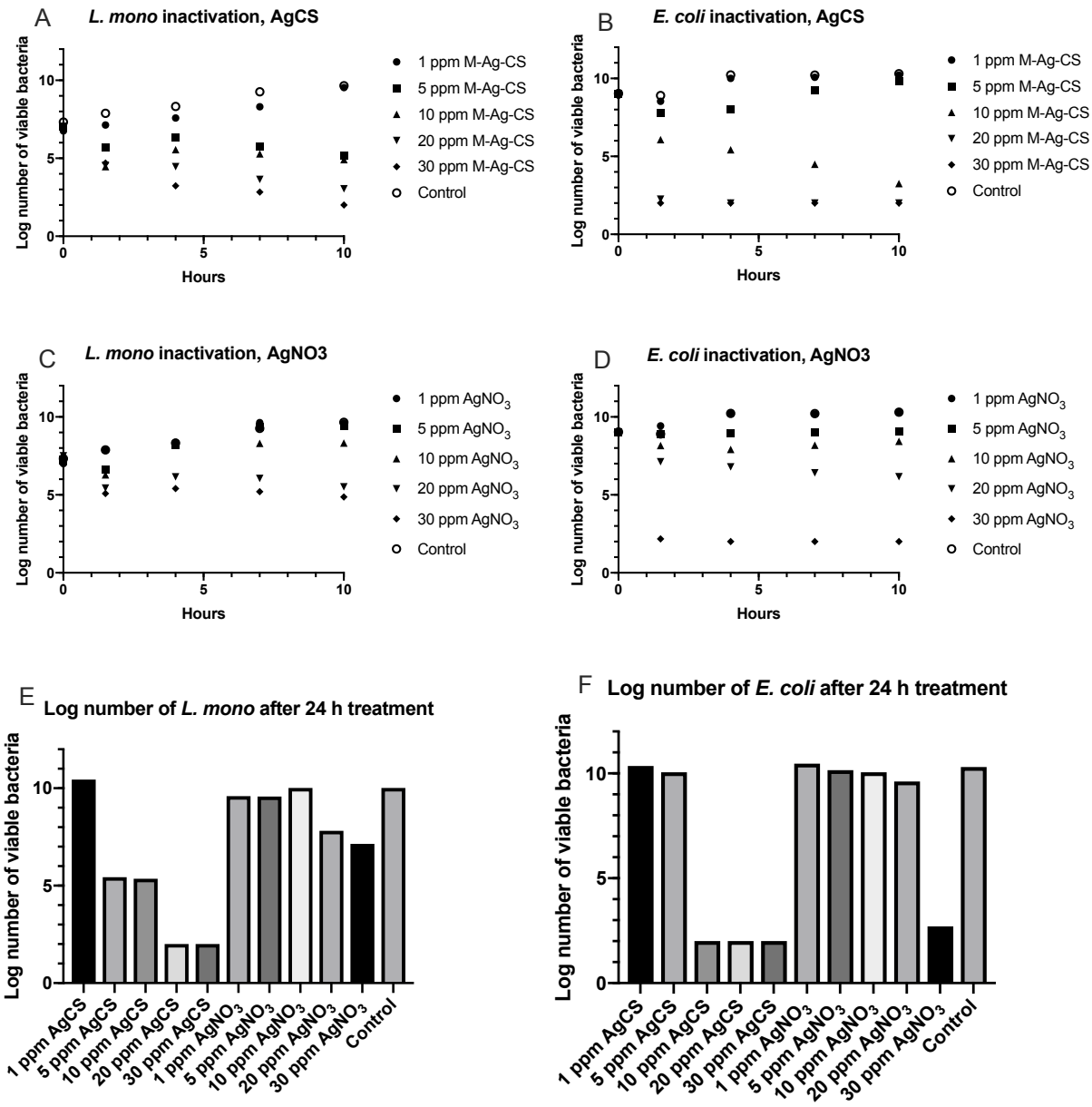


**Figure 4-5**. Bacteria inactivation of *E. coli* and *L. monocytogenes* by Ag-CS at concentrations of 1, 2, 5, 10, 20, 30 ppm Ag equivalents in TSB. Bacteria cells were exposed to Ag-CS for 0, 1.5, 4, 7, 10, and 24 h before enumeration.

### 4.4.5 Antimicrobial activity of Ag-CS coatings on shrimps and strawberries during cold storage

To study the antimicrobial activity of Ag-CS when applied on food, shrimps were dipped in different Ag-CS solutions at the total concentration of 10 $\mu$g/mL Ag equivalents. Shrimps that were dipped in water were used as a control. The treated and control shrimps were stored at 4°C for 12 days, and their quality was examined by 1) observing by eyes and recording appearance changes during storage (Figure 4-6), and 2) measuring total volatile basic nitrogen (TVB-N) after storage (Table 4-2). Visually, the control shrimps presented 13 dark spots in total, whereas the L-Ag-CS, M-Ag-CS, and H-Ag-CS coated shrimps had 8, 7, and 4 black spots in total. The appearance of dark spots was associated with spoilage of shrimps due to the enzymatic oxidation of phenolic compounds. Chemically, after 12 days of storage at 4°C, all Ag-CS-coated shrimps showed lower spoilage levels than control group. The control shrimps had a TVB-N level (78.2±2.6 mg/100g for control shrimp) 3 times higher than all Ag-CS-coated shrimps (19.3±1.4 mg/100g for L-Ag-CS coated shrimp, 14.6±1.9 mg/100g for M-Ag-CS coated shrimp, and 12.2±1.1 mg/100g for H-Ag-CS coated shrimp). The TVB-N level of meat reflects tissue decomposition and has long been used as an indicator of freshness for fishery products. In Australia and Japan, the maximum level of TVB-N for acceptable quality products of shrimps is over 30 mg/ 100g shrimp meat. Both of these results demonstrate the potential applications of Ag-CS on food

products as antimicrobial coating materials to extend shelf life of shrimps and slow down the rate of food spoilage.

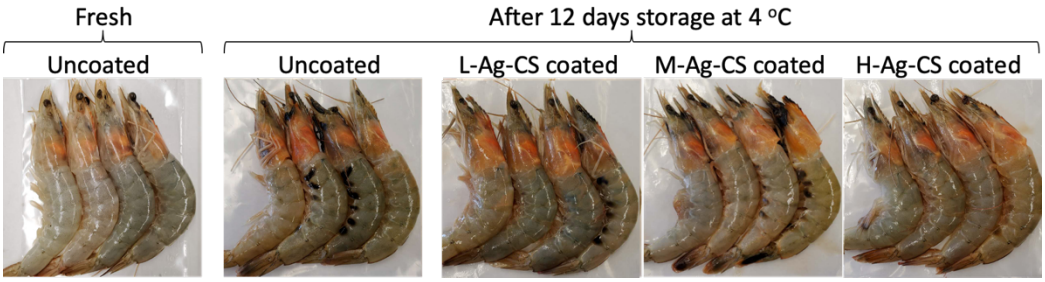


**Figure 4-6**. Appearance changes of coated and uncoated shrimps during cold storage. Shrimps were dip coated in Ag-CS coating solutions with final concentration of 10 $\mu$g/mL Ag equivalent, or DI water for uncoated shrimp. Pictures were taken after 12 days of storage at 4 ˚C.

**Table 4-2. Average TVB-N (mg/100g shrimp meat) compared to fresh shrimps.**

| TVB-N (mg/100g shrimp meat) | | | | |
|---|---|---|---|---|
| **Fresh** | **After 12 days storage at 4 ˚C** | | | |
| Uncoated | Uncoated | L-Ag-CS coated | M-Ag-CS coated | H-Ag-CS coated |
| 4±1.2 | 78.2±2.6 | 19.3±1.4 | 14.6±1.9 | 12.2±1.1 |

To estimate the safety of the Ag-CS coating, the Ag residual level in shrimps and the distribution of Ag residual in shrimps after storage were measured. The results showed that M-Ag-CS treated shrimps contained 0.145 mg Ag per kg of shrimp meat, and contained 1.88 mg Ag per kg of shrimp head & shell. These results indicated that most

Ag was accumulated at the shell of shrimp. Though currently there is no guideline value for Ag allowance in foods or drinking water. In a report "Ag as a drinking-water disinfectant" provided by the World Health Organization, it was suggested that, where Ag salts are used for drinking-water disinfection, a concentration of 0.1 mg/L could be tolerated without risk to health (a concentration that would give a total dose over a 70-year period of half of the human No Observable Adverse Effect Level of 10g Ag intake during lifetime). Although Ag content in treated shrimp meat (0.145 mg/kg) is slightly higher than the 0.1 mg/L, which is the suggested threshold for Ag disinfected drinking water, considering the daily intake amount of shrimp and drinking water, the total intake amount of Ag from treated shrimps could be tolerated without risk to health.

Strawberries were also involved to study the effectiveness of Ag-CS as an antimicrobial coating material. Fresh organic strawberries were coated by M-Ag-CS (10 $\mu$g/mL Ag equivalents) and stored at 4$^{o}$C. After 8 days storage, the uncoated strawberries showed large dark decay area on the strawberries, while no large decay area presented in M-Ag-CS coated strawberries (Figure 4-7). The results indicated that uncoated strawberries underwent faster decay than coated strawberries, and the M-Ag-CS coating effectively extended the shelf-life of strawberries under 4°C.

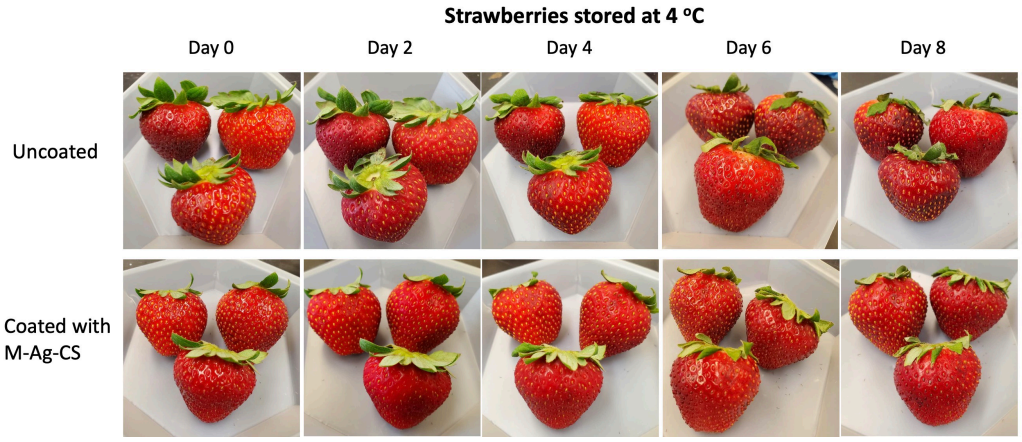


**Figure 4-7**. Appearance changes of coated and uncoated strawberries during cold storage. Strawberries were dip coated by M-Ag-CS coating solution with final concentration of 10 $\mu$g/mL Ag equivalent, and DI water was used for the group of uncoated strawberries. Pictures were taken every other day for a total 8 days storage at 4°C.

## *4.5 Conclusion*

In this study, the bacteria inhibition and inactivation properties of Ag-CS have been carefully studied. The Ag-CS with three substitution degrees were synthesized through a two-step chemical modification. Ag-CS at all substitution degrees presented a higher antimicrobial efficacy than that of AgOAc at the same Ag equivalents. Moreover, the antimicrobial effects of Ag-CS varied in different conditions. L-Ag-CS offered the highest antimicrobial effect in liquid medium at high volume, for the combined effect of Ag induced antimicrobial activity and CS induced co-precipitation of CS and bacteria cells. H-Ag-CS on agar possessed the strongest antimicrobial effects than M-Ag-CS and L-Ag-CS for its high local concentration of Ag. In the bacteria inactivation

test, M-Ag-CS demonstrated stronger bacteria inactivation properties than $AgNO_3$ at the same concentrations of Ag equivalents against *E. coli* and *L. monocytogenes* . Further application of Ag-CS on shrimps and strawberries for shelf life extension confirmed the strong antimicrobial activity of Ag-CS on food products. All these properties ensured the Ag-CS as a promising potent antimicrobial coating material with great potentials to be used in the food area.

# Chapter 5: Summary and Future Perspectives

In the past decades, many work have been conducted on the development of Ag-based antimicrobial agents, and greatly enriched the characteristics of food packaging materials. However, more efforts are needed to improve the efficiency and safety of Ag-based antimicrobial agents. AgNCs and Ag-CS were distinguished from other Ag-based antimicrobial agents for their 1) unique structures: the ultrasmall particles size (~2 nm) of AgNCs and the coreless structure of Ag-CS; 2) great potential of endowing high antimicrobial efficiency against several bacteria strains. However, limited studies have been conducted on investigating their antimicrobial properties and exploring potential applications in food areas. In this dissertation, AgNCs and Ag-CS were thoroughly studied for their preparation, characterization, chemical properties, antimicrobial efficacy, and safety. Several experiments were carried out and results indicated that AgNCs and Ag-CS presented a stronger antimicrobial efficiency over $AgNO_3$ or AgOAc.

Both AgNCs and Ag-CS are considered new as antimicrobial agents, and their applications in food areas have rarely been studied. To further explore the applications of AgNCs and Ag-CS, several directions could be considered: 1) Investigating the incorporation of AgNCs and Ag-CS into commonly used packaging materials, the stability, distribution, and compatibility of incorporated AgNCs and Ag-CS in different packaging materials (e.g. plastics, cardboard, paper) should be studied, and the

incorporation methods and techniques need to be established; 2) Improving the antimicrobial effects of AgNCs and Ag-CS by combining them with other antimicrobial agents, and study their hurdle effects, thus to lower the application dose of AgNCs and Ag-CS and to enhance the safety of AgNCs and Ag-CS; 3) Understanding the antimicrobial mechanism of AgNCs and Ag-CS *in vitro* and *in vivo*. In the *in vitro* study, changes of cell membrane, oxidative stress in cells, and DNA/RNA proliferations in cells that resulted by exposing to AgNCs and Ag-CS should be monitored. In the *in vivo* study, changes to tissues, organs and life spans of animals exposed to AgNCs and Ag-CS should be recorded; 4) Studying the metabolism of AgNCs and Ag-CS in animal models by monitoring changes on their stabilities, sizes, and structures after entering animals. Meanwhile, the dissociation of AgNCs and Ag-CS and corresponded dissociated substances should also be investigated and quantified. 5) Studying the migration procedure of AgNCs or Ag-CS from packaging materials into food products and the distribution of them in food products to ensure the safety. 6) Guidelines and regulations remain to be established for the incorporation of AgNCs and Ag-CS into food packaging systems as antimicrobial agents.

# Bibliography


(1) Huang, Y.; Mei, L.; Chen, X.; Wang, Q. Recent Developments in Food Packaging Based on Nanomaterials. *Nanomaterials (Basel, Switzerland)* **2018**, *8* (10). https://doi.org/10.3390/nano8100830.

(2) Mousavi Khaneghah, A.; Hashemi, S. M. B.; Limbo, S. Antimicrobial Agents and Packaging Systems in Antimicrobial Active Food Packaging: An Overview of Approaches and Interactions. *Food and Bioproducts Processing* **2018**, *111*, 1–19. https://doi.org/10.1016/j.fbp.2018.05.001.

(3) Bondarenko, O. M.; Sihtmäe, M.; Kuzmičiova, J.; Ragelienė, L.; Kahru, A.; Daugelavičius, R. Plasma Membrane Is the Target of Rapid Antibacterial Action of Silver Nanoparticles in Escherichia Coli and Pseudomonas Aeruginosa. *Int J Nanomedicine* **2018**, *13*, 6779–6790. https://doi.org/10.2147/IJN.S177163.

(4) Biswas, M. C.; Tiimob, B. J.; Abdela, W.; Jeelani, S.; Rangari, V. K. Nano Silica-Carbon-Silver Ternary Hybrid Induced Antimicrobial Composite Films for Food Packaging Application. *Food Packaging and Shelf Life* **2019**, *19*, 104–113. https://doi.org/10.1016/j.fpsl.2018.12.003.

(5) Hoseinnejad, M.; Jafari, S. M.; Katouzian, I. Inorganic and Metal Nanoparticles and Their Antimicrobial Activity in Food Packaging Applications. *Critical Reviews in Microbiology* **2018**, *44* (2), 161–181. https://doi.org/10.1080/1040841X.2017.1332001.

(6) Gyawali, R.; Ibrahim, S. A. Natural Products as Antimicrobial Agents. *Food Control* **2014**, *46*, 412–429. https://doi.org/10.1016/j.foodcont.2014.05.047.

(7) Hammer, K. A.; Carson, C. F.; Riley, T. V. Antimicrobial Activity of Essential Oils and Other Plant Extracts. *Journal of Applied Microbiology* **1999**, *86* (6), 985–990. https://doi.org/10.1046/j.1365-2672.1999.00780.x.

(8) Jayasena, D. D.; Jo, C. Essential Oils as Potential Antimicrobial Agents in Meat and Meat Products: A Review. *Trends in Food Science & Technology* **2013**, *34* (2), 96–108. https://doi.org/10.1016/j.tifs.2013.09.002.

(9) Abdallah, E. M. Plants: An Alternative Source for Antimicrobials. *Journal of Applied Pharmaceutical Science* 5.

(10) Guo, J.; Sun, W.; Kim, J. P.; Lu, X.; Li, Q.; Lin, M.; Mrowczynski, O.; Rizk, E. B.; Cheng, J.; Qian, G.; Yang, J. Development of Tannin-Inspired Antimicrobial Bioadhesives. *Acta Biomaterialia* **2018**, *72*, 35–44. https://doi.org/10.1016/j.actbio.2018.03.008.

(11) de Almeida Roger, J.; Magro, M.; Spagnolo, S.; Bonaiuto, E.; Baratella, D.; Fasolato, L.; Vianello, F. Antimicrobial and Magnetically Removable Tannic Acid Nanocarrier: A Processing Aid for Listeria Monocytogenes Treatment for Food Industry Applications. *Food Chemistry* **2018**, *267*, 430–436. https://doi.org/10.1016/j.foodchem.2017.06.109.

(12) Keymanesh, K.; Soltani, S.; Sardari, S. Application of Antimicrobial Peptides in Agriculture and Food Industry. *World J Microbiol Biotechnol* **2009**, *25* (6), 933–944. https://doi.org/10.1007/s11274-009-9984-7.

(13) Shin, J. m.; Gwak, J. w.; Kamarajan, P.; Fenno, J. c.; Rickard, A. h.; Kapila, Y. l. Biomedical Applications of Nisin. *Journal of Applied Microbiology* **2016**, *120* (6), 1449–1465. https://doi.org/10.1111/jam.13033.

(14) Thallinger, B.; Prasetyo, E. N.; Nyanhongo, G. S.; Guebitz, G. M. Antimicrobial Enzymes: An Emerging Strategy to Fight Microbes and Microbial Biofilms. *Biotechnology Journal* **2013**, *8* (1), 97–109. https://doi.org/10.1002/biot.201200313.

(15) Berlemont, R. Distribution and Diversity of Enzymes for Polysaccharide Degradation in Fungi. *Sci Rep* **2017**, *7*. https://doi.org/10.1038/s41598-017-00258-w.

(16) Kanmani, P.; Rhim, J.-W. Physical, Mechanical and Antimicrobial Properties of Gelatin Based Active Nanocomposite Films Containing AgNPs and Nanoclay. *Food Hydrocolloids* **2014**, *35*, 644–652. https://doi.org/10.1016/j.foodhyd.2013.08.011.

(17) Park, E.-S.; Moon, W.-S.; Song, M.-J.; Kim, M.-N.; Chung, K.-H.; Yoon, J.-S. Antimicrobial Activity of Phenol and Benzoic Acid Derivatives. *International Biodeterioration & Biodegradation* **2001**, *47* (4), 209–214. https://doi.org/10.1016/S0964-8305(01)00058-0.

(18) Kumar, Rajesh; Umar, Ahmad; Kumar, Girish; Nalwa, H. S. Antimicrobial Properties of ZnO Nanomaterials: A Review. *Ceramics International* **2017**, *43* (5), 3940–3961. https://doi.org/10.1016/j.ceramint.2016.12.062.

(19) Noshirvani, N.; Ghanbarzadeh, B.; Rezaei Mokarram, R.; Hashemi, M. Novel Active Packaging Based on Carboxymethyl Cellulose-Chitosan-ZnO NPs Nanocomposite for Increasing the Shelf Life of Bread. *Food Packaging and Shelf Life* **2017**, *11*, 106–114. https://doi.org/10.1016/j.fpsl.2017.01.010.

(20) Sandwich-Architectured Poly(lactic acid)–Graphene Composite Food Packaging Films | ACS Applied Materials & Interfaces https://pubs-acs-org.proxy-um.researchport.umd.edu/doi/abs/10.1021/acsami.6b02498 (accessed Oct 8, 2020).

(21) Liu, S.; Zeng, T. H.; Hofmann, M.; Burcombe, E.; Wei, J.; Jiang, R.; Kong, J.; Chen, Y. Antibacterial Activity of Graphite, Graphite Oxide, Graphene Oxide, and Reduced Graphene Oxide: Membrane and Oxidative Stress. *ACS Nano* **2011**, *5* (9), 6971–6980. https://doi.org/10.1021/nn202451x.

(22) Xie, J.; Hung, Y.-C. UV-A Activated TiO2 Embedded Biodegradable Polymer Film for Antimicrobial Food Packaging Application. *LWT* **2018**, *96*, 307–314. https://doi.org/10.1016/j.lwt.2018.05.050.

(23) Subhapriya, S.; Gomathipriya, P. Green Synthesis of Titanium Dioxide (TiO2) Nanoparticles by Trigonella Foenum-Graecum Extract and Its Antimicrobial Properties. *Microbial Pathogenesis* **2018**, *116*, 215–220. https://doi.org/10.1016/j.micpath.2018.01.027.

(24) Mehrabani, M. G.; Karimian, R.; Rakhshaei, R.; Pakdel, F.; Eslami, H.; Fakhrzadeh, V.; Rahimi, M.; Salehi, R.; Kafil, H. S. Chitin/Silk Fibroin/TiO2 Bio-Nanocomposite as a Biocompatible Wound Dressing Bandage with Strong Antimicrobial Activity. *International Journal of Biological Macromolecules* **2018**, *116*, 966–976. https://doi.org/10.1016/j.ijbiomac.2018.05.102.

(25) Amirsoleimani, M.; Khalilzadeh, M. A.; Sadeghifar, F.; Sadeghifar, H. Surface Modification of Nanosatrch Using Nano Silver: A Potential Antibacterial for Food Package Coating. *J Food Sci Technol* **2018**, *55* (3), 899–904. https://doi.org/10.1007/s13197-017-2996-7.

(26) Dakal, T. C.; Kumar, A.; Majumdar, R. S.; Yadav, V. Mechanistic Basis of Antimicrobial Actions of Silver Nanoparticles. *Front. Microbiol.* **2016**, *7*. https://doi.org/10.3389/fmicb.2016.01831.

(27) Sondi, I.; Salopek-Sondi, B. Silver Nanoparticles as Antimicrobial Agent: A Case Study on E. Coli as a Model for Gram-Negative Bacteria. *Journal of Colloid and Interface Science* **2004**, *275* (1), 177–182. https://doi.org/10.1016/j.jcis.2004.02.012.

(28) Rai, M. k.; Deshmukh, S. d.; Ingle, A. p.; Gade, A. k. Silver Nanoparticles: The Powerful Nanoweapon against Multidrug-Resistant Bacteria. *Journal of Applied Microbiology* **2012**, *112* (5), 841–852. https://doi.org/10.1111/j.1365-2672.2012.05253.x.

(29) Javani, S.; Lorca, R.; Latorre, A.; Flors, C.; Cortajarena, A. L.; Somoza, Á. Antibacterial Activity of DNA-Stabilized Silver Nanoclusters Tuned by Oligonucleotide Sequence. *ACS Appl. Mater. Interfaces* **2016**, *8* (16), 10147–10154. https://doi.org/10.1021/acsami.6b00670.

(30) Sharma, M.; Padmavathy, N.; Remanan, S.; Madras, G.; Bose, S. Facile One-Pot Scalable Strategy to Engineer Biocidal Silver Nanocluster Assembly on Thiolated PVDF Membranes for Water Purification. *RSC Advances* **2016**, *6* (45), 38972–38983. https://doi.org/10.1039/C6RA03143A.

(31) S. Alahmadi, N.; W. Betts, J.; Heinze, T.; M. Kelly, S.; Koschella, A.; D. Wadhawan, J. Synthesis and Antimicrobial Effects of Highly Dispersed, Cellulose-Stabilized Silver/Cellulose Nanocomposites. *RSC Advances* **2018**, *8* (7), 3646–3656. https://doi.org/10.1039/C7RA12280B.

(32) Ibrahim, Z.; Ahmad, W. A.; Baba, A. B. Bioaccumulation of Silver and the Isolation of Metal-Binding Protein from P.Diminuta. *Brazilian Archives of Biology and Technology* **2001**, *44* (3), 223–225. https://doi.org/10.1590/S1516-89132001000300001.

(33) Geyik, A. G.; Çeçen, F. Exposure of Activated Sludge to Nanosilver and Silver Ion: Inhibitory Effects and Binding to the Fractions of Extracellular Polymeric Substances. *Bioresource Technology* **2016**, *211*, 691–697. https://doi.org/10.1016/j.biortech.2016.03.157.

(34) Mohite, B. V.; Koli, S. H.; Patil, S. V. Heavy Metal Stress and Its Consequences on Exopolysaccharide (EPS)-Producing Pantoea Agglomerans. *Appl Biochem*

*Biotechnol* **2018**, *186* (1), 199–216. https://doi.org/10.1007/s12010-018-2727-1.

(35) Gudipaty, S. A.; McEvoy, M. M. The Histidine Kinase CusS Senses Silver Ions through Direct Binding by Its Sensor Domain. *Biochimica et Biophysica Acta (BBA) - Proteins and Proteomics* **2014**, *1844* (9), 1656–1661. https://doi.org/10.1016/j.bbapap.2014.06.001.

(36) Liao, X.; Yang, F.; Li, H.; So, P.-K.; Yao, Z.; Xia, W.; Sun, H. Targeting the Thioredoxin Reductase–Thioredoxin System from Staphylococcus Aureus by Silver Ions. *Inorg. Chem.* **2017**, *56* (24), 14823–14830. https://doi.org/10.1021/acs.inorgchem.7b01904.

(37) Tambosi, R.; Liotenberg, S.; Bourbon, M.-L.; Steunou, A.-S.; Babot, M.; Durand, A.; Kebaili, N.; Ouchane, S. Silver and Copper Acute Effects on Membrane Proteins and Impact on Photosynthetic and Respiratory Complexes in Bacteria. *mBio* **2018**, *9* (6), e01535-18. https://doi.org/10.1128/mBio.01535-18.

(38) Duan, X.; Peng, D.; Zhang, Y.; Huang, Y.; Liu, X.; Li, R.; Zhou, X.; Liu, J. Sub-Cytotoxic Concentrations of Ionic Silver Promote the Proliferation of Human Keratinocytes by Inducing the Production of Reactive Oxygen Species. *Frontiers of Medicine* **2018**, *12* (3), 289–300. https://doi.org/10.1007/s11684-017-0550-7.

(39) Wu, Y.; Zhang, L.; Zhou, Y.; Zhang, L.; Li, Y.; Liu, Q.; Hu, J.; Yang, J. Light-Induced ZnO/Ag/RGO Bactericidal Photocatalyst with Synergistic Effect of Sustained Release of Silver Ions and Enhanced Reactive Oxygen Species. *Chinese Journal of Catalysis* **2019**, *40* (5), 691–702. https://doi.org/10.1016/S1872-2067(18)63193-6.

(40) Martínez-Castañón, G. A.; Niño-Martínez, N.; Martínez-Gutierrez, F.; Martínez-Mendoza, J. R.; Ruiz, F. Synthesis and Antibacterial Activity of Silver Nanoparticles with Different Sizes. *J Nanopart Res* **2008**, *10* (8), 1343–1348. https://doi.org/10.1007/s11051-008-9428-6.

(41) Mafuné, Fumitaka; Kohno, J.; Takeda, Y.; Kondow, T.; Sawabe, H. Structure and Stability of Silver Nanoparticles in Aqueous Solution Produced by Laser Ablation. *J. Phys. Chem. B* **2000**, *104* (35), 8333–8337. https://doi.org/10.1021/jp001803b.

(42) Yu, D.; Yam, V. W.-W. Hydrothermal-Induced Assembly of Colloidal Silver Spheres into Various Nanoparticles on the Basis of HTAB-Modified Silver Mirror Reaction. *J. Phys. Chem. B* **2005**, *109* (12), 5497–5503. https://doi.org/10.1021/jp0448346.

(43) Chen, Y.-H.; Yeh, C.-S. Laser Ablation Method: Use of Surfactants to Form the Dispersed Ag Nanoparticles. *Colloids and Surfaces A: Physicochemical and Engineering Aspects* **2002**, *197* (1), 133–139. https://doi.org/10.1016/S0927-7757(01)00854-8.

(44) Morones, J. R.; Elechiguerra, J. L.; Camacho, A.; Holt, K.; Kouri, J. B.; Ramírez, J. T.; Yacaman, M. J. The Bactericidal Effect of Silver Nanoparticles.

*Nanotechnology* **2005**, *16* (10), 2346–2353. https://doi.org/10.1088/0957-4484/16/10/059.

(45) Agnihotri, S.; Mukherji, S.; Mukherji, S. Size-Controlled Silver Nanoparticles Synthesized over the Range 5–100 Nm Using the Same Protocol and Their Antibacterial Efficacy. *RSC Adv.* **2013**, *4* (8), 3974–3983. https://doi.org/10.1039/C3RA44507K.

(46) Zheng, K.; Setyawati, M. I.; Leong, D. T.; Xie, J. Antimicrobial Silver Nanomaterials. *Coordination Chemistry Reviews* **2018**, *357*, 1–17. https://doi.org/10.1016/j.ccr.2017.11.019.

(47) Gnanadhas, D. P.; Ben Thomas, M.; Thomas, R.; Raichur, A. M.; Chakravortty, D. Interaction of Silver Nanoparticles with Serum Proteins Affects Their Antimicrobial Activity *In Vivo*. *Antimicrobial Agents and Chemotherapy* **2013**, *57* (10), 4945–4955. https://doi.org/10.1128/AAC.00152-13.

(48) Ivask, A.; Visnapuu, M.; Vallotton, P.; Marzouk, E. R.; Lombi, E.; Voelcker, N. H. Quantitative Multimodal Analyses of Silver Nanoparticle-Cell Interactions: Implications for Cytotoxicity. *NanoImpact* **2016**, *1*, 29–38. https://doi.org/10.1016/j.impact.2016.02.003.

(49) Fayaz, A. M.; Balaji, K.; Girilal, M.; Yadav, R.; Kalaichelvan, P. T.; Venketesan, R. Biogenic Synthesis of Silver Nanoparticles and Their Synergistic Effect with Antibiotics: A Study against Gram-Positive and Gram-Negative Bacteria. *Nanomedicine: Nanotechnology, Biology and Medicine* **2010**, *6* (1), 103–109. https://doi.org/10.1016/j.nano.2009.04.006.

(50) Ruden, S.; Hilpert, K.; Berditsch, M.; Wadhwani, P.; Ulrich, A. S. Synergistic Interaction between Silver Nanoparticles and Membrane-Permeabilizing Antimicrobial Peptides. *Antimicrobial Agents and Chemotherapy* **2009**, *53* (8), 3538–3540. https://doi.org/10.1128/AAC.01106-08.

(51) Akram, F. E.; El-Tayeb, T.; Abou-Aisha, K.; El-Azizi, M. A Combination of Silver Nanoparticles and Visible Blue Light Enhances the Antibacterial Efficacy of Ineffective Antibiotics against Methicillin-Resistant Staphylococcus Aureus (MRSA). *Annals of Clinical Microbiology and Antimicrobials* **2016**, *15* (1), 48. https://doi.org/10.1186/s12941-016-0164-y.

(52) He, D.; Dorantes-Aranda, J. J.; Waite, T. D. Silver Nanoparticle—Algae Interactions: Oxidative Dissolution, Reactive Oxygen Species Generation and Synergistic Toxic Effects. *Environ. Sci. Technol.* **2012**, *46* (16), 8731–8738. https://doi.org/10.1021/es300588a.

(53) Lotfi, S.; Ahari, H.; Sahraeyan, R. The effect of silver nanocomposite packaging based on melt mixing and sol–gel methods on shelf life extension of fresh chicken stored at 4 °C https://onlinelibrary.wiley.com/doi/abs/10.1111/jfs.12625 (accessed Jun 21, 2019). https://doi.org/10.1111/jfs.12625.

(54) Wu, Z.; Zhou, W.; Pang, C.; Deng, W.; Xu, C.; Wang, X. Multifunctional Chitosan-Based Coating with Liposomes Containing Laurel Essential Oils and

Nanosilver for Pork Preservation. *Food Chemistry* **2019**, *295*, 16–25. https://doi.org/10.1016/j.foodchem.2019.05.114.

(55) Yu, Z.; Wang, W.; Kong, F.; Lin, M.; Mustapha, A. Cellulose Nanofibril/Silver Nanoparticle Composite as an Active Food Packaging System and Its Toxicity to Human Colon Cells. *International Journal of Biological Macromolecules* **2019**, *129*, 887–894. https://doi.org/10.1016/j.ijbiomac.2019.02.084.

(56) Vishnuvarthanan, M.; Rajeswari, N. Preparation and Characterization of Carrageenan/Silver Nanoparticles/Laponite Nanocomposite Coating on Oxygen Plasma Surface Modified Polypropylene for Food Packaging. *J Food Sci Technol* **2019**, *56* (5), 2545–2552. https://doi.org/10.1007/s13197-019-03735-4.

(57) Kostic, D.; Vukasinovic-Sekulic, M.; Armentano, I.; Torre, L.; Obradovic, B. Multifunctional Ternary Composite Films Based on PLA and Ag/Alginate Microbeads: Physical Characterization and Silver Release Kinetics. *Materials Science and Engineering: C* **2019**, *98*, 1159–1168. https://doi.org/10.1016/j.msec.2019.01.074.

(58) Kadam, D.; Momin, B.; Palamthodi, S.; Lele, S. S. Physicochemical and Functional Properties of Chitosan-Based Nano-Composite Films Incorporated with Biogenic Silver Nanoparticles. *Carbohydrate Polymers* **2019**, *211*, 124–132. https://doi.org/10.1016/j.carbpol.2019.02.005.

(59) Jokar, M.; Pedersen, G. A.; Loeschner, K. Six Open Questions about the Migration of Engineered Nano-Objects from Polymer-Based Food-Contact Materials: A Review. *Food Additives & Contaminants: Part A* **2017**, *34* (3), 434–450. https://doi.org/10.1080/19440049.2016.1271462.

(60) Pillai, K. V.; J. Gray, P.; Tien, C.-C.; Bleher, R.; Sung, L.-P.; Duncan, T. V. Environmental Release of Core–Shell Semiconductor Nanocrystals from Free-Standing Polymer Nanocomposite Films. *Environmental Science: Nano* **2016**, *3* (3), 657–669. https://doi.org/10.1039/C6EN00064A.

(61) Weiner, R. G.; Sharma, A.; Xu, H.; Gray, P. J.; Duncan, T. V. Assessment of Mass Transfer from Poly(Ethylene) Nanocomposites Containing Noble-Metal Nanoparticles: A Systematic Study of Embedded Particle Stability. *ACS Appl. Nano Mater.* **2018**, *1* (9), 5188–5196. https://doi.org/10.1021/acsanm.8b01241.

(62) Hannon, J. C.; Kerry, J. P.; Cruz-Romero, M.; Azlin-Hasim, S.; Morris, M.; Cummins, E. Kinetic Desorption Models for the Release of Nanosilver from an Experimental Nanosilver Coating on Polystyrene Food Packaging. *Innovative Food Science & Emerging Technologies* **2017**, *44*, 149–158. https://doi.org/10.1016/j.ifset.2017.07.001.

(63) Soleimani, J.; Ghanbarzadeh, B.; Dehghannya, J.; Baheri, I. S.; Sorouraddin, S. M. Comparative Numerical Study of Titanium and Silver Nano-Particles Migration from Nano-Composite of Polystyrene into Simulants on Experimental Data Basis. *International Journal of Food Engineering* **2017**, *13* (12). https://doi.org/10.1515/ijfe-2017-0091.

(64) Chen, H.-B.; Hu, C.-Y. Influence of PP Types on Migration of Zinc from Nano-ZnO/PP Composite Films. *Packaging Technology and Science* **2018**, *31* (11), 747–753. https://doi.org/10.1002/pts.2411.

(65) Hannon, J. C.; Kerry, J. P.; Cruz-Romero, M.; Azlin-Hasim, S.; Morris, M.; Cummins, E. Migration Assessment of Silver from Nanosilver Spray Coated Low Density Polyethylene or Polyester Films into Milk. *Food Packaging and Shelf Life* **2018**, *15*, 144–150. https://doi.org/10.1016/j.fpsl.2018.01.002.

(66) Cushen, M.; Kerry, J.; Morris, M.; Cruz-Romero, M.; Cummins, E. Evaluation and Simulation of Silver and Copper Nanoparticle Migration from Polyethylene Nanocomposites to Food and an Associated Exposure Assessment. *J. Agric. Food Chem.* **2014**, *62* (6), 1403–1411. https://doi.org/10.1021/jf404038y.

(67) Hannon, J. C.; Kerry, J. P.; Cruz-Romero, M.; Azlin-Hasim, S.; Morris, M.; Cummins, E. Human Exposure Assessment of Silver and Copper Migrating from an Antimicrobial Nanocoated Packaging Material into an Acidic Food Simulant. *Food and Chemical Toxicology* **2016**, *95*, 128–136. https://doi.org/10.1016/j.fct.2016.07.004.

(68) Metak, A. M.; Nabhani, F.; Connolly, S. N. Migration of Engineered Nanoparticles from Packaging into Food Products. *LWT - Food Science and Technology* **2015**, *64* (2), 781–787. https://doi.org/10.1016/j.lwt.2015.06.001.

(69) Jo, Y.-K.; Kim, B. H.; Jung, G. Antifungal Activity of Silver Ions and Nanoparticles on Phytopathogenic Fungi. *Plant Disease* **2009**, *93* (10), 1037–1043. https://doi.org/10.1094/PDIS-93-10-1037.

(70) Silva, J. M. de S. e; Pastorello, M.; Kobarg, J.; Cardoso, M. B.; Mazali, I. O. Selective Synthesis of Silver Nanoparticles onto Potassium Hexaniobate: Structural Organisation with Bactericidal Properties https://onlinelibrary.wiley.com/doi/abs/10.1002/cphc.201300855 (accessed Jun 19, 2019). https://doi.org/10.1002/cphc.201300855.

(71) Yuan, X.; Setyawati, M. I.; Tan, A. S.; Ong, C. N.; Leong, D. T.; Xie, J. Highly Luminescent Silver Nanoclusters with Tunable Emissions: Cyclic Reduction–Decomposition Synthesis and Antimicrobial Properties. *NPG Asia Materials* **2013**, *5* (2), e39. https://doi.org/10.1038/am.2013.3.

(72) Mosselhy, D. A.; El-Aziz, M. A.; Hanna, M.; Ahmed, M. A.; Husien, M. M.; Feng, Q. Comparative Synthesis and Antimicrobial Action of Silver Nanoparticles and Silver Nitrate. *J Nanopart Res* **2015**, *17* (12), 473. https://doi.org/10.1007/s11051-015-3279-8.

(73) Kaloti, M.; Kumar, A. Synthesis of Chitosan-Mediated Silver Coated γ-$Fe_2O_3$ (Ag–γ-$Fe_2O_3$@Cs) Superparamagnetic Binary Nanohybrids for Multifunctional Applications. *The Journal of Physical Chemistry C* **2016**, *120* (31), 17627–17644. https://doi.org/10.1021/acs.jpcc.6b05851.

(74) Chaudhari, A. A.; Jasper, S. L.; Dosunmu, E.; Miller, M. E.; Arnold, R. D.; Singh, S. R.; Pillai, S. Novel Pegylated Silver Coated Carbon Nanotubes Kill Salmonella but They Are Non-Toxic to Eukaryotic Cells. *Journal of*

*Nanobiotechnology* **2015**, *13* (1), 23. https://doi.org/10.1186/s12951-015-0085-5.

(75) Dasgupta, N.; Ranjan, S.; Rajendran, B.; Manickam, V.; Ramalingam, C.; Avadhani, G. S.; Kumar, A. Thermal Co-Reduction Approach to Vary Size of Silver Nanoparticle: Its Microbial and Cellular Toxicology. *Environ Sci Pollut Res* **2016**, *23* (5), 4149–4163. https://doi.org/10.1007/s11356-015-4570-z.

(76) Kumari, R.; Brahma, G.; Rajak, S.; Singh, M.; Kumar, S. Antimicrobial Activity of Green Silver Nanoparticles Produced Using Aqueous Leaf Extract of Hydrocotyle Rotundifolia. *Orient Pharm Exp Med* **2016**, *16* (3), 195–201. https://doi.org/10.1007/s13596-016-0236-8.

(77) Silvan, J. M.; Zorraquin-Peña, I.; Gonzalez de Llano, D.; Moreno-Arribas, M. V.; Martinez-Rodriguez, A. J. Antibacterial Activity of Glutathione-Stabilized Silver Nanoparticles Against Campylobacter Multidrug-Resistant Strains. *Front. Microbiol.* **2018**, *9*. https://doi.org/10.3389/fmicb.2018.00458.

(78) Sharma, R.; Singh, P.; Dharela, R.; Singh Chauhan, G.; Chauhan, K. Thiourea Functionalized β-Cyclodextrin as Green Reducing and Stabilizing Agent for Silver Nanocomposites with Enhanced Antimicrobial and Antioxidant Properties. *New Journal of Chemistry* **2017**, *41* (21), 12645–12654. https://doi.org/10.1039/C7NJ00759K.

(79) Huang, X.; Pang, Y.; Liu, Y.; Zhou, Y.; Wang, Z.; Hu, Q. Green Synthesis of Silver Nanoparticles with High Antimicrobial Activity and Low Cytotoxicity Using Catechol-Conjugated Chitosan. *RSC Advances* **2016**, *6* (69), 64357–64363. https://doi.org/10.1039/C6RA09035D.

(80) Wan, X.; Zhuang, L.; She, B.; Deng, Y.; Chen, D.; Tang, J. In-Situ Reduction of Monodisperse Nanosilver on Hierarchical Wrinkled Mesoporous Silica with Radial Pore Channels and Its Antibacterial Performance. *Materials Science and Engineering: C* **2016**, *65*, 323–330. https://doi.org/10.1016/j.msec.2016.04.058.

(81) Jena, S.; Singh, R. K.; Panigrahi, B.; Suar, M.; Mandal, D. Photo-Bioreduction of Ag+ Ions towards the Generation of Multifunctional Silver Nanoparticles: Mechanistic Perspective and Therapeutic Potential. *Journal of Photochemistry and Photobiology B: Biology* **2016**, *164*, 306–313. https://doi.org/10.1016/j.jphotobiol.2016.08.048.

(82) Farrag, M.; Mohamed, R. A. Ecotoxicity of ~1nm Silver and Palladium Nanoclusters Protected by L-Glutathione on the Microbial Growth under Light and Dark Conditions. *Journal of Photochemistry and Photobiology A: Chemistry* **2016**, *330*, 117–125. https://doi.org/10.1016/j.jphotochem.2016.07.027.

(83) Mei, L.; Teng, Z.; Zhu, G.; Liu, Y.; Zhang, F.; Zhang, J.; Li, Y.; Guan, Y.; Luo, Y.; Chen, X.; Wang, Q. Silver Nanocluster-Embedded Zein Films as Antimicrobial Coating Materials for Food Packaging. *ACS Appl. Mater. Interfaces* **2017**, *9* (40), 35297–35304. https://doi.org/10.1021/acsami.7b08152.

(84) Carbone, M.; Donia, D. T.; Sabbatella, G.; Antiochia, R. Silver Nanoparticles in Polymeric Matrices for Fresh Food Packaging. *Journal of King Saud University - Science* **2016**, *28* (4), 273–279. https://doi.org/10.1016/j.jksus.2016.05.004.

(85) Sadeghnejad, A.; Aroujalian, A.; Raisi, A.; Fazel, S. Antibacterial Nano Silver Coating on the Surface of Polyethylene Films Using Corona Discharge. *Surface and Coatings Technology* **2014**, *245*, 1–8. https://doi.org/10.1016/j.surfcoat.2014.02.023.

(86) Zhao, Q.; Wang, C.; Liu, Y.; Wang, S. Bacterial Adhesion on the Metal-Polymer Composite Coatings. *International Journal of Adhesion and Adhesives* **2007**, *27* (2), 85–91. https://doi.org/10.1016/j.ijadhadh.2006.01.001.

(87) Bahrami, A.; Rezaei Mokarram, R.; Sowti Khiabani, M.; Ghanbarzadeh, B.; Salehi, R. Physico-Mechanical and Antimicrobial Properties of Tragacanth/Hydroxypropyl Methylcellulose/Beeswax Edible Films Reinforced with Silver Nanoparticles. *International Journal of Biological Macromolecules* **2019**, *129*, 1103–1112. https://doi.org/10.1016/j.ijbiomac.2018.09.045.

(88) Orsuwan, A.; Shankar, S.; Wang, L.-F.; Sothornvit, R.; Rhim, J.-W. Preparation of Antimicrobial Agar/Banana Powder Blend Films Reinforced with Silver Nanoparticles. *Food Hydrocolloids* **2016**, *60*, 476–485. https://doi.org/10.1016/j.foodhyd.2016.04.017.

(89) Jin, R.; Zeng, C.; Zhou, M.; Chen, Y. Atomically Precise Colloidal Metal Nanoclusters and Nanoparticles: Fundamentals and Opportunities. *Chem. Rev.* **2016**, *116* (18), 10346–10413. https://doi.org/10.1021/acs.chemrev.5b00703.

(90) Yang, J.; Jin, R. New Advances in Atomically Precise Silver Nanoclusters. *ACS Materials Letters* **2019**. https://doi.org/10.1021/acsmaterialslett.9b00246.

(91) Lee, T.-H.; Dickson, R. M. Discrete Two-Terminal Single Nanocluster Quantum Optoelectronic Logic Operations at Room Temperature. *PNAS* **2003**, *100* (6), 3043–3046. https://doi.org/10.1073/pnas.0635474100.

(92) Xie, Y.-P.; Shen, Y.-L.; Duan, G.-X.; Han, J.; Zhang, L.-P.; Lu, X. Silver Nanoclusters: Synthesis, Structures and Photoluminescence. *Mater. Chem. Front.* **2020**, *4* (8), 2205–2222. https://doi.org/10.1039/D0QM00117A.

(93) Zhang, L.; Wang, E. Metal Nanoclusters: New Fluorescent Probes for Sensors and Bioimaging. *Nano Today* **2014**, *9* (1), 132–157. https://doi.org/10.1016/j.nantod.2014.02.010.

(94) Yu, H.; Rao, B.; Jiang, W.; Yang, S.; Zhu, M. The Photoluminescent Metal Nanoclusters with Atomic Precision. *Coordination Chemistry Reviews* **2019**, *378*, 595–617. https://doi.org/10.1016/j.ccr.2017.12.005.

(95) Díez, I.; A. Ras, R. H. Fluorescent Silver Nanoclusters. *Nanoscale* **2011**, *3* (5), 1963–1970. https://doi.org/10.1039/C1NR00006C.

(96) Wang, X.; Xu, S.; Xu, W. Synthesis of Highly Stable Fluorescent Ag Nanocluster @ Polymer Nanoparticles in Aqueous Solution. *Nanoscale* **2011**, *3* (11), 4670–4675. https://doi.org/10.1039/C1NR10590F.

(97) Chakraborty, I.; Udayabhaskararao, T.; Deepesh, G. K.; Pradeep, T. Sunlight Mediated Synthesis and Antibacterial Properties of Monolayer Protected Silver Clusters. *J. Mater. Chem. B* **2013**, *1* (33), 4059–4064. https://doi.org/10.1039/C3TB20603C.

(98) Xu, J.; Zhu, X.; Zhou, X.; Khusbu, F. Y.; Ma, C. Recent Advances in the Bioanalytical and Biomedical Applications of DNA-Templated Silver Nanoclusters. *TrAC Trends in Analytical Chemistry* **2020**, *124*, 115786. https://doi.org/10.1016/j.trac.2019.115786.

(99) Zhang, F.; A. Smolen, J.; Zhang, S.; Li, R.; N. Shah, P.; Cho, S.; Wang, H.; E. Raymond, J.; L. Cannon, C.; L. Wooley, K. Degradable Polyphosphoester-Based Silver-Loaded Nanoparticles as Therapeutics for Bacterial Lung Infections. *Nanoscale* **2015**, *7* (6), 2265–2270. https://doi.org/10.1039/C4NR07103D.

(100) Gagnon, J.; D. Clift, M. J.; Vanhecke, D.; E. Widnersson, I.; Abram, S.-L.; Petri-Fink, A.; A. Caruso, R.; Rothen-Rutishauser, B.; M. Fromm, K. Synthesis, Characterization, Antibacterial Activity and Cytotoxicity of Hollow TiO 2 -Coated CeO 2 Nanocontainers Encapsulating Silver Nanoparticles for Controlled Silver Release. *Journal of Materials Chemistry B* **2016**, *4* (6), 1166–1174. https://doi.org/10.1039/C5TB01917F.

(101) Tokura, S.; Ueno, K.; Miyazaki, S.; Nishi, N. Molecular Weight Dependent Antimicrobial Activity by Chitosan. In *New Macromolecular Architecture and Functions*; Kamachi, M., Nakamura, A., Eds.; Springer: Berlin, Heidelberg, 1996; pp 199–207. https://doi.org/10.1007/978-3-642-80289-8_21.

(102) Zheng, L.-Y.; Zhu, J.-F. Study on Antimicrobial Activity of Chitosan with Different Molecular Weights. *Carbohydrate Polymers* **2003**, *54* (4), 527–530. https://doi.org/10.1016/j.carbpol.2003.07.009.

(103) Kashiri, M.; Cerisuelo, J. P.; Domínguez, I.; López-Carballo, G.; Muriel-Gallet, V.; Gavara, R.; Hernández-Muñoz, P. Zein Films and Coatings as Carriers and Release Systems of Zataria Multiflora Boiss. Essential Oil for Antimicrobial Food Packaging. *Food Hydrocolloids* **2017**, *70*, 260–268. https://doi.org/10.1016/j.foodhyd.2017.02.021.

(104) Smart Packaging Technologies for Fast Moving Consumer Goods | Wiley Online Books https://onlinelibrary.wiley.com/doi/book/10.1002/9780470753699 (accessed Dec 9, 2019).

(105) Sharma, V. K.; Yngard, R. A.; Lin, Y. Silver Nanoparticles: Green Synthesis and Their Antimicrobial Activities. *Advances in Colloid and Interface Science* **2009**, *145* (1), 83–96. https://doi.org/10.1016/j.cis.2008.09.002.

(106) Wakshlak, R. B.-K.; Pedahzur, R.; Avnir, D. Antibacterial Activity of Silver-Killed Bacteria: The "Zombies" Effect. *Scientific Reports* **2015**, *5* (1), 9555. https://doi.org/10.1038/srep09555.

(107) Gao, P.; Nie, X.; Zou, M.; Shi, Y.; Cheng, G. Recent Advances in Materials for Extended-Release Antibiotic Delivery System. *The Journal of Antibiotics* **2011**, *64* (9), 625–634. https://doi.org/10.1038/ja.2011.58.

(108) Richter, A. P.; Brown, J. S.; Bharti, B.; Wang, A.; Gangwal, S.; Houck, K.; Cohen Hubal, E. A.; Paunov, V. N.; Stoyanov, S. D.; Velev, O. D. An Environmentally Benign Antimicrobial Nanoparticle Based on a Silver-Infused Lignin Core. *Nature Nanotechnology* **2015**, *10* (9), 817–823. https://doi.org/10.1038/nnano.2015.141.

(109) Chinnapongse, S. L.; MacCuspie, R. I.; Hackley, V. A. Persistence of Singly Dispersed Silver Nanoparticles in Natural Freshwaters, Synthetic Seawater, and Simulated Estuarine Waters. *Science of The Total Environment* **2011**, *409* (12), 2443–2450. https://doi.org/10.1016/j.scitotenv.2011.03.020.

(110) Nanotechnology Safety Concerns Revisited | Toxicological Sciences | Oxford Academic https://academic-oup-com.proxy-um.researchport.umd.edu/toxsci/article/101/1/4/1655301 (accessed Oct 8, 2020).

(111) Laaksonen, T.; Ruiz, V.; Liljeroth, P.; M. Quinn, B. Quantised Charging of Monolayer-Protected Nanoparticles. *Chemical Society Reviews* **2008**, *37* (9), 1836–1846. https://doi.org/10.1039/B713681C.

(112) Photoinduced Electron Transfer of DNA/Ag Nanoclusters Modulated by G-Quadruplex/Hemin Complex for the Construction of Versatile Biosensors | Journal of the American Chemical Society https://pubs-acs-org.proxy-um.researchport.umd.edu/doi/abs/10.1021/ja3089857 (accessed Oct 8, 2020).

(113) Wang, Y.; Dai, C.; Yan, X.-P. Fabrication of Folate Bioconjugated Near-Infrared Fluorescent Silver Nanoclusters for Targeted in Vitro and in Vivo Bioimaging. *Chemical Communications* **2014**, *50* (92), 14341–14344. https://doi.org/10.1039/C4CC06329E.

(114) Dadmehr, M.; Hosseini, M.; Hosseinkhani, S.; Reza Ganjali, M.; Sheikhnejad, R. Label Free Colorimetric and Fluorimetric Direct Detection of Methylated DNA Based on Silver Nanoclusters for Cancer Early Diagnosis. *Biosensors and Bioelectronics* **2015**, *73*, 108–113. https://doi.org/10.1016/j.bios.2015.05.062.

(115) Self-Stratified Antimicrobial Acrylic Coatings via One-Step UV Curing | ACS Applied Materials & Interfaces https://pubs-acs-org.proxy-um.researchport.umd.edu/doi/abs/10.1021/acsami.5b04633 (accessed Oct 8, 2020).

(116) Shang, L.; Dong, S. Silver Nanocluster-Based Fluorescent Sensors for Sensitive Detection of Cu( Ii ). *Journal of Materials Chemistry* **2008**, *18* (39), 4636–4640. https://doi.org/10.1039/B810409C.

(117) Zhang, Y.; Niu, Y.; Luo, Y.; Ge, M.; Yang, T.; Yu, L. (Lucy); Wang, Q. Fabrication, Characterization and Antimicrobial Activities of Thymol-Loaded Zein Nanoparticles Stabilized by Sodium Caseinate–Chitosan Hydrochloride Double Layers. *Food Chemistry* **2014**, *142*, 269–275. https://doi.org/10.1016/j.foodchem.2013.07.058.

(118) Moradi, M.; Tajik, H.; Razavi Rohani, S. M.; Mahmoudian, A. Antioxidant and Antimicrobial Effects of Zein Edible Film Impregnated with Zataria Multiflora Boiss. Essential Oil and Monolaurin. *LWT - Food Science and Technology* **2016**, *72*, 37–43. https://doi.org/10.1016/j.lwt.2016.04.026.

(119) Ruparelia, J. P.; Chatterjee, A. K.; Duttagupta, S. P.; Mukherji, S. Strain Specificity in Antimicrobial Activity of Silver and Copper Nanoparticles. *Acta Biomaterialia* **2008**, *4* (3), 707–716. https://doi.org/10.1016/j.actbio.2007.11.006.

(120) Huang, W.; Xu, H.; Xue, Y.; Huang, R.; Deng, H.; Pan, S. Layer-by-Layer Immobilization of Lysozyme–Chitosan–Organic Rectorite Composites on Electrospun Nanofibrous Mats for Pork Preservation. *Food Research International* **2012**, *48* (2), 784–791. https://doi.org/10.1016/j.foodres.2012.06.026.

(121) Malhotra, B.; Keshwani, A.; Kharkwal, H. Antimicrobial Food Packaging: Potential and Pitfalls. *Front. Microbiol.* **2015**, *6*. https://doi.org/10.3389/fmicb.2015.00611.

(122) Li, X.; Fu, T.; Li, B.; Yan, P.; Wu, Y. Riboflavin-Protected Ultrasmall Silver Nanoclusters with Enhanced Antibacterial Activity and the Mechanisms. *RSC Advances* **2019**, *9* (23), 13275–13282. https://doi.org/10.1039/C9RA02079A.

(123) Halbes-Letinois, U.; Weibel, J.-M.; Pale, P. The Organic Chemistry of Silver Acetylides. *Chem. Soc. Rev.* **2007**, *36* (5), 759–769. https://doi.org/10.1039/B602151B.

(124) Devlieghere, F.; Vermeulen, A.; Debevere, J. Chitosan: Antimicrobial Activity, Interactions with Food Components and Applicability as a Coating on Fruit and Vegetables. *Food Microbiology* **2004**, *21* (6), 703–714. https://doi.org/10.1016/j.fm.2004.02.008.

(125) Dutta, P. K.; Tripathi, S.; Mehrotra, G. K.; Dutta, J. Perspectives for Chitosan Based Antimicrobial Films in Food Applications. *Food Chemistry* **2009**, *114* (4), 1173–1182. https://doi.org/10.1016/j.foodchem.2008.11.047.

(126) Coma, V.; Martial-Gros, A.; Garreau, S.; Copinet, A.; Salin, F.; Deschamps, A. Edible Antimicrobial Films Based on Chitosan Matrix. *Journal of Food Science* **2002**, *67* (3), 1162–1169. https://doi.org/10.1111/j.1365-2621.2002.tb09470.x.

(127) Gregorio-Jauregui, K. M.; Pineda, M. G.; Rivera-Salinas, J. E.; Hurtado, G.; Saade, H.; Martinez, J. L.; Ilyina, A.; López, R. G. One-Step Method for Preparation of Magnetic Nanoparticles Coated with Chitosan https://www.hindawi.com/journals/jnm/2012/813958/ (accessed Oct 21, 2020). https://doi.org/10.1155/2012/813958.

(128) Bao, H.; Li, L.; Leong, W. C.; Gan, L. H. Thermo-Responsive Association of Chitosan-Graft-Poly(N-Isopropylacrylamide) in Aqueous Solutions. *J. Phys. Chem. B* **2010**, *114* (32), 10666–10673. https://doi.org/10.1021/jp105041z.

(129) McCabe-Sellers, B. J.; Beattie, S. E. Food Safety: Emerging Trends in Foodborne Illness Surveillance and Prevention. *Journal of the American*

*Dietetic Association* **2004**, *104* (11), 1708–1717. https://doi.org/10.1016/j.jada.2004.08.028.

(130) Guan, Y.; Teng, Z.; Mei, L.; Zhang, J.; Wang, Q.; Luo, Y. An Entrapped Metal-Organic Framework System for Controlled Release of Ethylene. *Journal of Colloid and Interface Science* **2019**, *533*, 207–215. https://doi.org/10.1016/j.jcis.2018.08.057.